Statistical Mechanics of Distribution Networks

DIAR NASIEV

Doctor Of Philosophy

– ASTON UNIVERSITY –

September 2009

ASTON UNIVERSITY

Statistical Mechanics of Distribution Networks

DIAR NASIEV

Doctor Of Philosophy, 2009

Thesis Summary

This thesis presents an analysis of the stability of complex distribution networks.

We present a stability analysis against cascading failures. We propose a spin [binary] model, based on concepts of statistical mechanics. We test macroscopic properties of distribution networks with respect to various topological structures and distributions of microparameters. The equilibrium properties of the systems are obtained in a statistical mechanics framework by application of the replica method. We demonstrate the validity of our approach by comparing it with MonteCarlo simulations. We analyse the network properties in terms of phase diagrams and found both qualitative and quantitative dependence of the network properties on the network structure and macroparameters. The structure of the phase diagrams points at the existence of phase transition and the presence of stable and metastable states in the system.

We also present an analysis of robustness against overloading in the distribution networks. We propose a model that describes a distribution process in a network. The model incorporates the currents between any connected hubs in the network, local constraints in the form of Kirchoff's law and a global optimizational criterion. The flow of currents in the system is driven by the consumption. We study two principal types of model: infinite and finite link capacity. The key properties are the distributions of currents in the system. We again use a statistical mechanics framework to describe the currents in the system in terms of macroscopic parameters. In order to obtain observable properties we apply the replica method. We are able to asses the criticality of the level of demand with respect to the available resources and the architecture of the network. Furthermore, the parts of the system, where critical currents may emerge, can be identified. This, in turn, provides us with the characteristic description of the spread of the overloading in the systems.

Keywords: Distribution networks, complex networks, statistical physics, replica method.

Contents

List of Figures

To
my family.

Acknowledgements

First and foremost I am grateful to my supervisor Dr Jort van Mourik for the support, encouragement and much needed guidance offered to me during my studies at Aston.

I wish to thank NCRG members; Professor David Lowe, Professor David Saad, Professor Ian Nabney, Davide D'Alimonte for their excellent lectures and assistance during my years at Aston.

I am also grateful to Reimer Kühn with whom I closely collaborated.

Thanks to Dr Laura Rebollo-Neira who kept me busy with marking!

My sincerest thanks to Vicky Bond and Kanchan Patel for assistance with my numerous visa applications.

Special thanks to my fellow colleagues Alexis Boukouvalas, Michel Randrianandrasana, Rajeswari Matam, Jack Raymond, Erik Casagrande, Ming Sivaraksa, Thomas Bermudez, András Joó, Harry Goldingay,Michail Vrettas,Martin Shcroeder, James Bowley, Ben Tocher, Richard Jones who made my life in Birmingham enjoyable.

To Remi Barillec, Chris Chu, Sergej Lubovnikov and Matt Williams I am especially grateful for footie games.

To my volleyball loving friends Jovana, Annalisa, Tomoyo, Rike, Pavel, Anthony , Rosen, Piotr and Rafal thank you for playing game (and Arnold! and Alex!).

I would also like to thank my dear friends Dorota, Magdalena, Maciek, Kristina, Rokas and Jolanta.

To my (work) supervisors Sheila and Ilona I will be always grateful.

During my years at Aston I have been receiving the strongest emotional support from my family and friends in Russia and Kazakhstan. I feel so much grateful to my mother for help and encouragement.

1 Introduction

CONTENTS

1.1 Complex networks, motivation.

The field of complex networks has grown from the research of many other fields of science and spans many research areas. Stemming from mathematics [1] and social science [2, 3] the field of complex networks attracts a lot of interest from various scientific communities and in a period of rapid development.

Complex networks arise naturally in many fields of science. Having understood the behaviour or properties of individual objects and interactions between objects, researchers attempt to look into properties of the groups of interacting objects. While it is possible to analyse small groups or groups that have special order, the analysis of large groups, with just basic knowledge of the objects and interactions, is still an open question in many cases and is the subject of the study of complex networks.

1.1.1 Applications of complex networks.

There are many applications of complex networks in various fields. In social studies [2, 3, 4, 5] the networks are statistically measured to address the questions of the status, influence or role of an individual. The structure of social networks reveals social division or cohesiveness. From the epidemiological point of view, social networks are interesting as a distribution network to study the spread of diseases [1, 6, 7, 8]. The social interactions in this context could assist in the discovery of new strategies for avoiding or containing future epidemics. In biochemical networks, some unexpected features are found, that are significant in understanding of the evolution of organisms [9, 10].

Technological networks are another type of network of interest. The term "technological" refers to various communication and transport networks [11], electrical power grids [12, 13], the Internet [14, 15, 16], as well as other man-made networks. The remarkable growth of networks of this type completely changed our education and entertainment, commerce and communication. It is very hard to underestimate the importance of these networks as they have become a backbone of modern society, and without these networks, even day to day tasks become surprisingly hard to accomplish.

Technological networks are a particularly fruitful application of complex networks.

The studies of such networks proved to be useful in design of new algorithms for search [17, 18], implementation of the computation/resource sharing [19], analysis of robustness and vulnerability [20, 21, 22, 23, 24].

1.1.2 Robustness of complex networks.

In this thesis we focus on the stability issues of complex distribution networks. We focus on networks where some kind of distribution process is in action such as electrical power distribution, rail/road transportation, information distribution on the Internet. Thus, electrical power distribution is a process of delivering electrical energy to consumers. The power grid connects generating power plants to multiple transmission and distribution substations. Therefore, the success of the distribution process depends on the functioning of substations and transmission lines in the network. Similarly, transportation of people and commodities is achieved by use of various transport networks, and both the transport links and the transport hubs are critical to the transportation. Finally, information distribution on the Internet is a process of sending/receiving electronic documents between computers connected to the Internet. The Internet is a network of computers and physical connections between them. The distribution depends on the functioning of many computers and connections between them.

The typical state of any distribution network is the functional one, that is the service is delivered throughout the whole network. However, everyday we experience traffic jams, sometimes the absence of Internet connection and very rare power outages. All these indicate that the corresponding network does not function to an expected level. In particular, the grid lock on the roads signals that the road capacity is less than the actual traffic, the absence of Internet connections could be caused by hardware problems or cable faults, the power outage by transmission line or substation faults.

However, the malfunction of some parts of the network usually does not affect the whole network [25]. Thus, the traffic problems in one part of the city do not affect traffic in other parts; nonfunctioning servers on the Internet affect only users that connect to them, broken transmission lines cause outages in particular locations.

Moreover, the design of the core of such networks allows multiple routes between any locations, computers or substations. This built-in network redundancy, allows avoidance of problem spots, decreasing stress on the malfunctioning parts of the network [22]. This is especially important in such systems due to the systematic character of observed failures [26]. It is known that many routers, websites or Web pages malfunction everyday, but still the overall functioning of the whole system remains intact. Similarly, studies of power grids show many low level failures in the systems, yet the overall distribution in general is unaffected [26].

On the other hand, interconnectedness of network elements may appear to have negative effects as well. A traffic jam could develop into a total grid lock, or an accident on the main power station could trigger a blackout in the power grid. The same mechanism that makes networks robust to local failures could help in propagating such failures through the network. The question now is under what conditions a network's function could be affected by failures [20]. Why do failures in the networks sometimes pass unnoticed, while sometimes they trigger a cascade of failures causing damage to large parts of the network? What level of failures could cause such critical damage? To what degree does the network's structure influence robustness of the network?

Typically, distribution networks would operate below their maximum capacity level [27]. Occasionally, due to different factors like the malfunction of some elements in the network or increases of the flow, transported through the network, some parts of the network have to operate at their critical level. This may cause failures of these parts and increase stress on the neighbours. This process spreads in such a fashion from some parts of the network to others. The failed parts affect neighbours, which in turn affect their neighbours, causing a cascade of failures [28].

By "capacity" we mean the maximum allowed flow through a link [29]. Of course, the capacity of the motorway is bigger than that of the country lane, or the capacity of high-voltage transmission line is bigger than that of the low-voltage line. However, the capacity of the whole network is not just a sum of its elements. In order to estimate capacity of the whole network from the capacities of its individual elements we need an approach that allows the description of the individual elements and their interactions, and

also takes into account the structural properties of the network [30].

1.2 Statistical mechanics of disordered systems.

Statistical mechanics is a field of physics that relates macroscopic properties of large groups of interacting objects with the microscopic description of the system entities and interactions between them. Based on simplified or even incomplete descriptions of interacting objects, theoretical models reproduce remarkable agreement with the qualitative behaviour of real systems. One of the most successful applications is the SK model of spin glasses.

1.2.1 Sherrington-Kirkpatrick (SK) model.

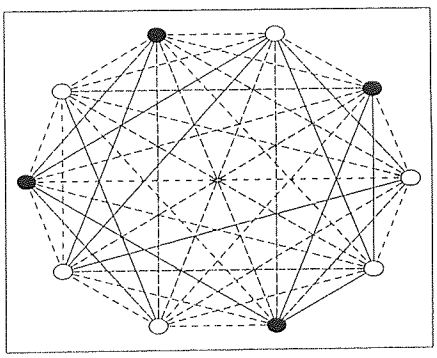

Figure 1.1: Fully connected network on which SK model is defined. The solid lines represent ferromagnetic interactions and dashed lines represent antiferromagnetic interactions between spins. Dark and light nodes indicate spin ± 1.

The Sherrington-Kirkpatrick (SK) model is a model of magnetism in spin glasses (ferromagnetic materials with impurities) [31]. Random placements of impurities leads to the phenomenon of frustration and thereby to dependencies on distance, which can be ferromagnetic or antiferromagnetic, and leads to non-trivial properties of spin glasses and to spin glass phase in particular [32].

The SK model describes a system of N spins, the spins can take values $\{\pm 1\}$. The interactions between spins are described by anti-/ferromagnetic couplings J_{ij}. The positive(ferromagnetic) couplings stimulates parallel alignment of the spins, while negative

(antiferromagnetic) stimulates antiparallel alignment. The equilibrium properties of the system are described by the Hamiltonian

$$H = -\frac{1}{2}\sum_{ij}^{N} J_{ij} s_i s_j - h\sum_{i}^{N} s_i. \tag{1.1}$$

The thermodynamic limit is obtained for a large system size ($N \to \infty$). As the energy density should be independent of the size of the system the distribution of J should be appropriately scaled. It turns out that the presence of the J's introduces correlations between spins. For fixed J's in zero magnetic field at high temperature the magnetisation ($m = \frac{1}{N}\sum_i s_i$) is zero, just like in usual ferromagnets. However, in the low temperature region in the absence of an external magnetic field two different phases have been found. The local magnetisation at the low temperature becomes exposed to the disorder J. To account for this effect the so-called Edwards-Anderson order parameter is introduced

$$q = \frac{1}{N}\sum_{i=1}^{N} m_i^2, \quad \text{where} \quad m_i \equiv \langle s_i \rangle. \tag{1.2}$$

The two phases are then distinguished by the pair (m, q). Cooling the system leads to either spin glass phase ($m = 0, q > 0$) or the ferromagnetic phase ($m \neq 0$).

1.2.2 Replica method.

The replica method applied to study the SK model [32] will be used throughout this thesis extensively. The details of the application of replica steps depend on the details of the particular problem. Here we present the key ideas of the replica method.

The presence of random long range interactions (called disorder) in the SK model introduces correlations between spins (s) in the system. The quenched or frozen disorder (J), as opposed to annealed disorder, appears in the form of fixed random variables that do not evolve with time or evolve much more slowly compared to physical observable. The distribution of the variable that represents the disorder is assumed to be known. From the computational point of view the presence of disorder introduces considerable difficulties.

The partition function in the presence of disorder J is

$$Z_J = \operatorname*{Tr}_s e^{-\beta H_J[s]} \tag{1.3}$$

and the free energy density

$$f_J = -\frac{1}{\beta N} \ln Z_J. \tag{1.4}$$

Other properties of the system can be calculated from the free energy density. In a system with annealed disorder, the physical quantities could be calculated directly through averaging of the partition function (Z_J), but in the presence of the quenched disorder the calculation of (1.4) is not simple, so we have to use the replica method. We start with introduction of the n replicas of the system. Each replica is subject to the same quenched disorder J. With each replica we associate a set of spin variables $S^\alpha = \{s_1^\alpha, \ldots, s_N^\alpha\}$. The partition function of the n-fold replicated system is

$$\langle Z_J^n \rangle = \langle \operatorname*{Tr}_{s^\alpha} e^{\beta\left(\frac{1}{2}\sum_\alpha \sum_{ij} J_{ij} s_i^\alpha s_j^\alpha + h \sum_\alpha \sum_i s_i^\alpha\right)} \rangle. \tag{1.5}$$

The thermodynamically relevant terms in the exponent now become dependent on the inter-replica correlations $\sum_i s_i^{\alpha_1} s_i^{\alpha_2}$. The simplest case of inter-replica correlations is replica symmetry. Replica symmetry (RS) assumes that all inter-replica correlations are independent of the replicas in question. Note that different assumptions about the inter-replica correlations could be made, leading to hierarchy of solutions, different levels of replica symmetry breaking(RSB) [33].

Next, we use the identity

$$\langle \ln Z_J \rangle = \lim_{n \to 0} \frac{\langle Z_J^n \rangle - 1}{n}. \tag{1.6}$$

Finally, we can compute the average of the free energy density

$$\langle f_J \rangle = -\frac{1}{\beta N} \langle \ln Z_J \rangle. \tag{1.7}$$

Provided that fluctuations of the disorder variables is proportional to $(1/N^{\frac{1}{2}})$, for the

large system the difference between the free energy density and the average of the free energy density becomes negligible

$$\langle f_J \rangle^2 - \langle f_J^2 \rangle = O\left(\frac{1}{N}\right). \tag{1.8}$$

To calculate physical observable properties we would have to take two limits $N \to \infty$ and $n \to 0$. The free energy of the system is obtained

$$F = -\lim_{N\to\infty} \lim_{n\to 0} \frac{1}{\beta N} \langle Z_J^n \rangle \tag{1.9}$$

In the limiting procedure the dependence on the integer n is continued to the real numbers.

The replica method has proven to be successful to study disordered models. The applications of this method can be found not only in physics, but also in biological models [34, 35, 36] and mathematical optimisation problems [37, 38, 39, 40].

1.2.3 Optimisation

In the second part of the thesis (**capacity**) physical properties of interest - distributions of currents in power-grids - are obtained by finding the systems ground state. In particular, the flow of currents in a network obtained as a solution of an optimisation problem with the cost function represented by a partition function. In our case the cost function is dependent on a high number of parameters (individual resistances) and optimisation is quite difficult.

There are known parallels between the statistical mechanics and combinatorial optimisation problems [37, 40]. In such problems one must find the minimum of a function which depends on many variables. The typically high number of variables in such problems makes finding minima of that function quite difficult. However, it is possible to map such problems on spin glasses. Then a configuration of variables corresponds to a configuration of the spins, the cost function corresponds to the energy function in the spin glass, the optimal configuration to a ground state, and the minimal cost to the ground state

energy. Spin models have been applied to many NP-complete combinatorial optimisation problems like TSP, matching, assignment [38, 39].

Not all combinatorial optimisation problems can be tackled by statistical mechanics. There are qualitative differences between say spin glasses and hard optimisation problems. In statistical mechanical problems one might know very little about the system, and normally one is interested in some macroscopic properties. In contrast, in optimisation problems we usually have a lot of information about the problem and are interested in the detailed answers. While statistical mechanics provides with the most probable solution, we consider that solution not as optimal but as an improvement on the existing one.

As has been noticed, the problems that arise in the analysis of combinatorial optimisation problems are harder than in normal spin glasses due to the necessity to find an optimal solution. The difficulties arise from the fact that the one has to find *true minima* of the cost function. The number of metastable states in spin glasses depend on the external factors like temperature. As temperature decreases the number of the metastable states in the system increases. The ground state energy then should be calculated at zero temperature. Considering that replica symmetric solution of the SK model tends to give a very bad approximation at low temperature, analysis of the optimisation problem is rather difficult [32]. However, it has been shown for some problems like TSP, matching or assignment, the replica symmetric solution at zero temperature reaches the true minimum of the cost function [38, 39].

1.3 Graphical models

1.3.1 From real world problems to abstract models.

Historically, studies of complex networks, like early studies of social networks, have focused on the structural properties of such networks. In many cases it is assumed that properties of objects and interactions are known and qualitatively similar. Under these assumptions some social, biological and physical networks can be studied . The World Wide Web and the Internet also could be thought of as a large collection of qualitatively

similar objects. Given this object homogeneity, the properties of the system will depend on the structural characteristics of the underlying network. An understanding of the network's structure and its influence on the final properties of a complex network is thus very important [12].

In mathematics, graph theory is a natural tool to study the structure of a network. Some particular networks can be represented as graphs, the network's nodes and interactions represented by the vertices and the edges. Such a representation produces a clear view of the network structure, sometimes allowing insightful simplifications. For example, the properties of a network with a star-like structure heavily depend on the properties of the central node(s) and not so much on the dangling nodes, while the nodes in a chain-like network are all equally important. For networks with directed interactions, like the Web or biochemicals networks, directed graphs enable source-destination representation. Directed representations, for instance, could be useful to identify generators/distributors/consumers in power networks.

1.3.2 Lattices.

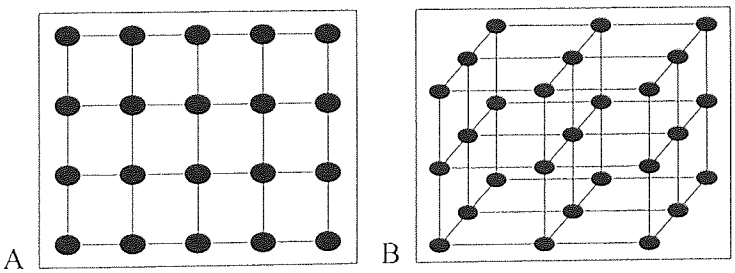

Figure 1.2: Examples of lattices. **A**, two-dimensional grid. **B**, three-dimensional grid.

Regular graphs are a good starting point for many physical networks. The regular underlying structures can be found in many real physical systems, e.g. crystalls. Therefore it is useful to model such systems on lattices. From the mathematical point of view the treatment of models on lattices is much simpler, i.e. compared to unregular structures.

Other regular structures like trees, chains, stars (Figure1.3) also provide simplified mathematical analysis of the networks.

However, such structures do not typically represent real-world networks. For instance,

it is highly uncharacteristic for any social or technological network to exhibit strong order. In contrast, many real networks highlight a high degree of irregularity. The number of friends varies significantly from person to person (depends on personal characteristics), or the number of links on the page of a big media site is considerably higher than on the one's personal page. It is proposed that such networks could be modelled by random graphs [41].

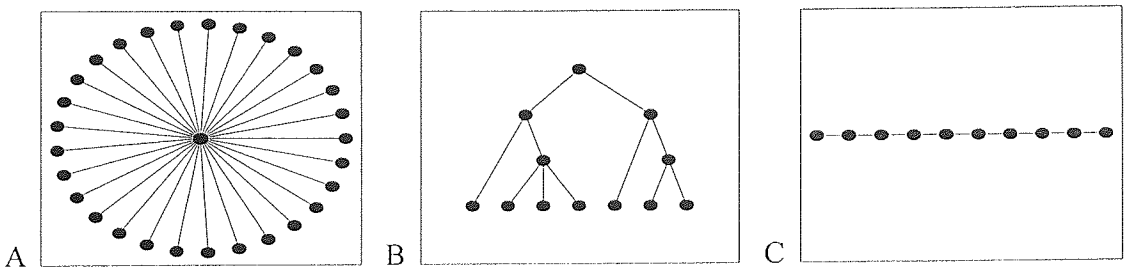

Figure 1.3: Examples of regular structures. **A**, Star-like structure. **B**, a tree. **C**, a chain.

1.3.3 Exponential and regular random graphs.

Figure 1.4: Schematic illustration of exponential random graph. A graph contains 150 nodes and 225 links (average connectivity $C = 3$). Only 25 nodes (17%) are reached by the five most connected nodes.

The exponential random graph model was introduced by Erdős and Renyi [42]. The random graph $G(V,E)$ obtained by considering a set of nodes $V = \{v_i\}$, and links $E = \{e_{ij}\}$ between given pairs of nodes (v_i, v_j) are all drawn independently with probability p. This construction method produces so-called $G(N,p)$ random graphs. Another way to construct an exponential random graph is to define the size N, the number of links M and then randomly assign the links to the pairs of nodes. Such graphs are called $G(N,M)$ random graphs. For large graphs both models produce qualitatively similar graphs. In this work, we will use the $G(N,M)$ version to generate large exponential random graphs.

We also consider regular random graphs. The regular random graph with the average connectivity C is a graph where each node has C links. In cases when C is not an integer, the number of links is either $[C]$ or $[C]+1$

Exponential random graphs have been extensively studied over the years [42, 43]. Structurally, exponential random graphs are different from regular random graphs. Statistically the difference between structures is assessed by average connectivity[1], clustering

[1]The average connectivity is typically denoted by C and is an average of connectivities of each node c_i, $C = \frac{1}{N}\sum_i c_i$

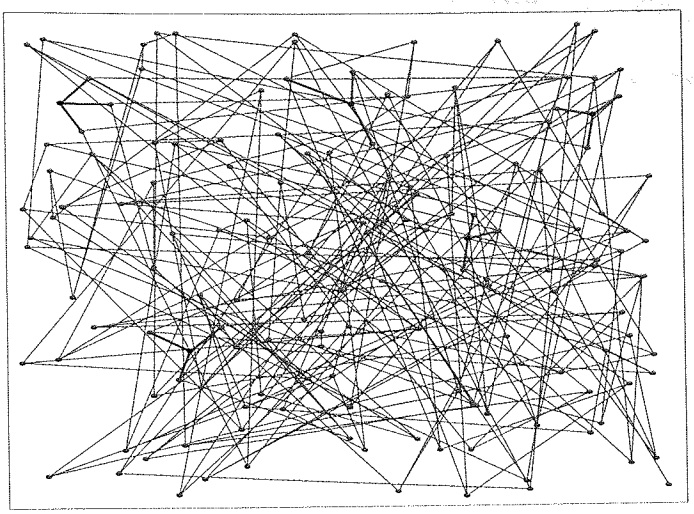

Figure 1.5: Schematic illustration of regular random graph. A graph contains 150 nodes and 225 links (average connectivity $C = 3$). All nodes have the same number of links. Only 15 nodes (10%) are reached by the five most connected nodes.

coefficient[2] and degree distribution[3]. The average connectivity is the average number of connections each node in the graph has; the clustering coefficient measures the degree to which nodes tend to cluster together; the degree distribution is a distribution of the nodes connectivities or degrees. For regular and exponential random graphs of the same size and the same average connectivity the clustering coefficient is much higher for the regular graphs, while the average length between any two nodes is much smaller in exponential random graphs. The degree distribution for regular random graphs is a delta peak(if C is an integer, otherwise is a weighted sum of two delta peaks), and follows a Poison distribution for exponential random graphs [42].

The key differences between random graphs and lattices are: *periodicity* and *dimensionality*. The lattices are the periodic structures and can be embedded into space of finite dimensionality. On the other hand, the infinite random graphs are non-periodic and infinite dimensional structures.

[2]The local clustering coefficient can be defined as $C_i = \frac{\sum_{jk} c_{ij} c_{jk} c_{ki}}{k_i(k_i-1)/2}$

[3]The degree distribution denoted as P(L) is a distribution of degrees or connectivities or coordination numbers.

1.3.4 Small world networks, scale-free networks

Random graph models proved to be insightful and useful in many cases [44, 45], but still are far from being a realistic representation of many systems. Empirical evidence of many social and technological networks shows that such networks feature properties of both regular and random structures. Even the earliest experiments [3] reported higher than random clustering coefficient and small average shortest path. Indeed, in a typical social network, chances that one's friends are friends themselves are quite high, i. e. a group of friends form a clique (fully connected subgraph) and that makes it very similar to lattices. On the other hand, the so called small-world property has been highlighted for many different types of networks. The small-world property means that any two individuals in the network are separated by a small number of intermediaries. The "six degrees of separation" [3] is the manifestation of these property in the human population, or 19 clicks between any two pages in the World Wide Web [46].

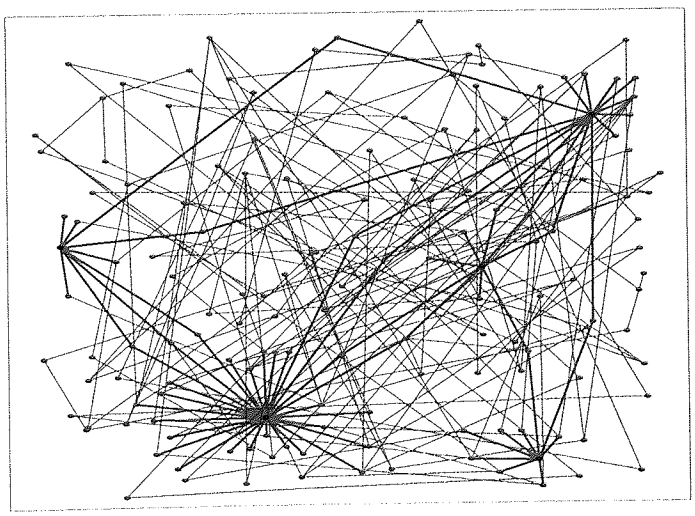

Figure 1.6: Schematic illustration of scale-free random graph. A graph contains 150 nodes and 225 links (average connectivity $C = 3$). The majority of the nodes have a few links but a few nodes have a large number of links. In the scale-free graph 67 nodes (46%) are reached by the five most connected nodes.

The networks that exhibit the small-world property are called small world networks, and have been extensively studied in the last two decades [41, 13]. The models of small world networks introduced by Strogatz and Watts are between the regular and random

graphs, and provide a better description of biological, social and technological networks [41] . For all of them, measured properties and properties predicted based on the corresponding models of small world networks are qualitatively similar. However, more detailed analysis shows some significant differences between different networks [12].

One particular class of small world networks that has been found to be a good approximation of real networks are scale-free networks. Discovered by A. -L. Barabasi and R. Albert [47], it has been found that power grids, social networks, biological, chemical networks can be modeled as scale-free networks.

Scale-free networks are characterised by a power law degree distribution. The structure of various networks have been probed and it has been reported that many real networks are actually scale-free. It was also suggested that there are certain mechanisms responsible for the developing scale-free structure. Namely, these mechanisms are growing and preferential attachment. Growing is observed in any real network as new nodes are added to the network. The second mechanism is responsible for the connections in the network, new nodes more likely to be connected to the nodes with higher connectivities. Preferential attachment can be observed in the Internet and social networks [47].

1.4 Stability analysis of distribution networks.

Various factors contribute to the formation of network structures. All parts of even the simplest of organisms evolve to ensure survival. Power grids are generally planned by engineers to distribute electrical energy as efficiently as possible, while the Internet has spread all over the globe without any central administration and without any preventive safety measures. Correspondingly, different technological, biological and social networks display diverse and non-trivial network structure. Yet, despite of the diverse nature of these networks they all exhibit a high degree of tolerance against failures.

By failures we refer to an uncommon state of the network's nodes and links. Failures could be negative as well as positive. Examples of failures are a broken server in the Internet, a broken electrical transmission line in the power grid, a sick person in the social network, a useful application (or invention), a new political or cultural opinion. It has been

recognised that the spread of failures significantly depend on the structural properties of the network. Stability analysis is applied to identify features of the networks that contribute to the spread/eradication of failures [6, 7, 48].

Also, we realise that at least two different types of failures can be considered, and stability analysis depends significantly on the type of failures under consideration. Suppose one is going to inflict damage to a component of a network. Without any knowledge of the system any component of the system is equally likely to be damaged. This will constitute a *random failure* or *random removal*. In real networks random failures take place due to mechanical (electrical, electronic, etc) problems or natural events. In contrast, with the knowledge of the network properties, one could decide to damage the most important components of the system. Damaging the main router in the Internet or a high-voltage transmission line from the power station will constitute an *attack* or *selective removal*. An attack is a more elaborate case of failures, as it needs an intricate knowledge if not of the system, at least of the structural properties of the underlying network. In stability analysis the random failures and attacks should be distinguished [20].

Often the robustness of the network is looked at in the context of the development of global cascades [21, 25]. This strange phenomena can be referred as "robust yet fragile" nature of many complex systems. Many of the natural and technological systems display a high degree of robustness : systems appear stable for long periods of time, withstanding many externally inflicted failures (living organism, functioning power grid) However, suddenly and often unexplained the system collapses, i.e. develops a large cascade of failures.

A wide spectrum of research disciplines contributes to understanding properties of complex networks and conditions necessary to develop cascades of failures. The obvious approach is to investigate the structural properties of the networks. For the generic models of exponential random graphs and scale-free networks it has been found that both types of structures display a high degree of tolerance against random failures, with the scale-free networks outperforming random graphs. However, subject to a targeted attack, random graphs appear to be significantly more robust than scale-free networks. Robustness of the network is measured by estimating the size of the largest component and monitoring sizes

of small clusters [20].

It was suggested that the reason for this behaviour of scale-free networks is the existence of the hubs. These are highly connected nodes and highly beneficial in the context of spreading information in the information network for example. But in case of attacks the hubs are targeted first. It has been shown that removal of even a modest number of highly connected nodes in scale-free networks causes significant changes to the network structure often with a catastrophic effects to a networks' robustness. The disintegration of scale-free structures could become apparent after removal of as little as 5% of the highly connected nodes (this is a fragmentation threshold). Continued removal leads to the fragmentation of the network into many isolated clusters.

However, if subjected to random failures, scale-free networks display a remarkable degree of robustness. Even for unrealistically high rates of failures (for up to 45% of the nodes) the network functioning remains mainly intact. It appears that one giant component (cluster) is observed at all stages of random removal. The size of this cluster slowly decreases and no threshold for fragmentation is observed [20].

For random graphs both types of failures (attacks and random failures) cause qualitatively similar damage. For the attacks the fragmentation threshold is reported to be at 28% of the order of the graph. The fragmentation process is very similar to a scale-free fragmentation under attacks. This behaviour is attributed to a homogeneity of the random network, the damage from elimination of any of the nodes is approximately the same [20].

Similar techniques have been applied to real networks. Both the Internet and World Wide Web appeared to exhibit scale-free like fragmentation. Different values of fragmentation thresholds have been reported, otherwise qualitatively the same. For the Internet the *random* elimination of 2.5% of the nodes does not cause any statistically significant change to the average shortest path of the largest component, yet *selective removal* of the same proportion of the nodes causes three-fold increase of average shortest path. The critical point in the attack mode is at 3% of the order of the graph. For the World Wide Web response to the failures is very similar, despite the directedness of the links. Under random failures the network stays intact as a large cluster, but under attacks the system falls apart abruptly after removal of 6.7% of the nodes [20].

In many networks not only the nodes could be damaged, but the connections between them as well. In [49] both node and edge failures are considered in the analysis. The functionality of the network is measured by characteristic path length. Also, from the local point of view, the evolution of the clustering coefficient and nodes betweenness is monitored. Four different strategies, the degree-based (calculated before the start of the removal process or recalculated after each removal) and betweenness-based[4] (calculated before the start of the removal process or recalculated after each removal), applied for the node attacks. For the random graphs all strategies result in qualitatively similar fragmentation process, the degree-based strategies resulted in a slower fragmentation. For the scale-free structures the fragmentation starts considerably earlier than for random networks, and without any significant difference between degree-based and betweenness-based attacks.

For the analysis of edge attacks the edge degree is introduced as a product of degrees of the nodes connected by the edges. Both random graphs and scale-free networks show similar response to edge removal. Moreover, the edge removal in the random graphs, confirms that high degree edges are responsible for the networks vulnerability.

Analysis of node and edge removal were performed in scientific collaboration networks and computer networks of Internet traffic. Both networks display similar response to the edge attacks, while under node attacks show very distinct behaviour. The average shortest path length increases almost linearly for the former and logarithmically for the latter with decrease of the size of a network [50].

So far, only static structures have been considered and various aspects of networks robustness and vulnerability explored. More realistic analysis should take into account processes on the network is studied in [24, 25]. Introduction of such processes brings out the dynamical aspects into consideration. Now the load of traffic flowing through each link can potentially damage those links, so the failures appear as part of the processes on the network, rather than due to some external factors. The simple threshold model is introduced for the link failure and the diversion of the load from the damaged parts of the

[4]Betweenness is a centrality measure of a node in a graph. It characterises how many shortest paths go through this node relative to the total number of shortest paths in a graph.

network is also assumed. In this set up, the scale-free networks are able to handle traffic up to some critical average load. Below this level the network faces partial congestions that start to build up local bottlenecks and small instabilities might trigger global blackouts with a finite probability. Above the critical load level any small instability leads to complete network collapse.

Other studies adopt similar approaches to study real world networks like power grids. The study, focused on the North American Power Grid [26], assumes the simplified load distribution and illustrates the possibility of blackouts for this particular network. Unlike effects of node and edge removal in the static network, the load-based induced failures display increased rate of fragmentation. Moreover, load-based removal with dynamical recalculation of the load appear to resemble real cascades in the network.

1.5 Thesis outline.

This thesis deals with stability and capacity of distribution networks.

In the first part (**Stability of distribution networks**) of the thesis, the nodes and links are looked at as processes which can fail due to low maintenance levels. Occurrence of failures is determined not only by individual properties of the nodes and links but also by the current state of the network. The failure of a network element happens if the levels of maintenance fall below certain thresholds. As maintenance levels depend on the functioning of network elements, the failure of some elements can lead to a catastrophic breakdown of the network.

In the second part (**Capacity of distribution networks**) of the thesis we look at the load based failures. Occurrence of such failures is related to the physical constraints of the network elements. In a distribution network with relatively low loads such failures are rare. However, in a distribution network with high loads, such failures may lead to global congestion of the system.

Stability of distribution networks. To address a problem of random failures in the distribution network we adopt a statistical mechanical approach. We introduce a spin model of distribution networks. The model is inspired by statistical mechanics

spin models with random long range interactions, and enables us to couple the microscopic description of interactions with graphical models. We test macroscopic properties of distribution networks with respect to various topological structures and distributions of microparameters. Moreover, we investigate the conditions for the development of the global cascades of failures. Monte-Carlo simulations on finite networks are also presented to validate the theoretical analysis.

We analyse network properties in terms of phase diagrams. We identified key phases of the network states as well as dynamic and thermodynamic phase transitions. We observe phase transition for all network structures which we considered (exponential, regular and scale-free random graphs). We confirm the beneficial role of redundancy in networks of all types. However, some qualitative differences have been noticed between homogeneous and heterogeneous structures.

In addition to a phase transition that points out that random failures in distribution networks may trigger large blackouts, we identified a coexistence region. The importance of this phase is the undetectability of a metastable states through the standard set of observables. Also, once in the metastable state the system might experience a large blackout without any external influences, but only driven to a collapse by internal random failures.

Capacity of distribution networks. We introduce **capacity** of the transmission link in a DC current distribution network. The current that goes through a link can not exceed the link's capacity. The distribution of the current at a node is governed by Kirchhoff's law. The objective is to minimise dissipation of the energy in a system. Structurally, we split the whole network into three parts : networks of producers, distributors and receivers.

Again we use a statistical mechanical approach. We study macroscopic properties of distribution networks with respect to various topological structures and distributions of microparameters. We consider two main cases: the **Infinite Capacity (IC)** model and **Finite Capacity (FC)** model[5].

[5]In this case we set maximal capacity of the links.

We analyse distribution network properties in terms of distributions of currents. In the IC model the the key characteristics of the current distributions[6] exhibit linear dependence on the load in the network. In the FC model we additionally consider a fraction of a number of maximal currents in the network, denoted by f_c . This measure reflects the level of congestion in the network.

We identify phases of a system using a FC model: operational and critical. The characterisation of these phases is based on the f_c. We also find only one phase in the IC model. This phase corresponds to the operational phase of the FC model.

Also we are able to identify the subnetworks that develop critical currents first. This could have implications in the analysis of complex networks' stability against overload, as well as provide us with the tools to monitor the spread of load induced failures through the network.

By using IC and FC models we will confirm the beneficial role of redundancy and analyse network properties with respect to system parameters and topological structures.

[6] We look at mean and standard deviation of distributions

2 Stability of distribution networks

CONTENTS

2.1 Introduction

The present chapter is based on the work [51] and is focused on the stability issues of complex networks against random failures. Problems that occur in the financial sector or in the most advanced technological networks like power grids are well documented. While the nature, structure and functionality of such systems is completely different, the global character of the failures observed in both types of systems is common for such large complex networks. The understanding of this phenomenon has attracted researchers from many different fields of science and recent advantages in complex networks analysis encourages applications of new methods and techniques.

This is partly a response to the fact that modern societies are increasingly relying on network based technologies, including mobile and land-line telecommunication, the Internet or, lately, grid computing, but also on traditional transport infrastructure, such as rail or road networks. Much of the interest is also fuelled by the realisation that complex systems in biology [52, 53, 54], chemistry [55], sociology [4], and economy[56, 57] can be analysed using various network related techniques and paradigms [58, 59]. The issues here are to understand the workings of a given complex system in terms of properties of the underlying network, and given some fundamental understanding has been obtained, perhaps go further and characterise the way in which the efficiency of a system would depend on properties of the network.

Network properties of interest include statistical measures characterising structural and topological aspects globally over a network, such as the degree distribution, clustering coefficients, centrality, percolation thresholds, and more, as well as more specific information concerning, e. g. , the presence or absence of certain motifs in (local) connectivity patterns.

Connectivity issues aside, both the nodes and the links in a network may be further characterised by (graded) quality measures. The capacity of a specific directed information channel, the current carrying capacity of a power line, or just a distance between two nodes in a net would constitute examples of graded link properties, whereas the computing power of a server, the capacity of a local water reservoir, the susceptibility of an

individual to infection by a virus (or an opinion, or by the desire to acquire a new gadget) would be examples of properties specifically associated with "nodes".

It goes without saying that functionality as well as efficiency of network based operations will depend to various degrees on the properties of a given network. Points of concern then are robustness or efficiency, and - on a more basic level - of functionality against unexpected failures of links or nodes, or the resilience of network based operations against directed attacks [20, 22, 23, 50]. Clearly these issues have implications in the realm of biological evolution; they would have to influence design decisions in engineering contexts, or political decisions, e. g. when setting up supply infrastructure. On a day-to-day basis, financial institutions are nowadays required to set aside capital to cover financial losses incurred by process failures (operational risk); as processes in organisations would normally be set up in a way to mutually support each other, collective effects creating the possibility of extreme events in large process networks are clearly relevant and need to be properly quantified in order to set aside the right amount of capital. Erring in either direction would be costly (for different reasons) and affect the competitiveness of the organisation in question.

The present investigation is concerned with the issues of resilience of network functionality against random failures or directed attacks in supply infrastructure and distribution networks, such as power grids, various forms of information transfer networks (telephone, Internet), traffic systems (logistics), or metabolic networks, where these issues are particularly relevant [60, 61]. Failures of nodes and/or links can be threaten the basic functionality of the network and if cascading through the system (or affecting hubs of central importance), even lead to a global breakdown. Examples are major blackouts in power grids , massive gridlock in traffic system, or death of an organism.

We shall look at a simplified setting in which the breakdown of a link or node is triggered when the level of maintenance or support it receives falls below a given threshold, leaving the case where failures are induced by loads exceeding critical levels to Chapter 3. The simplified setting renders our model generalisation of previously studied models for operational risk [60, 61] that includes dynamical properties link variables in the analysis.

Next, we introduce our model, describing its coupled link and node dynamics and

interpreting the parameters of the model in terms of unconditional and conditional probabilities for link and node failure. Conditions are identified under which the system can be analysed using thermodynamic equilibrium methods. The statistical mechanics approach to analyse long term properties of the model under these conditions is briefly outlined. Results in terms of a phase diagram characterising the collective behaviour of the system , given its model parameters are presented and discussed. The phase diagram is confirmed qualitatively and quantitatively by simulations on explicit realisations of the graph, thus confirming the validity of our approach. We finish with a summary and an outlook on future lines of research.

2.2 Model.

The distribution network can be thought of as a dynamical structure on a graph. The distribution centres and lines represented by the set of nodes or vertices V and the set of the links or the edges E respectively, defining the graph $G(V,E)$.

We assume that both the centres and the lines can fail. That is the functioning network element might suddenly break due to some internal or external factors. Furtermore, we assume that any failed element might recover becoming functioning again. To model this situation, we associate dynamical variables to each node and each link. The node (i) carries a dynamical variable v_i that can be either 1 or 0. Similarly, with each link (ij) we associate a dynamical variable e_{ij} that can also be either 1 or 0. For both variables the 0 value represents a failed element, while 1 represents a fully functioning network element.

For the network of N nodes the underlying structure is fully defined by the connectivity matrix $\mathbf{c} = \{c_{ij} : i,j = 1,\ldots,N\}$. The undirected graph is then described by a symmetric matrix. The value $c_{ij} = 1$ indicates that there is a connection between nodes (i) and (j), otherwise $c_{ij} = 0$. The average connectivity defined as

$$C = \frac{1}{N}\sum_{(ij)} c_{ij}.^{1} \tag{2.1}$$

[1] The (ij) denotes summation over all pairs of i and j without repetition.

In our analysis we consider network structures with finite average connectivity. First of all, such networks are sparse. Indeed, most of the real systems are sparse, that is any given node is connected to a small fraction of the network. The large number of connections would be, of course, beneficial from the distributional point of view, but the limited nature of available resources limits the maintenance of large numbers of direct links. Secondly, as the network grows, the number of connections increases. However, the increase in the number of connections typically matches (is proportional to) the increase in the number of the nodes. Therefore, for any given node, the number of connections stays the same, finite. In physics, such networks are referred to as sparse networks with finite connectivity. Such networks are dissimilar to networks with dilution. For the diluted case the number of connections per node is growing, but at a slower rate than the network size.

We primarily focus on three types of network structures : regular random graphs (unimodal or bimodal), the exponential random graphs and scale-free networks.

Regular random graphs

We consider finite regular random graphs and specify the degree distribution as follows. We nominate the set of coordination numbers $\{L_i : i = 1, \ldots, N\}$. Then the degree distribution is given by

$$P(L) = \frac{1}{N} \sum_i \delta_{L,L_i}, \tag{2.2}$$

where L - is a degree or connectivity of a node. The average degree can be calculated as

$$C = \sum_L LP(L). \tag{2.3}$$

If C is an integer then all $L_i \equiv C$ and the degree distribution

$$P_C(L) = \delta(L - C). \tag{2.4}$$

If C is not an integer the degree distribution

$$P_C(L) = x\delta(L-[C]) + (1-x)\delta(L-[C]+1), \quad \text{where} \quad x \in [0,1]. \tag{2.5}$$

The $[C]$ gives an integer part of C. In any case the average connectivity of the graph is C.

Exponential random graphs

We consider exponential random graphs which are determined by the following probability distribution

$$P(c) = \prod_{(ij)} \left[\left(1 - \frac{C}{N}\right) \delta_{c_{ij},0} + \frac{C}{N} \delta_{c_{ij},1} \right] \delta_{c_{ij},c_{ji}}, \tag{2.6}$$

i.e. every possible link (ij) is present with probability $\frac{C}{N}$. This typically results in a random graph where the coordination numbers L_i of the nodes are Poisson distributed with parameter C (the average connectivity). The degree distribution is

$$P_C(L) = \frac{C^L}{L!} e^{-C}. \tag{2.7}$$

Scale-free random graphs

For the scale-free graphs the degree distribution follows a power law. We use the following form

$$P_C(L) = sL^{-\gamma(C)}, \quad \gamma(C) > 1 \quad L = m, m+1, \ldots, K, \tag{2.8}$$

where m and K are the smallest and largest possible numbers of connections and s is a normalisation constant. In a finite network of order N, the largest connectivity K can be estimated from

$$\int_K^\infty P(L)\mathrm{d}L = \frac{1}{N}, \tag{2.9}$$

resulting in

$$K \approx mN^{\frac{1}{\gamma(C)-1}}. \tag{2.10}$$

The parameter γ for real networks is in the range $1-5$ and the smallest connectivity m is usually 1 or 2.

The main statistical characteristic of the networks is their degree distribution, denoted as $P_C(L)$. Although the degree distribution does not fully describe the network structure (one should take a closer look at correlations in the network), it is sufficient in the present model. [2]

2.2.1 Dynamics

A dynamical evolution of the node and link variables on the graph can be described and motivated by analogy with previous operational risk modelling [60] as follows. The node support is defined as

$$h_i = \sum_{j(\neq i)} c_{ij} e_{ij} (a_{ij} v_j + b_{ij}) + \mu_i, \tag{2.11}$$

and a link support as

$$h_{ij} = \tilde{a}_{ij} v_i v_j + \tilde{b}_{ij} (v_i + v_j) + d_{ij}. \tag{2.12}$$

In these expressions, the parameter a_{ij} would quantify the contribution of node j to the support of i, while b_{ij} could describe external support to i that is funnelled through the link (ij), while μ_i would describe a baseline support independent of the dynamical state of the system itself.

Similarly, $\tilde{a}_{ij}$ would describe a contribution to the maintenance of link (ij) that originates from a collaboration of the nodes connected by it, while $\tilde{b}_{ij}$ would quantify separate contributions from adjacent functioning nodes which would exist without collaboration, and d_{ij} would again characterise a baseline support independent of the dynamical state of the system.

[2] explained in section 2.3.5, Calculation of observable properties.

We propose a probabilistic asynchronous dynamics which stipulates that vertices and nodes fail, if they receive less than a critical threshold support. Without loss of generality the thresholds can be taken to be zero by appropriate definition of baseline support levels. Thus, in formal terms we have

$$v_i(t+\Delta t) = \Theta(h_i(t)+\xi_i(t)), \tag{2.13}$$

$$e_{ij}(t+\Delta t) = \Theta(h_{ij}(t)+\xi_{ij}(t)) \tag{2.14}$$

where $\Theta(x)$ function defined as

$$\Theta(x) = \begin{cases} 1, & x \geq 0, \\ 0, & x < 0. \end{cases}$$

and the node and edge noises $\xi_i(t)$ and $\xi_{ij}(t)$ are taken to be independent and white, and either zero mean Gaussians with variances σ and $\tilde{\sigma}$, respectively:

$$\langle \xi_i(t)\xi_j(t')\rangle = \sigma^2\delta_{ij}\delta_{t,t'}, \tag{2.15}$$

$$\langle \xi_{ij}(t)\xi_{kl}(t')\rangle = \hat{\sigma}^2\delta_{(ij),(kl)}\delta_{t,t'}, \tag{2.16}$$

or thermal noises with probability density functions:

$$p(\xi_i) = \frac{1}{2}\frac{\mathrm{d}}{\mathrm{d}\xi_i}\tanh\left(\frac{\beta\xi_i}{2}\right), \tag{2.17}$$

$$p(\xi_{ij}) = \frac{1}{2}\frac{\mathrm{d}}{\mathrm{d}\xi_{ij}}\tanh\left(\frac{\hat{\beta}\xi_{ij}}{2}\right). \tag{2.18}$$

By the integrating over the noises in equations (2.13)-(2.14) one obtains,

$$P(v_i(t+\Delta t)=1) = \langle v_i(t+\Delta t)\rangle = \phi\left(\frac{h_i(t)}{\sigma}\right), \tag{2.19}$$

$$P(e_{ij}(t+\Delta t)=1) = \langle e_{ij}(t+\Delta t)\rangle = \phi\left(\frac{h_{ij}(t)}{\tilde{\sigma}}\right), \tag{2.20}$$

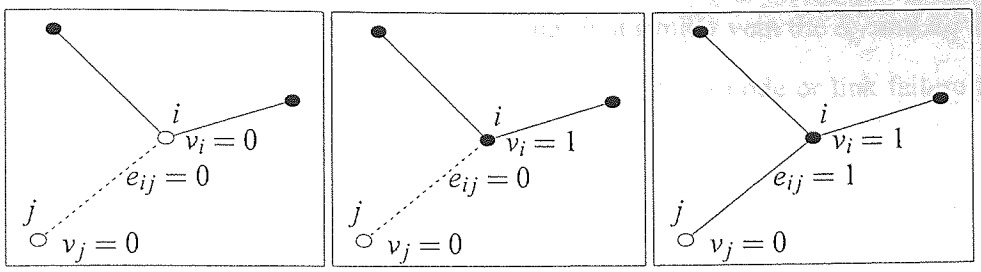

Figure 2.1: Evolution of node and link variables. Filled circles and full lines represent operational nodes and links respectively. Correspondingly, the empty circles and dashed lines represent non-operational nodes and links. Transition from the first slide to the second: dynamics of the node variable. In the first slide, the central node is non-operational, assuming support of two operational nodes is greater than support of the bottom node, the central node changes its state. Transition from the second to the third slide: dynamics of the link variables. Now the only non-operational link is supported by bottom (non-operational node) and central (operational node). Providing, support of the central node is greater than support of the bottom node, the link becomes operational.

in the case of Gaussian noises, with $\phi(x)$ denoting the integrated unit-variance normal density, while the corresponding result for the thermal noise model would be

$$P(v_i(t+\Delta t)=1) = \langle v_i(t+\Delta t)\rangle = \phi_\beta\left(h_i(t)\right), \tag{2.21}$$

$$P(e_{ij}(t+\Delta t)=1) = \langle e_{ij}(t+\Delta t)\rangle = \phi_\beta\left(h_{ij}(t)\right), \tag{2.22}$$

with

$$\phi_\beta(x) = \frac{1}{2}\left[1+\tanh\left(\frac{\beta x}{2}\right)\right]. \tag{2.23}$$

The collective properties of the system do not crucially depend on which noise model is chosen as long as the levels are properly matched. Therefore in what follows we work with the thermal noise model for which standard statistical mechanics methods work best.

Note that the current formulation of the dynamics is in terms of resources or the lack of them as responsible for the functioning or the failure of nodes and links. In particular, one would sensibly expect the parameters a_{ij} and $\tilde{a}_{ij}$ as well as the b_{ij} and $\tilde{b}_{ij}$ to be positive within this interpretation. The case where failure of links or nodes is triggered by load levels exceeding certain critical values is left to Chapter 3.

The parameters d_{ij} and μ_i are related to the a priori probability that the isolated link

(ij) or the isolated node i, respectively, are up. In a similar vein the a_{ij} and $\tilde{a}_{ij}$ as well as the b_{ij} and $\tilde{b}_{ij}$ can be related to conditional probability of node or link failure for given configurations of node and link-states.

In the present investigation we will restrict our attention to a case in which the model parameters satisfy a number of symmetry relations, which ensure that the long time behaviour of the system can be described by thermodynamic equilibrium theory. These are

$$\forall_{ij}: \quad a_{ij} = \tilde{a}_{ij}, \quad b_{ij} = \tilde{b}_{ij}, \tag{2.24}$$

and

$$\forall_{i<j}: \quad a_{ij} = a_{ji}, \quad b_{ij} = b_{ji}, \tag{2.25}$$

as well as $a_{ii} = 0$ and $b_{ii} = 0$ and equality of noises of the link and node dynamics,

$$\beta = \tilde{\beta}. \tag{2.26}$$

These conditions together are sufficient to ensure that the stochastic dynamics (2.21) and (2.22) satisfies detailed balance with respect to the Gibbs-Boltzmann equilibrium distribution at inverse temperature β that is generated by the energy function

$$H = -\sum_{(ij)} c_{ij} e_{ij} \left[a_{ij} v_i v_j + b_{ij}(v_i + v_j) + d_{ij} \right] - \sum_i \mu_i v_i. \tag{2.27}$$

This feature allows one to study the collective behaviour of the distribution networks by the methods of equilibrium statistical mechanics, which greatly simplifies the analysis, and will be the main focus of the remainder of this Chapter. For the details of the detailed balance see (B.1).

Clearly a full dynamical study is required whenever any of the symmetry assumptions is violated. However, it is well known that thermodynamic equilibrium theory often gives a fair qualitative description, provided the violations are not too drastic.

2.3 Theoretical analysis.

2.3.1 Replica method.

For the analysis of the model described in the previous section, we use the replica method for sparsely connected systems [44, 62, 63, 64]. In contrast to the previous models studied with this method, we have a new ingredient that not only the nodes but also the links have dynamical variables, though we shall find that this introduces only minor complications in the analysis. The general strategy is to calculate the free energy of the model, from which all relevant thermodynamic quantities can be derived. The free energy is expected to be self-averaging, entailing that, in the large system limit and under very general conditions on the disorder distribution in the model (i. e. $\mathbf{c}, a_{ij}, b_{ij}, d_{ij}$ and μ_i), the average of the free energy over all disorder configurations coincides with its typical value: the free energy on any explicit realization of the problem drawn from this ensemble will be equal to the average with probability approaching 1 in the large N limit.

Given the Hamiltonian (2.27), the disorder dependent partition function Z and the free energy F are obtained from :

$$\begin{aligned} Z(\mathbf{c},\{a,b,d,\mu\}) &= \operatorname*{Tr}_{v}\operatorname*{Tr}'_{e}\exp(-\beta H), \\ F(\mathbf{c},\{a,b,d,\mu\}) &= -\ln(Z(\mathbf{c},\{a,b,d,\mu\})), \end{aligned}$$

where Tr' denotes a trace over those e_{ij} for which $c_{ij} = 1$.

In order to average the free energy over the disorder, we use the replica method,

$$\langle \ln Z \rangle_{D,c_{ij}} = \lim_{n\to 0} \frac{1}{n} \ln \langle Z^n \rangle_{D,c_{ij}},$$

so that we have to calculate the average of the replicated partition function $\langle Z^n \rangle_{D,c_{ij}}$ as follows:

$$\langle Z^n\rangle_{D,c_{ij}} = \left\langle \operatorname*{Tr}_{\{\nu^\alpha\}} \operatorname*{Tr}'_{\{e^\alpha\}} \exp\left[\beta\sum_\alpha\left(\sum_{(ij)} c_{ij}e_{ij}^\alpha[a_{ij}\nu_i^\alpha\nu_j^\alpha + b_{ij}(\nu_i^\alpha+\nu_j^\alpha)+d_{ij}] + \sum_i \mu_i\nu_i^\alpha\right)\right]\right\rangle_{D,c_{ij}} . \tag{2.28}$$

Here $\langle\rangle_D$ indicates the average over the disorder. At this point we do not yet need to specify the disorder distribution for the $\{a_{ij}, b_{ij}, d_{ij}, \mu_i\}$. We start by performing the average over the connectivity matrix $\mathbf{c}$ and the trace over the link variables $\{e^\alpha\}$, which can be easily done as the replicated partition sum factorises over these variables. This is a well-known fact, which has been extensively used in the study of Ising models with annealed bond disorder [65].

2.3.2 Order pararmeters, Conjugate variables

Details of the following steps can be found in (B.2). We introduce the order parameter

$$\rho(\tilde{\nu}) \equiv \frac{1}{N}\sum_{i=1}^N \delta_{\tilde{\nu},\tilde{\nu}_i}, \quad \tilde{\nu}\equiv\{\nu^\alpha : \alpha = 1,\ldots,n\}, \tag{2.29}$$

and its conjugate $\hat{\rho}(\tilde{\nu})$ to enforce the definition of the order parameter. Then, the expression for the replicated partition function becomes

$$\langle Z^n\rangle_D = \int \mathrm{d}\rho(\tilde{\nu})\mathrm{d}\hat{\rho}(\tilde{\nu}) \exp\left[N\left\{\frac{C}{2}G_l[\rho] - G_m[\rho,\hat{\rho}] + G_s[\hat{\rho}]\right\}\right]. \tag{2.30}$$

The functionals appearing in (2.30) are given by

$$\begin{aligned} G_l &= \operatorname*{Tr}_{\tilde{\nu}}\left[\rho(\tilde{\nu})\operatorname*{Tr}_{\tilde{w}}\left[\rho(\tilde{w})\left\langle\prod_\alpha\left(1+e^{\beta[a\nu^\alpha w^\alpha + b(\nu^\alpha+w^\alpha)]+d}\right)\right\rangle_{a,b,d}\right]\right] - 1, \\ G_m &= \operatorname*{Tr}_{\tilde{\nu}}[\rho(\tilde{\nu})\hat{\rho}(\tilde{\nu})], \\ G_s &= \ln\left\langle \operatorname*{Tr}_{\tilde{\nu}} e^{\beta[\mu|\tilde{\nu}|+\hat{\rho}(\tilde{\nu})]}\right\rangle_\mu , \end{aligned} \tag{2.31}$$

where we have used the shorthand $|\tilde{\nu}| \equiv \sum_\alpha \nu^\alpha$. For the details of calculations see B.3

2.3.3 Replica symmetry assumptions

For the analytic continuation $n \to 0$ we need to make an ansatz about the symmetry between the replicas, and assume replica symmetry (RS). The simplest form of RS ansatz is :

$$\rho(\tilde{v}) = \int_0^\infty d\pi(x) \frac{x^{|\tilde{v}|}}{(1+x)^n}, \tag{2.32}$$

$$\hat{\rho}(\tilde{v}) = \lambda_0 \int_0^\infty d\hat{\pi}(x) \frac{\hat{x}^{|\tilde{v}|}}{(1+\hat{x})^n}, \tag{2.33}$$

where $\pi(x)$ and $\hat{\pi}(x)$ are probability functions over non-negative variable x.

Further introducing

$$C_0 = 1 + e^{\beta d}, \quad C_1 = 1 + e^{\beta(b+d)}, \tag{2.34}$$

$$C_2 = 1 + e^{\beta(a+2b+d)}, \quad \{x_l\}_L = \prod_{l=1}^{L} x_l, \tag{2.35}$$

and following standard reasoning, we arrive at the typical RS free energy per node

$$F = -\frac{1}{\beta}\left(\frac{C}{2} G_l[\pi] - C G_m[\pi, \hat{\pi}] + G_s[\hat{\pi}]\right), \tag{2.36}$$

where

$$\begin{aligned} G_l &= \int_0^\infty d\pi(x_1) d\pi(x_2) \left\langle \ln\left[C_0 + C_1(x_1 + x_2) + C_2 x_1 x_2\right]\right\rangle_{a,b,d}, \\ G_m &= \int_0^\infty d\pi(x) d\hat{\pi}(\hat{x}) \ln\left[1 + x\hat{x}\right], \\ G_s &= \sum_L P_C(L) \int_0^\infty \{d\hat{\pi}(\hat{x}_l)\}_L \left\langle \ln\left[1 + e^{\beta\mu}\{\hat{x}\}_L\right]\right\rangle_\mu. \end{aligned} \tag{2.37}$$

2.3.4 Saddle point equations

It is understood that equation (2.36) has to be evaluated in the saddle point with respect to π and $\hat{\pi}$. This implies that π and $\hat{\pi}$ have to satisfy the self-consistency equations

$$\pi(x) = \sum_L \frac{LP_C(L)}{C} \int_0^\infty \{d\hat{\pi}(\hat{x}_l)\}_{L-1} \langle \delta(x - e^{\beta\mu}\{\hat{x}_l\}_{L-1}) \rangle_\mu, \tag{2.38}$$

$$\hat{\pi}(\hat{x}) = \int_0^\infty d\pi(x) \left\langle \delta\left(\hat{x} - \frac{C_1 + C_2 x}{C_0 + C_1 x}\right) \right\rangle_{a,b,d} \tag{2.39}$$

2.3.5 Calculation of observable properties

From the free energy, one can obtain physically relevant quantities (see B.4), such as the fraction m_n of working nodes

$$m_n = \sum_L P_C(L) \int_0^\infty \{d\hat{\pi}(\hat{x}_l)\}_L \left\langle \frac{e^{\beta\mu}\{\hat{x}_l\}_L}{1 + e^{\beta\mu}\{\hat{x}_l\}_L} \right\rangle_\mu, \tag{2.40}$$

the fraction of working links,

$$m_e = \int_0^\infty d\pi(x_1) d\pi(x_2) \left\langle \frac{M_0 + M_1(x_1 + x_2) + M_2 x_1 x_2}{C_0 + C_1(x_1 + x_2) + C_2 x_1 x_2} \right\rangle_{a,b,d}, \tag{2.41}$$

in which $M_i = C_i - 1$, and the internal energy,

$$\begin{aligned} U &= -\frac{C}{2} \int_0^\infty d\pi(x_1) d\pi(x_2) \left\langle \frac{E_0 + E_1(x_1 + x_2) + E_2 x_1 x_2}{C_0 + C_1(x_1 + x_2) + C_2 x_1 x_2} \right\rangle_{a,b,d} \\ &\quad - \sum_L P_C(L) \int_0^\infty \{d\hat{\pi}(\hat{x}_l)\}_L \left\langle \frac{\mu e^{\beta\mu}\{\hat{x}_l\}_L}{1 + e^{\beta\mu}\{\hat{x}_l\}_L} \right\rangle_\mu, \end{aligned}$$

with $E_0 = de^{\beta d}$, $E_1 = (b+d)e^{\beta(b+d)}$ and $E_2 = (a+2b+d)e^{\beta(a+2b+d)}$.

One should note that the inverse temperature β can be absorbed into the parameters a, b, d, μ and is only used to derive some of the physical quantities. In what follows, we implicitly assume that $\beta = 1$.

At this point one should also note that although the links are dynamical variables, it was not necessary to introduce a separate order parameter to describe the link distribution. It turns out that in any such model the trace over the link variable (irrespective of the type

of variable) can be carried out directly as the partition function can be written in a form that factorises over the links.

It should be noted that the saddle-point equations (2.39) can only be solved numerically using, e. g. a population dynamics algorithm[66]. The analysis of these equations, and the implications that different types of solution have concerning the possible occurrence of sudden global system failures are presented in the next section.

2.4 Results

We solve equations (2.39) numerically for fixed $\beta = 1$ and various connectivities C and distributions of a, b, d and μ, using a population dynamics algorithm. The size of populations in population dynamics is 10000.

After extensive numerical experiments we have obtained the full (at least five-dimensional) phase diagram, and we find that the parameter space can be qualitatively divided into four distinctive regions:

- (O) the operational state ($m_n \backsimeq 1$) is the only stable solution,
- (N) the non-operational state ($m_n \backsimeq 0$) is the only stable solution,
- (CO) the coexistence of the stable operational state with a metastable non-operational state,
- (CN) the coexistence of the stable non-operational state with a metastable operational state.

We have not found any region where more than two locally stable phases coexist. The boundaries between the single-solution and multiple-solution regions are spinodal surfaces (associated with dynamical transitions).

As plots of phase diagrams in more than two dimensions are not easy two interpret quantitatively, we have restricted ourselves to presenting two-dimensional plots in the (a, μ) plane (see figures (2.4.2)-(2.13)), for several combinations of the other parameters,

thus indicating the major trends and characteristics of the full phase diagram. In all plots, the numerical precision is of the order of the line widths.

We refer to the boundary between the (O) and (CO) regions as the upper spinodal, and the boundary between the (N) and (CN) regions as the lower spinodal. The upper spinodal demarcates the locations in parameter space where the non-operational (N) phase ceases to exist as a metastable phase, while the lower spinodal gives the locations where the operational (O) phase becomes unstable. The boundary between the (CO) and (CN) regions is given by the surface in parameter space where the free energies of the two solutions coincide, i. e. they mark the thermodynamic equilibrium transition.

The two spinodals and the thermodynamic transition may meet (end) in lines (more precisely, lower dimensional surfaces) of critical points (analogous to critical points of liquid-gas systems), so that it is always possible to go from the (O) region to the (N) region continuously, following some path through the phase diagram that avoids any transitions.

Except when explicitly mentioned, all plots shown have been made for constant parameters $\forall x_{ij} = x$, with $x = \{a, b, d, \mu\}$. We have also solved the model with varying parameters, e.g. $x_{ij} \sim N(\langle x \rangle, \sigma)$. The general tendency is that an increase in the variance σ leads to a reduction of the (CO) and (CN) regions (pulling the spinodals closer to the transition), while the thermodynamic transition remains virtually unchanged. This implies that an increase in the variability of the resources reduces the region where the working system is locally stable, thus increasing the likelihood of sudden system failures.

Since both m_n and m_e depend on the same distributions π and $\hat{\pi}$, either observable can be used to monitor the dynamical transitions. In general, any discontinuity in m_n corresponds to a discontinuity in the same direction in m_e, although the amplitude of the discontinuity depends on the relative strength of various parameters (see figures (2.2)-(2.4)).

2.4.1 Coexistence regions

The (CO) and (CN) regions are of particular interest with respect to the possible occurrence of sudden global system failures. Starting from the a state where the working system

is globally stable, one may , by gradually increasing the average load or by gradually reducing the available resources , push the system over the thermodynamic transition into a region where the operational (O) phase no longer corresponds to the global minimum of the free energy, without realising it, as there are no detectable signatures of such a (first order) equilibrium transition.

If the system is pushed further in this direction, it will certainly collapse once the spinodal is reached. However, as long as the system is still relatively close to the equilibrium transition point, it may continue to operate for a very long time until a rare unfavourable fluctuation tips it over the edge, and a global collapse takes place. Both the system size and the distance from spinodal will determine the likelihood that rare unfavourable fluctuations actually manage to destabilise the system. The time before the collapse occurs, fluctuates wildly, hence it is impossible to accurately predict the timing of global system failures.

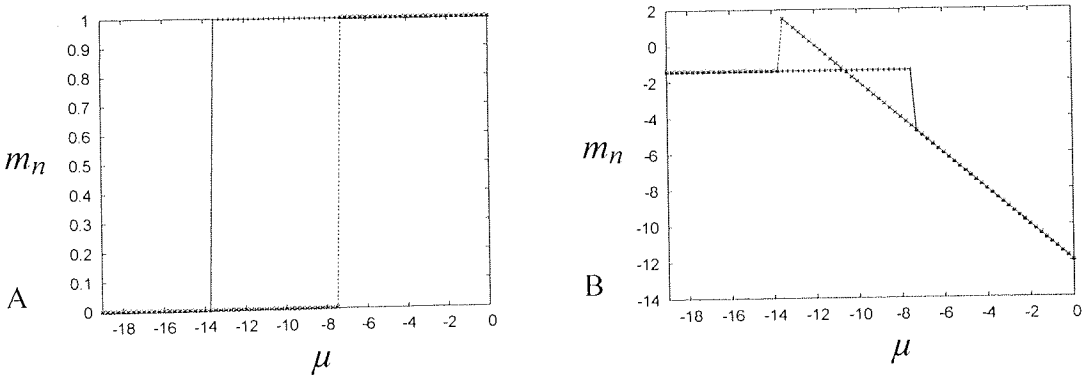

Figure 2.2: Population dynamics on regular random graph case. (A) Hysteresis of m_n as a function of μ with parameters C=4, $\langle a \rangle$= 6. The symbols '+' indicate that we started from the (O) solution, while 'x' indicate that we started from the (N) solution. (B) The free energy profile across transition.

.

2.4.2 Monte-Carlo simulations

In order to confirm the validity of our analytical solution, we have also performed Monte Carlo simulations of the model using a variant where node and link variable are pooled and random sequentially updated according to the Metropolis algorithm. The order of the

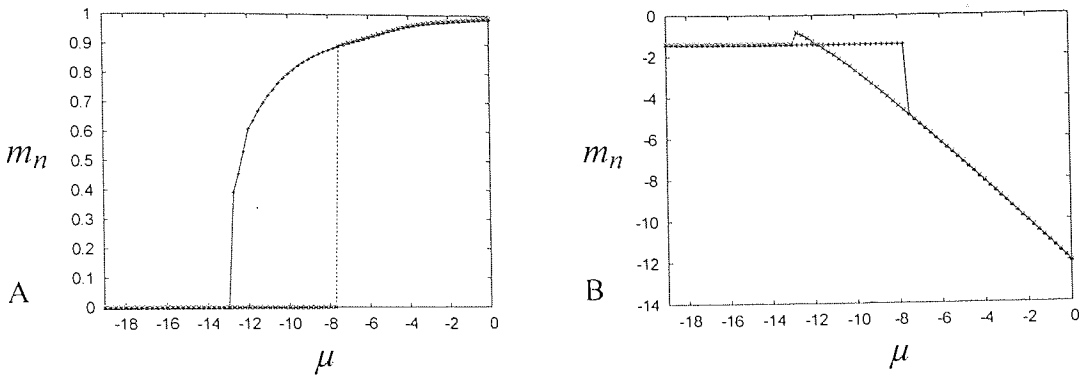

Figure 2.3: Population dynamics on exponential random graph. (A) Hysteresis of m_n as a function of μ with parameters C=4, $\langle a \rangle$= 6. The symbols '+' indicate that we started from the (O) solution, while 'x' indicate that we started from the (N) solution. (B) The free energy profile across transition.

.

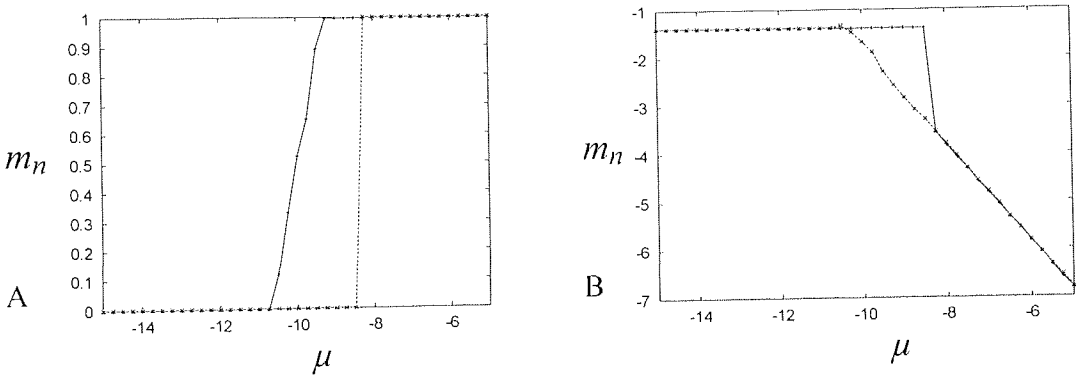

Figure 2.4: Population dynamics on scale-free random graph. (A) Hysteresis of m_n as a function of μ with parameters C=3.8, $\langle a \rangle$= 6, $m1$ = 2. The symbols 'x' indicate that we started from the (O) solution, while '+' indicate that we started from the (N) solution. (B) The free energy profile across transition.

.

graphs is 100 and the measurements are taken by averaging over 1000 graph realizations. In general, our simulation results for spinodals coincide with the theoretical predictions obtained by population dynamics.

The difference between the theoretical predictions and the Monte Carlo simulations can be attributed to a small sizes of systems in Monte Carlo simulations. Only relatively small systems can be simulated and analysed. We present one-dimensional phase diagrams to illustrate agreement between population dynamics and Monte Carlo simulations, see figure (2.4.2).

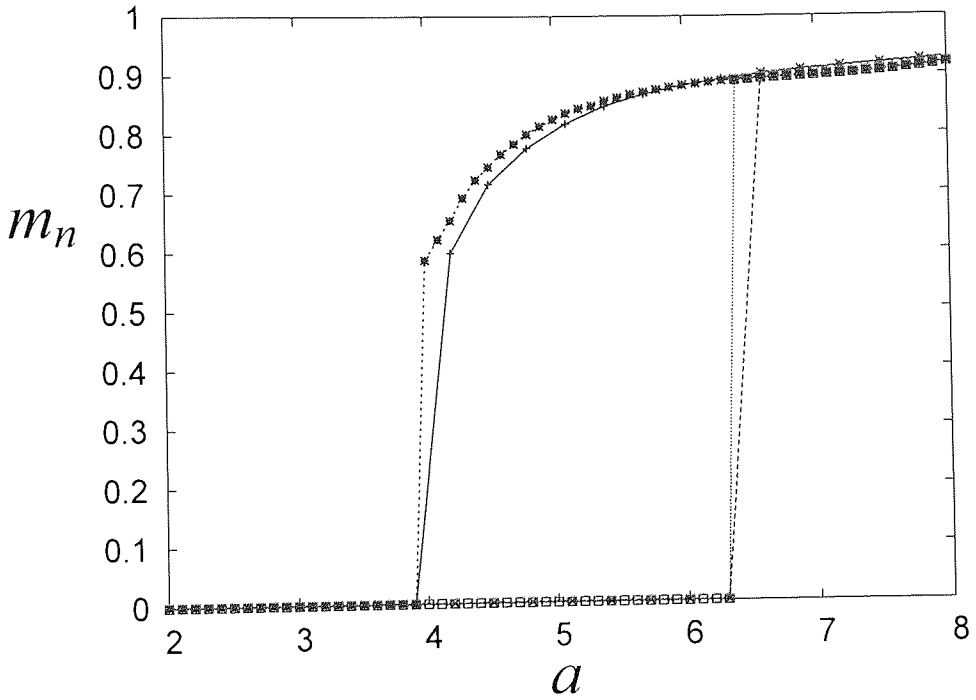

Figure 2.5: Fraction of working nodes (m_n) : population dynamics and Monte Carlo simulation on exponential random graphs. Results of population dynamics are depicted by '+' and 'x' lines, while results of Monte Carlo simulations are depicted by square and star lines. The size of the system in Monte Carlo simulations is 100, the fraction of working nodes (m_n) computed by averaging over 1000 realizations of the exponential graphs. The size of population in population dynamics is 10000. In both cases we have $\mu = -8$, $b = 0$, $d = 0$. While the general agreement between two experiments is good, the differences are more pronounced around dynamic transitions and could be explained by the small sizes of the graphs in Monte Carlo simulations.

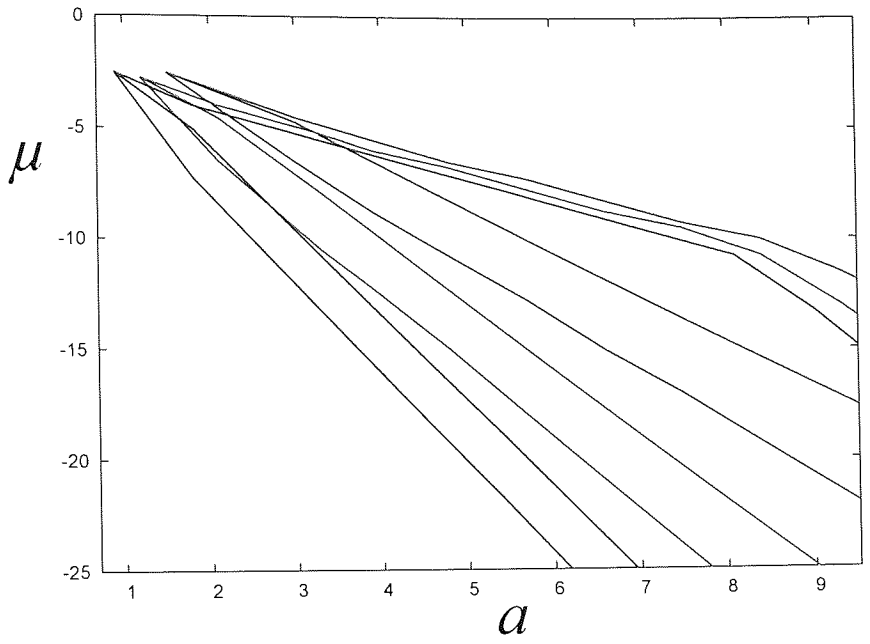

Figure 2.6: Population dynamics : phase diagram for regular random graphs, various connectivities. A section of phase diagram for regular random graph in the (a, μ) plane with b=0, d=0 for three different average connectivities: C=4 (red lines), C=6 (green lines) and C=8 (blue lines).

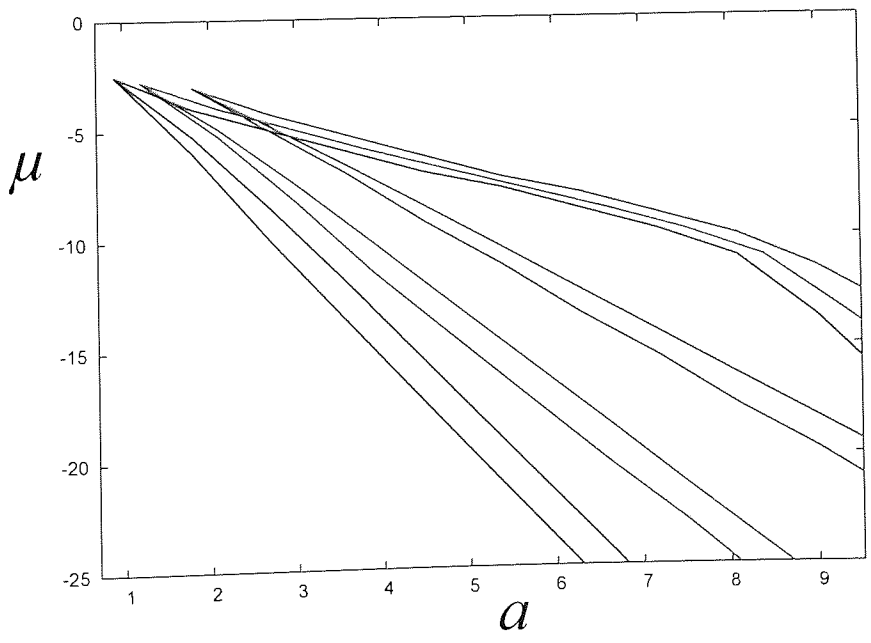

Figure 2.7: Population dynamics : phase diagram for regular random graphs, various connectivities. A section of phase diagram for exponential random graph in the (a, μ) plane with b=0, d=0 for three different average connectivities: C=4 (red lines), C=6 (green lines) and C=8 (blue lines).

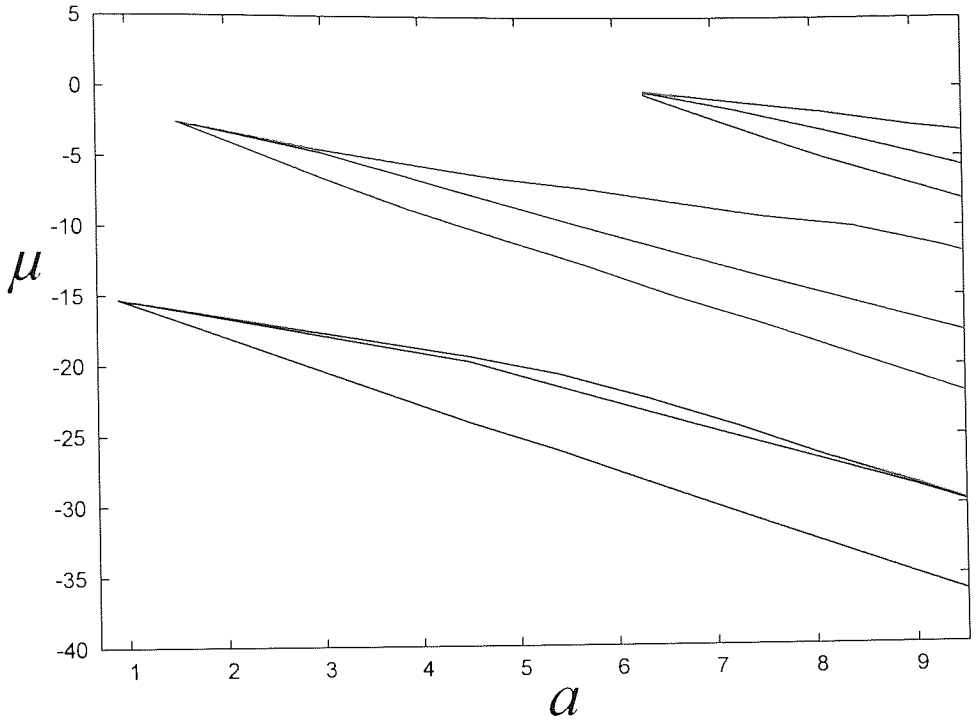

Figure 2.8: Population dynamics : phase diagram for regular random graphs, dependence on parameter b. A section of phase diagram for regular random graph in the (a, μ) plane with C=4, d=0 for three different values of parameter B: b=3 (red lines), b=0 (green lines) and b=-3 (blue lines).

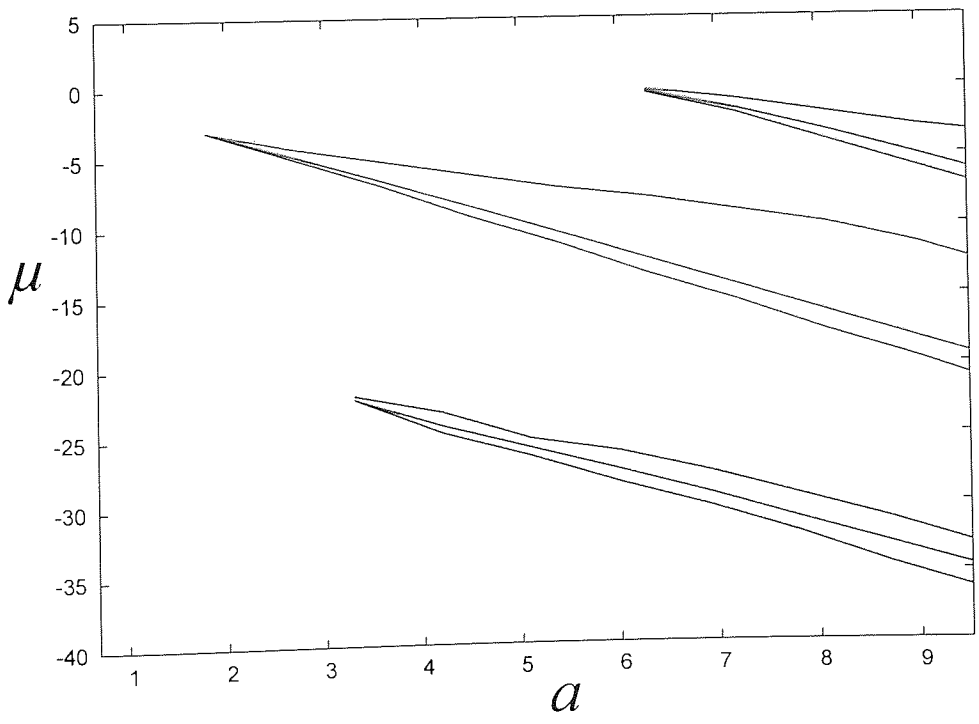

Figure 2.9: Population dynamics : phase diagram for exponential random graphs, dependence on parameter b. A section of phase diagram for regular random graph in the (a, μ) plane with C=4, d=0 for three different values of parameter B: b=3 (red lines), b=0 (green lines) and b=-3 (blue lines).

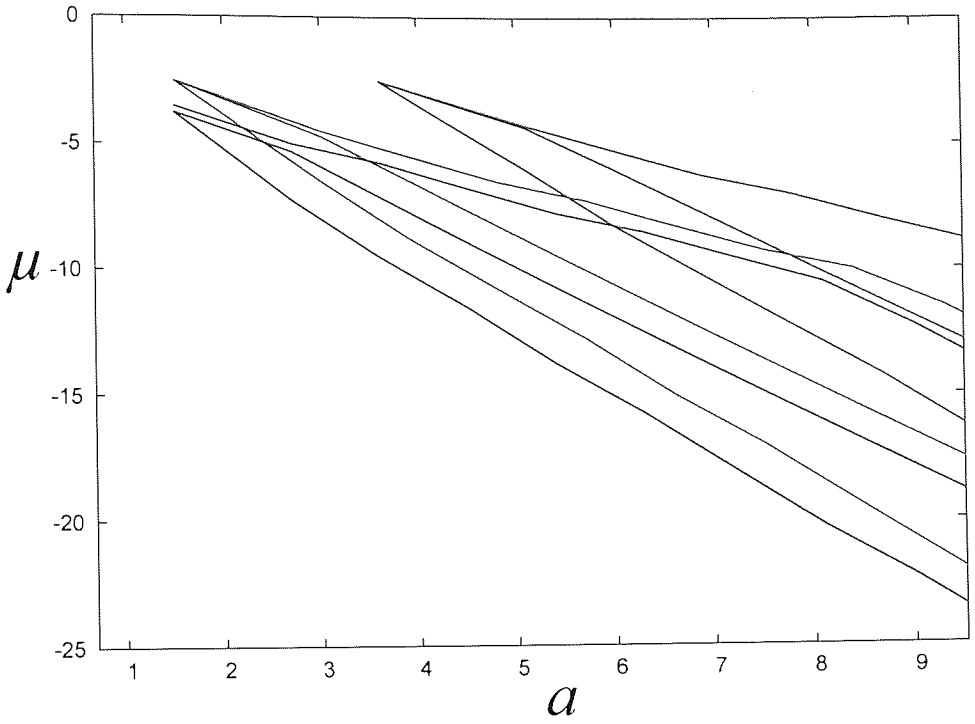

Figure 2.10: Population dynamics : phase diagram for regular random graphs, dependence on parameter d. A section of phase diagram for regular random graph in the (a, μ) plane with d=0, C=4 for three different values of parameter d: d=3 (red lines), d=0 (green lines) and d=-3 (blue lines).

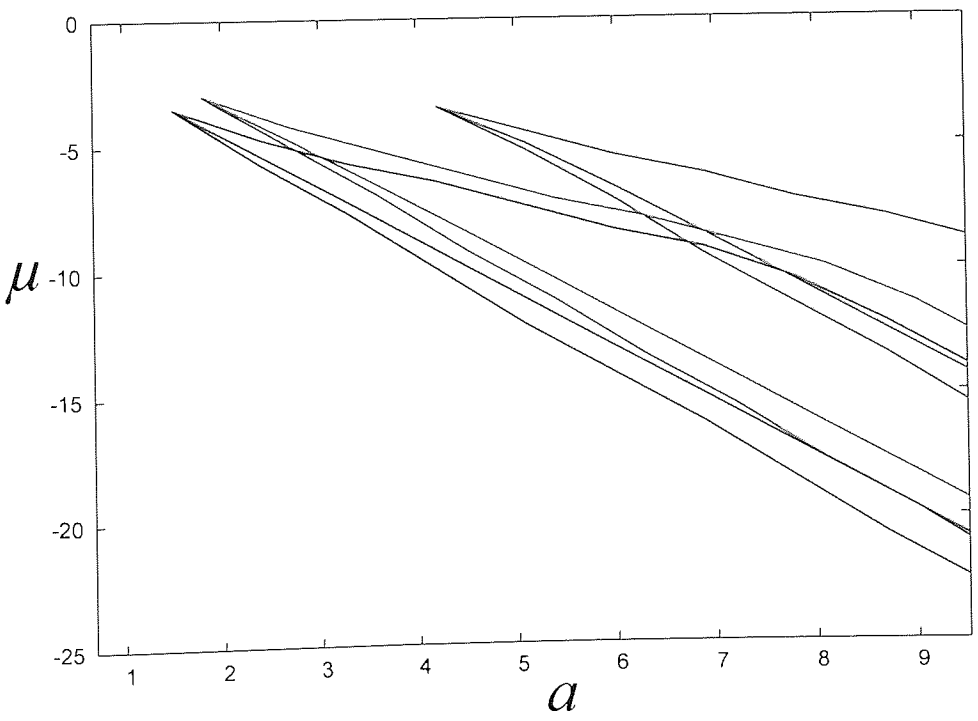

Figure 2.11: Population dynamics : phase diagram for exponential random graphs, dependence on parameter d. A section of phase diagram in the (a, μ) plane with b=0, C=4 for three different values of parameter d: d=3 (red lines), d=0 (green lines) and d=-3 (blue lines).

2.4.3 Scale-free random graphs

We also applied our model to study the stability of distribution networks on scale-free random graphs. General results on stability of scale-free networks suggest that random failures (based on the node removal [20]) have dramatically different impact compared to homogeneous graphs (regular or exponential random graphs). Indeed, finite scale-free networks disintegrate at higher fraction of the randomly removed nodes than exponential random graphs of similar order and size. While any finite scale-free system appears to have a percolation threshold, analytical calculations indicate that it is caused by finite size effects, and for the large scale-free networks the fraction of nodes to be removed to cause disintegration approaches 1 with the size of the network. In other words, scale-free networks display remarkable robustness against random failures.

However, in the current model we consider dynamical effects of node and link failures. Failed nodes and links are thought to have an effect on the neighbours that may not have sufficient resources to function due to loss of support from failed component. Such effects of random failures are believed to lead to cascading failures , affecting a large fraction of the network. The work by Watts [13] focuses on development of cascading failures in networks. The model he used for investigation assumes dynamical effects of random node failures (but not links). The main findings of the study confirms higher degree of robustness of scale-free networks compared to exponential random graphs.

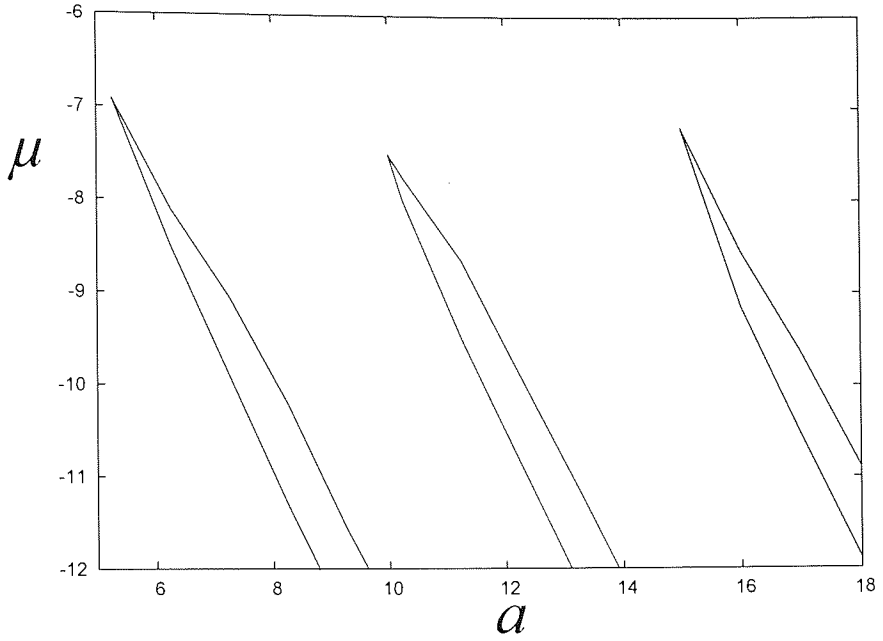

Figure 2.12: Population dynamics: phase diagrams for scale-free random graphs, dependence on the parameter d. A section of phase diagram for scale-free graph in the (a, μ) plane with C=4, b=0 for three different values of parameter d: d=0(red lines), d=-5(green lines) and d=-10(blue lines). For each, the top line is the upper spinodal [marking the boundary between the(CO) and the(O) region], the middle line is the equilibrium transition, and the bottom line is the lower spinodal [marking the boundary between the (CN) and the (N) region].

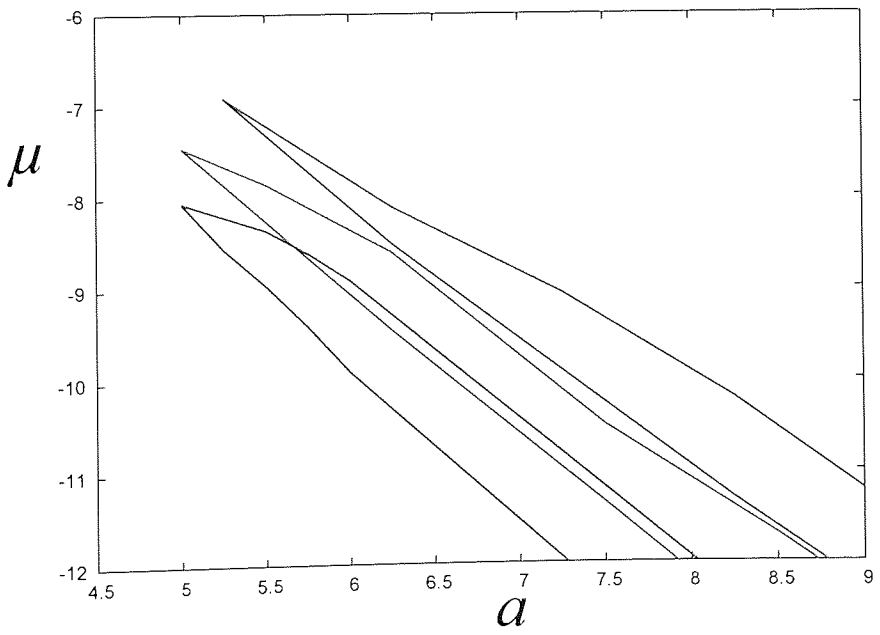

Figure 2.13: Population dynamics: phase diagrams for scale-free random graphs, various connectivities. A section of phase diagram in the (a, μ) plane with b=-1, d=5 for three different connectivities C: C=4 (red lines), C=6 (green lines) and C=8 (blue lines). For each, the top line is the upper spinodal , the middle line is the equilibrium transition, and the bottom line is the lower spinodal.

2.5 Conclusions

We have investigated the performance of distribution networks realised as sets of nodes interacting via dynamical links arranged on a random graph. We have formulated the coupled node and link dynamics in such a way that breakdown of a link or node is caused when a level of support it receives falls below a given threshold. We have identified conditions under which the collective behaviour of such systems can be analysed using equilibrium statistical mechanics, and we perform such an analysis using replica and mean-field techniques for finitely connected random systems.

The model generalises previous models of operational risk, in which link-dynamics is included as an essential new ingredient. Formally the conventional operational risk situation can be recovered by considering a limit in which the links are infinitely resilient against failure, thereby freezing out the dynamics of links.

A phase diagram characterising the global behaviour of the system and its dependence on the system parameters has been obtained , which confirms and quantifies intuitions one would have about such systems. In the region of parameter space of interest for an interpretation as distribution networks the system can be in one of two possible phases, an operational phase (O) where most nodes and links are up and running, and a non-operational phase (N) where most nodes and links are down. In certain regions of the parameter space, both phases can coexist. Theses are further divided into subregions where either the operational phase (CO) or the non-operational phase (CN) are the absolutely stable ones. These subregions are separated by the thermodynamic first order equilibrium transition. Coexistence regions are bounded by spinodal surfaces, which mark locations in parameter space where the metastable phases become unstable (and therefore cease to exist). We find that spinodals can meet in lower-dimensional surfaces of critical second-order transitions.

One observes the following main trends. By increasing average connectivity C, or by increasing the resilience of links against spontaneous failure (parameterised by $\langle d \rangle$), or to a lesser extent by increasing the resilience of nodes against spontaneous failure (parameterised by $\langle \mu \rangle$) the coexistence region is moved to lower values of the parameter

$\langle a \rangle$, which quantifies the individual contribution to node support as well as the cooperative link support. These trends are clearly in line with intuition one would have about systems of this type , concerning the beneficial roles of redundancy of resources or the reliability of nodes and links. There is a concurrent increase of the width of the coexistence region in the $\langle a \rangle - \langle \mu \rangle$ plane, though throughout most of the coexistence region the operational (O) phase appears to be the stable phase (the non-operational phase is the metastable one).

From the point of view of assessing the risk of failure of the net, the coexistence regions are clearly the most important regions in parameter space. In these regions, an all operational state of the system coexists with a non-operational state. Parameter changes, which drive the system into the coexistence region, would not be detectable in the collective behaviour of the system and, as already noted, the same is true, in particular, also for parameter changes that exchange the relative stabilities of the operational (O) and non-operational (N) phase. As a consequence, parameter changes that would result in making catastrophic breakdown of the system an event that is eventually bound to occur under normal operating conditions would go unnoticed.

In the present investigation we have restricted ourselves to situations in which the system parameters satisfy a set of symmetry relations, allowing us to use equilibrium methods to analyse collective behaviour. Nevertheless, proper dynamics techniques and /or numerical simulations would be required to study this issue in greater detail for the present model.

A more important point concerns the mechanisms triggering failures of nodes or links. In many distribution networks the dominant mechanism is related to traffic along certain links or through certain nodes exceeding critical values, which triggers the failure of a given element, and rerouting traffic appears as a crucial ingredient responsible for cascading failures in the system. This aspect is not covered in the present investigation, but is clearly of great importance.

3 Capacity of distribution networks

CONTENTS

3.1 Introduction

In the present chapter we focus on stability of complex networks, and, in particular, on stability associated with failures induced by loads exceeding critical levels of capacity of network elements. These types of failures are common in large complex networks [29, 67] and can be observed in most real networks, and typical manifestation of such failures are gridlock on the road network or critical slowing down of telecommunication networks. While the nature of failures is clearly defined, the influence on network stability are not yet investigated.

The failures under consideration are associated with finite capacity of network elements [30, 28]. Both the distribution lines and the centres in real networks are physically restricted [68], such as bandwith of communication line and power of a server, capacity of a stretch of a road and capacity of a road junction. For most of the time the functional state of these networks can be described as operational, e.g. "stable" Internet access or "freeflowing" road traffic. However, under some conditions we observe "overloading" of network elements, that in turn spreads over the rest of network [69]. The key question is then to understand conditions under which the "overloading" occurs and how such failures spread through the system [29, 8, 25].

Of course, the characteristics of individual elements affects development of critical loads in the system. In a simple system one may find the weakest link in a chain to have an idea of a strength of a system. For example the capacity of a backbone of a transcontinental gas/oil distribution system can be easily reduced by reducing capacity of any of intermediate parts like capacity of pipe or of oil refinery. Local capacity reduction in this case has a negative effect on the whole system.

Another factor that affects the stability of a system is a complexity of interconnections in a network structure [70, 26]. In a network environment redundancy of possible re-routing capabilities may be expected to have a positive effect on overall stability. However, stability of a system compounded by many subnetworks is not clear [28] and as we will show is nontrivial. We analyse network stability with respect to structural characteristics as well as properties of individual network elements.

The network stability against overloading failures has implications in various technological systems [26, 71] as well as biological[59], business and financial networks [56]. As mentioned before the physical characteristics of network parts in communication and transportation systems affect stability against overloading. In a biological context the functioning of an organism can be affected by critically congested blood/air vessels. In the business network, the collapse of a major player or a small specialised business can trigger problems in the supply chain, and could affect a large parts of a sector [41]. In financial networks the financial institutes assign capital against losses, and in case of insolvency other cooperative organisations may become insolvent themselves, sometimes affecting large parts of an economical sector or a whole economy.

We propose a model of a flow in distribution networks, the flow is realized as a set of currents that goes through the links. The amount of current in a link quantifies a **load** and does not exceed the links **capacity** [25]. In addition to a finite capacity requirement, we observe a balance relations at the nodes. The general flow is governed by a global optimisation criterion of a least overall dissipation of energy.

To analyse network stability against overloading failures, we concentrate on occurrences of the first maximal currents. Occurrence of the first overloadings in a system is indicative of a load strain in a system. Once a system reaches that state the overloaded parts of the system can be effectively discounted, while the rest of a system is not only close to critical load, but also has reduced load shedding capabilities. In other words occurrence of the critical loads in a system signals onset of the critical phase.

This Chapter is organised as follows. In Section (3.2) we introduce a model of a distribution network, the global flow is defined, as well as local constraints and global optimisation criteria. We apply a statistical mechanics approach to analyse properties of our system in Section (3.3). Then we analyse independently two characteristic cases of **infinite** link capacity (IC model in Section (3.4)) and of **finite** link capacity (FC model in Section (3.5)). Finally, we discuss and compare two models in Section (3.6) .

3.2 The model.

The distribution network can be thought of as a dynamical structure on the graph. The distribution centres and lines are represented by the set of nodes or vertices (V) and the set of links or edges (E) respectively. We denote the graph as $G(V,E)$. The graph structure is completely described by a symmetric connectivity matrix $c = \{c_{ij} : i,j = 1,\ldots,N\}$. , with $c_{ij} = 1$ if nodes i and j are connected, and $c_{ij} = 0$ otherwise.

3.2.1 The physical model of the flow in a network.

We introduce a physical model of the flow in the network and the optimisation criterion. The physical model of the flow strongly resembles the DC transmission network. In fact, the current transmission and distribution constraints are inspired by the direct current transmission networks. Indeed, we introduce the line resistances and direct currents, Kirchhoff's law-like constraints, and define a dissipation of the energy in terms of link resistance and electrical current. The global dissipation provides the optimisation criterion.

To each link we assign a **resistance** R_{ij} and a dynamical variable I_{ij} - **current**. Both resistances and currents are assumed to be continuous. The current that goes through the link is in fact a directed current. We use the following agreement: the current I_{ij} is going from the source node j to the sink node i. For the opposite current we have $I_{ji} = -I_{ij}$. Resistance, in contrast, is assumed to be independent of the direction.

The nodes in the network can be functionally separated into three distinctive classes as follows

- producers (we use index 'p' to index variables associated with these nodes),
- distributors (accordingly we use indices 'q' and 's'),
- receivers (we use index 'r').

Producers are the source nodes in the network, they have only the outgoing currents. Distributors are the nodes that have both incoming and outgoing currents. Finally, receivers

are the nodes that have only incoming currents. Such functional separation defines the general direction of the flow in the network from the producers through the distribution part of the network to the receivers.

Next, we assume the distribution constraint on the currents at each distribution node in the network. This constraint is, the sum of all incoming currents should be equal to the sum of all outgoing currents, and expressed as

$$\forall_q \quad \sum_{i(\neq q)} c_{qi} I_{qi} = 0. \tag{3.1}$$

For the receiver nodes we specify the level of demand in terms of currents by the set $\{I_r\}$. The constraint (3.1) for the receiver and producer nodes transforms to

$$\forall_r \quad \sum_q c_{rq} I_{rq} = I_r, \tag{3.2}$$

$$\forall_p \quad \sum_q I_{qp} = I_p. \tag{3.3}$$

The I_p's reflect the level of production, which, unlike the level of demand we do not specify. In fact, the specification of either level of production or level of demand is needed, as the other, through observed balance constraints (3.1), becomes the consequence of the first. For this reason we will not use last constraint (3.3), but use (3.1) and (3.2).

Finally, we introduce dissipation of the energy that is associated with the transmission of current through the link. We assume the DC-like form of dissipation

$$D_{ij} = R_{ij} I_{ij}^2, \tag{3.4}$$

and the global dissipation is just a sum of dissipations over all links

$$D = \sum_{(ij)} D_{ij}, \tag{3.5}$$

where (ij) denotes summation without repetitions.

3.2.2 Structure of the network.

The functional separation of the nodes into three distinctive categories imposes certain structural features. That is, we assume that producer nodes are not interlinked and only connected to the distribution nodes. Similarly, the receiver nodes do not connect to each other and only connect to the distribution nodes. On the other hand, the distribution nodes are inter-connected and also might be connected to both producer and receiver nodes. In other words, we observe three distinguished networks compounded by distributor-producer, distributor-distributor and distributor-receiver links respectively. These networks connect to each other by distribution nodes, but in terms of connectivity can be considered independently. We denote these networks as producer, distributor and receiver networks respectively.

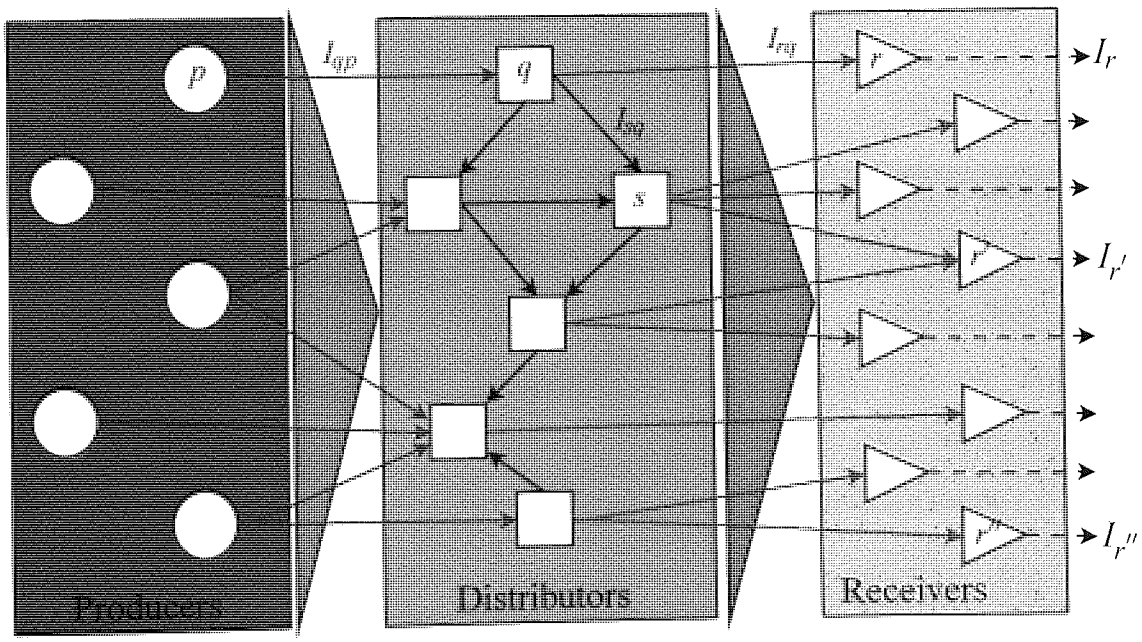

Figure 3.1: Schematic representation of network structure. Three sets of nodes are producers, distributors and receivers. We split the network into three subnetworks: producer subnetwork (blue links), receiver subnetwork (red links) and distribution subnetwork (solid black links). Consumption level at each receiver node is represented by dashed black arrow

A graph is fully determined by its connectivity matrix $\mathbf{c}$. For the graph of average connectivity C, the *a priori* probability of the link to be present is defined like

$$p_C(c_{ij}) = \frac{C}{N}\delta_{c_{ij},1} + \left(1 - \frac{C}{N}\right)\delta_{c_{ij},0}. \tag{3.6}$$

To enforce a particular degree distribution $P_C(L)$, where L is the node degree we use

$$P_C(L) = \frac{1}{N}\sum_i \delta_{L,L_i}, \tag{3.7}$$

for a given set of coordination numbers L_i. The full distribution of connectivity matrices $P_C(\mathbf{c})$ is defined by

$$P_C(\mathbf{c}) \sim \prod_{(ij)} p_C(c_{ij})\delta_{c_{ij},c_{ji}} \prod_i \delta_{L_i,\sum_{j(\neq i)} c_{ij}}. \tag{3.8}$$

As we have imposed constraints on the type of interactions between producer, distributor and receiver nodes, the full distribution can be factorised

$$\begin{aligned} P_C(\mathbf{c}) \sim & \prod_{qp} p_{C_p}(c_{qp})\delta_{c_{qp},c_{pq}} \prod_p \delta_{L_p,\sum_q c_{qp}} \\ & \times \prod_{(qs)} p_{C_q}(c_{qs})\delta_{c_{qs},c_{sq}} \prod_q \delta_{L_q,\sum_{s(\neq q)} c_{qs}} \\ & \times \prod_{qr} p_{C_r}(c_{qr})\delta_{c_{qr},c_{rq}} \prod_r \delta_{L_r,\sum_q c_{qr}}. \end{aligned} \tag{3.9}$$

In (3.9) the sets of L_p, L_q, L_r are drawn from the $P_{c_p}(L), P_{c_q}(L)$ and $P_{c_r}(L)$ respectively. The c_p, c_q and c_r are average connectivities of each subnetwork.

The connectivity model and parameterisation for the producer and the receiver networks are defined on the producer and receiver sides respectively. Thus, the degree distribution of the producer network $P_{c_p}(L)$ defines the degrees of the producer nodes. Similarly, the degree distribution of the receiver network $P_{c_r}(L)$ defines the degrees of the receiver nodes.

The degree distribution of the distribution network is denoted as $P_{c_q}(L)$. For the distribution network we consider a non-Poissonian random graph of average connectivity c_q [1].

The total number of nodes in the network is N. As we split nodes into three groups we obtain (N_p, N_q, N_r) - number of producers, distributors and receivers respectively. We

[1] We add another parameter - minimal connectivity ($m_q > 2$) to ensure we do not have oscillated (the nodes of degree 0) and dangling (the nodes of degree 1) nodes in distribution network.

have

$$N = N_p + N_q + N_r, \tag{3.10}$$

$$N_p = \lambda_p N, \tag{3.11}$$

$$N_q = \lambda_q N, \tag{3.12}$$

$$N_r = \lambda_r N, \tag{3.13}$$

$$\lambda_p + \lambda_q + \lambda_r = 1. \tag{3.14}$$

3.2.3 Simplified network diagram.

To aid understanding of key characteristics of the network we use network diagrams. In all figures we use the following signs to denote subnetworks (or network elements).

- ◯ - producers
- □ - distributors
- ▷ - receivers

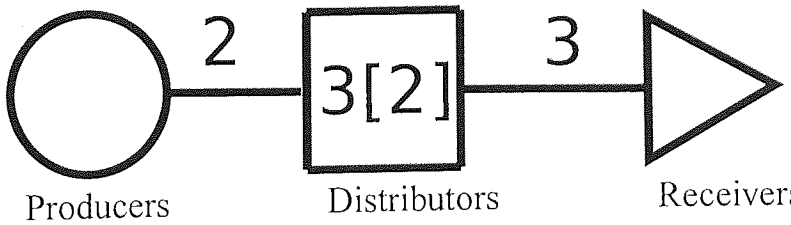

Figure 3.2: Example of a network diagram. Each producer has exactly 2 links, average connectivity in distributor network is 3 and lowest connectivity is 2, each receiver has exactly 3 links. The general direction of the flow in the network is from producers to distributors to receivers.

In our simulations we use a fixed number of connections per node in distributor and receiver networks. However, a random number of connections may be used as well as in (2.2).

3.3 Theoretical analysis

We follow standard steps of replica analysis [32]. We introduce n replicas and calculate the replicated partition function ($\langle Z^n \rangle_{c,R}$). The $\langle \ldots \rangle_{c,R}$ here means averaging over connectivities ($c = \{c_p, c_r, c_q\}$) and link resistances ($R = \{R_{ij}\}$). We assume that the disorder is quenched. To denote replicas we use index $\alpha = \{1, \ldots, n\}$.

The n-fold replicated partition function that includes both the constraints (3.1, 3.2) and the optimisation criterion (3.5) is given by

$$\langle Z^n \rangle_{c,R} = \left\langle \operatorname*{Tr}_{\widetilde{I}} \exp\left[-\beta \sum_{\alpha} \sum_{<ij>} c_{ij} R_{ij} I_{ij}^{\alpha^2} \right] \prod_{\alpha,q} \delta\left(\beta \left[\sum_i c_{qi} I_{qi}^{\alpha} \right] \right) \prod_{\alpha,r} \delta\left(\beta \left[I_r + \sum_q c_{qr} I_{qr}^{\alpha} \right] \right) \right\rangle_{c,R} . \tag{3.15}$$

Here, $\underline{I} = \{I_{ij}\}$ and $\widetilde{I} = \{I^{\alpha}\}$, so the trace is taken over all realizations of currents in all replicas. The <ij> denotes the links without repetitions. The constraints (3.1, 3.2) are scaled to match the exponential term. We use the integral representation of Dirac delta function : $\delta(u) = \frac{1}{2\pi} \int_{-\infty}^{\infty} dx e^{-\mathrm{i}ux}$. We introduce conjugate site variables x_q^{α} and x_r^{α}, and the partition function is transformed to

$$\langle Z^n \rangle_{c,R} = \left\langle \operatorname*{Tr}_{\widetilde{I}} \exp\left[-\beta \sum_{\alpha} \sum_{<ij>} c_{ij} R_{ij} I_{ij}^{\alpha^2} \right] \left(\prod_{\alpha,q} \int_{-\infty}^{\infty} \mathrm{d}x_q^{\alpha} e^{-\beta \mathrm{i} \sum_{\alpha,i} c_{qi} I_{qi}^{\alpha} x_q^{\alpha}} \right) \left(\prod_{\alpha,r} \int_{-\infty}^{\infty} \mathrm{d}x_r^{\alpha} e^{-\beta \mathrm{i} \left(\sum_{\alpha} x_r^{\alpha} \left(I_r + \sum_q c_{qr} I_{qr}^{\alpha} \right) \right)} \right) \right\rangle_{c,R} \tag{3.16}$$

The conjugate variables in (3.17) turn out to be a voltage-like potentials. It is useful to introduce short-hand notation for a replicated vector $\tilde{x} = (x^1, \ldots, x^n)$. Also, we introduce replica link weights

$$U^{qp}(\tilde{x}_q) \equiv \operatorname*{Tr}_{\widetilde{I}} \exp\left[-\beta \sum_{\alpha} \left(R_{qp} I_{qp}^{\alpha^2} + \mathrm{i} x_q^{\alpha} I_{qp}^{\alpha} \right) \right] \tag{3.17}$$

$$U^{qr}(\tilde{x}_q, \tilde{x}_r) \equiv \operatorname*{Tr}_{\widetilde{I}} \exp\left[-\beta \sum_{\alpha} \left(R_{qr} I_{qr}^{\alpha^2} + \mathrm{i} \left(x_r^{\alpha} - x_q^{\alpha} \right) I_{qr}^{\alpha} \right) \right] \tag{3.18}$$

$$U^{qs}(\tilde{x}_q, \tilde{x}_s) \equiv \operatorname*{Tr}_{\widetilde{I}} \exp\left[-\beta \sum_{\alpha} \left(R_{qs} I_{qs}^{\alpha^2} + \mathrm{i} \left(x_q^{\alpha} - x_s^{\alpha} \right) I_{qs}^{\alpha} \right) \right], \tag{3.19}$$

and the replica site weight

$$U^r(\tilde{x}_r) \equiv \exp\left(-\beta\sum_\alpha \mathrm{i}x^\alpha I_r\right) = \exp\left(-\beta\sum_\alpha V(x^\alpha)\right). \tag{3.20}$$

We start by performing the average over the connectivity. We recall that within our structure we have three distinctive subgraphs. Therefore, we can factorise the partition function and perform averaging over connectivity separately for each subgraph. In each case we can follow the standard steps [72]. Constraints on the local connectivities are enforced via the identity

$$\delta_{K_i,L_i} = \oint_{|z|=1} \frac{\mathrm{d}z_i}{2\pi\mathrm{i}z_i} z_i^{(K_i-L_i)}. \tag{3.21}$$

In our next step we introduce replica density functions

$$\rho^r(\tilde{x}) = \frac{1}{N_r}\sum_r z_r\delta(\tilde{x}-\tilde{x}_r), \quad \rho^q(\tilde{x}) = \frac{1}{N_q}\sum_q z_q\delta(\tilde{x}-\tilde{x}_q). \tag{3.22}$$

The physical meaning of order parameters turns out to be the mean-field voltage average. Enforcing the definitions of the replica density functions in terms of conjugate functions $\hat{\rho}^r(\tilde{x})$ and $\hat{\rho}^q(\tilde{x})$ we obtain the replicated partition function as a functional integral over the replica densities

$$\langle Z^n\rangle_R = \int D\{\rho^r,\rho^q,\hat{\rho}^r,\hat{\rho}^q\}\exp\left\{N\left(G_l[\rho^q,\rho^r]-G_m[\rho^q,\hat{\rho}^q,\rho^r,\hat{\rho}^r]+G_s[\hat{\rho}^q,\hat{\rho}^r]\right)\right\}, \tag{3.23}$$

where the first term denotes contribution of the "links" (to shorten expressions we use the

replica link weights)

$$G_l[\rho^q,\rho^r] = \lambda_q\Big[c_p(G_l^p[\rho^q]-1)+c_r(G_l^r[\rho^q,\rho^r]-1)+\frac{c_q}{2}(G_l^r[\rho^q]-1)\Big] \quad (3.24)$$

$$G_l^p[\rho^q] = \left\langle \int_{-\infty}^{\infty} d\tilde{x}\rho^q(\tilde{x})U^{qp}(\tilde{x}_q)\right\rangle_R, \quad (3.25)$$

$$G_l^q[\rho^q] = \left\langle \int_{-\infty}^{\infty} d\tilde{x}d\tilde{x}'\rho^q(\tilde{x})\rho^q(\tilde{x}')U^{qs}(\tilde{x},\tilde{x}')\right\rangle_R, \quad (3.26)$$

$$G_l^r[\rho^q,\rho^r] = \left\langle \int_{-\infty}^{\infty} d\tilde{x}d\tilde{x}'\rho^q(\tilde{x})\rho^r(\tilde{x}')U^{qr}(\tilde{x},\tilde{x}')\right\rangle_R, \quad (3.27)$$

the last term denotes contribution from the 'sites'

$$G_s[\hat{\rho}^q,\hat{\rho}^r] = \lambda_q G_n^q[\hat{\rho}^q]+\lambda_r G_n^r[\hat{\rho}^r], \quad (3.28)$$

$$G_s^q[\hat{\rho}^q] = \sum_L P_{C_q}(L)\ln\int_{-\infty}^{\infty} d\tilde{x}[\rho^q(\tilde{x})]^L, \quad (3.29)$$

$$G_s^r[\hat{\rho}^r] = \sum_L P_{C_r}(L)\left\langle \ln\int_{-\infty}^{\infty} d\tilde{x}\rho^{rL}(\tilde{x})U^r(\tilde{x},I_r)\right\rangle_{I_r}, \quad (3.30)$$

and the middle term is a mixed term

$$G_m[\rho^q,\hat{\rho}^q,\rho^r,\hat{\rho}^r] = \lambda_q G_m^q[\rho^q,\hat{\rho}^q]+\lambda_r G_m^r[\rho^r,\hat{\rho}^r], \quad (3.31)$$

$$G_m^q[\rho^q,\hat{\rho}^q] = \int_{-\infty}^{\infty} d\tilde{x}\rho^q(\tilde{x})\hat{\rho}^q(\tilde{x}), \quad (3.32)$$

$$G_m^r[\rho^r,\hat{\rho}^r] = \int_{-\infty}^{\infty} d\tilde{x}\rho^r(\tilde{x})\hat{\rho}^r(\tilde{x}). \quad (3.33)$$

3.3.1 Replica symmetry.

To calculate the partition function (3.23), the functionals needs to be calculated at the relevant saddle point and in order to do this we need to make an ansatz for the replicated densities and their conjugates which assumes that all replicas are indistinguishable under permutations. Here, both replicated densities and their conjugates are expressed as superpositions of products of single-replica functions, written in the Gibbsian form :

$$\rho^r(\tilde{x}) = \int D\psi\pi^r[\psi]\prod_\alpha \frac{e^{-\beta\psi(x^\alpha)}}{Z[\psi]}, \qquad \hat{\rho}^r(\tilde{x}) = \mu_r\int D\hat{\psi}\hat{\pi}^r[\hat{\psi}]\prod_\alpha \frac{e^{-\beta\hat{\psi}(x^\alpha)}}{Z[\hat{\psi}]}, \quad (3.34)$$

$$\rho^q(\tilde{x}) = \int D\psi\pi^q[\psi]\prod_\alpha \frac{e^{-\beta\psi(x^\alpha)}}{Z[\psi]}, \qquad \hat{\rho}^q(\tilde{x}) = \mu_q\int D\hat{\psi}\hat{\pi}^q[\hat{\psi}]\prod_\alpha \frac{e^{-\beta\hat{\psi}(x^\alpha)}}{Z[\hat{\psi}]}, \quad (3.35)$$

where $Z[\psi]\equiv\int dx e^{-\beta\psi(x)}$. The functions ψ and $\hat{\psi}$ are complex single-replica potentials that generate the Gibbs distribution. The π's and $\hat{\pi}$'s are probability functions over the

function spaces of single-replica functions.

We obtained prefactors μ_r and μ_q by collecting terms of the order of $O(1)$

$$\mu_r = \frac{\lambda_q}{\lambda_r} c_r, \qquad \mu_q = c_p + c_r + c_q, \tag{3.36}$$

Applying RS ansatz to (3.23) leads to the following expression of the functionals (3.24),(3.28) and (3.31) :

$$\begin{aligned} G_l &\simeq \lambda_q c_p \int D\pi^q[\psi^q] \left\langle \ln \frac{Z_1[\psi^q U^{qp}]}{Z[\psi^q]} \right\rangle_R \\ &+ \lambda_q c_r \int D\pi^q[\psi^q] D\pi^r[\psi^r] \left\langle \ln \frac{Z_2[\psi^q, \psi^r, U^{qr}]}{Z[\psi^q] Z[\psi^r]} \right\rangle_R \\ &+ \lambda_q \frac{c_q}{2} \int D\pi^q[\psi^q] D\pi^q[\psi^s] \left\langle \ln \frac{Z_2[\psi^q, \psi^s, U^{qs}]}{Z[\psi^q] Z[\psi^s]} \right\rangle_R, \end{aligned} \tag{3.37}$$

$$\begin{aligned} G_m &\simeq \lambda_r \int D\pi^r[\psi] D\hat{\pi}^r[\hat{\psi}] \ln \left[\frac{Z[\psi + \hat{\psi}]}{Z[\psi] Z[\hat{\psi}]} \right] \\ &+ \lambda_q \int D\pi^q[\psi] D\hat{\pi}^q[\hat{\psi}] \ln \left[\frac{Z[\psi + \hat{\psi}]}{Z[\psi] Z[\hat{\psi}]} \right]. \end{aligned} \tag{3.38}$$

$$\begin{aligned} G_s &\simeq \lambda_r \sum_{L=0}^{\infty} P_{c_r}(L) \int \{D\hat{\pi}^r[\hat{\psi}_l]\}_L \left\langle \ln \left[\frac{Z[\sum_{l=1}^L \hat{\psi}_l + V]}{\{Z[\hat{\psi}_l]\}_L} \right] \right\rangle_{I_r} \\ &+ \lambda_q \sum_{L=0}^{\infty} P_{c_q}(L) \int \{D\hat{\pi}^q[\hat{\psi}_l]\}_L \ln \left[\frac{Z[\sum_{l=1}^L \hat{\psi}_l]}{\{Z[\hat{\psi}_l]\}_L} \right], \end{aligned} \tag{3.39}$$

and the partition function can be expressed as

$$\langle Z^n \rangle_R \sim \int D\pi D\hat{\pi} \exp\{nN(G_l - G_m + G_s)\}. \tag{3.40}$$

Here we introduced short-hand notation

$$D\pi[\psi] = D\psi\pi[\psi], \quad D\pi_L = \prod_{l=1}^{L} D\pi[\psi_l], \tag{3.41}$$

$$Z_2[f, g, U^{ij}] = \int \mathrm{d}x\mathrm{d}x' e^{-\beta(f(x)+g(x'))} U^{ij}(x, x'), \tag{3.42}$$

$$Z_1[f, U^{qp}] = \int \mathrm{d}x e^{-\beta f(x)} U^{qp}(x). \tag{3.43}$$

It is understood that the expression (3.40) should be evaluated at the saddle point. The

corresponding saddle point equations are obtained by using stationarity conditions with respect to variations of π's and $\hat{\pi}$'s.

$$\hat{\pi}^r[\hat{\psi}^r] = \int D\pi^q[\psi^q]\,\langle\delta(\hat{\psi}^r - \Psi[\psi^q, U^{qr}])\rangle_R, \tag{3.44}$$

$$\hat{\pi}^q[\hat{\psi}^q] = \frac{c_p}{\mu_q}\langle U^{qp}\rangle_R + \frac{c_r}{\mu_q}\int D\pi^r[\psi^r]\,\langle\delta(\hat{\psi}^q - \Psi[\psi^r, U^{qr}])\rangle_R + \frac{c_q}{\mu_q}\int D\pi^q[\psi^q]\,\langle\delta(\hat{\psi}^q - \Psi[\psi^q, U^{qs}])\rangle_R, \tag{3.45}$$

$$\pi^r[\psi^r] = \sum_L \frac{LP_{c_r}(L)}{\mu_r}\int\{D\hat{\pi}^r[\hat{\psi}_l]\}_{L-1}\delta\left(\psi^r - \sum_{l=1}^{L-1}\hat{\psi}_l^r - V\right), \tag{3.46}$$

$$\pi^q[\psi^q] = \sum_L \frac{LP_{c_q}(L)}{\mu_q}\int\{D\hat{\pi}^q[\hat{\psi}_l]\}_{L-1}\delta\left(\psi^q - \sum_{l=1}^{L-1}\hat{\psi}_l^q\right), \tag{3.47}$$

where

$$\Psi[\psi, U^{ij}](x') = -\frac{1}{\beta}\ln\int dx\left(e^{-\beta\psi(x)}U^{ij}(x,x')\right). \tag{3.48}$$

The general way to solve saddle point equations is to use population dynamics algorithms [66]. The strategy is based on the sampling from distribution of functions $\pi[\psi]$ and the link disorder R to obtain $\hat{\pi}[\hat{\psi}]$, and sampling from distribution of functions $\hat{\pi}[\hat{\psi}]$, the corresponding degree distribution $P_C(L)$ and, if necessary, site disorder I_r. The updates can be done iteratively. Note that our single-replica functions are complex. Therefore, the updates in population dynamics have to be performed for complex functions. Due to particular form of single-replica functions (a quadratic real part and a linear imaginary part) the population dynamics can be easily performed without any complications.

3.3.2 Physical properties.

The relevant physical quantities now can be obtained from the averaged replicated partition function evaluated at the saddle point.

The **free energy per node** of the system is given by

$$F = -\frac{1}{\beta}[G_l - G_m + G_s] \tag{3.49}$$

The **distribution of currents** (in each of the subnetworks) is obtained by taking a derivative with respect to the corresponding conjugate variable of functionals in (3.37)

For example, to calculate the distribution of the receiver currents $P_r(I_{qr})$ we take the derivative with respect to the conjugate variable x_r of the second term in (3.37),

$$P_r(I_{qr}) = \int \mathrm{d}\pi[\psi^q]\mathrm{d}\pi[\psi^r] \left\langle \delta\left(I_{qr} - \frac{\frac{\partial}{\partial x^r}\left(Z_2[\psi^q,\psi^r,U^{qr}]\right)}{Z_2[\psi^q,\psi^r,U^{qr}]} \right) \right\rangle. \tag{3.50}$$

Similarly we obtain distributions of currents in producer and distribution networks

$$P_p(I_{qp}) = \int \mathrm{d}\pi[\psi^q] \left\langle \delta\left(I_{qp} - \frac{\frac{\partial}{\partial x^q}\left(Z_1[\psi^q,U^{qp}]\right)}{Z_2[\psi^q,U^{qp}]} \right) \right\rangle. \tag{3.51}$$

$$P_q(I_{qs}) = \int \mathrm{d}\pi[\psi^q]\mathrm{d}\pi[\psi^q] \left\langle \delta\left(I_{qs} - \frac{\frac{\partial}{\partial x^q}\left(Z_2[\psi^q,\psi^q,U^{qs}]\right)}{Z_2[\psi^q,\psi^r,U^{qs}]} \right) \right\rangle. \tag{3.52}$$

Also we define the **node load** - the sum of all currents passing through the given node, and calculate the **distribution of loads**

$$P^p(I_p) = \sum_L P_{c_p}(L) \int \left\{ \mathrm{d}P_p(I_l) \right\}_L \delta\left(I_p - \sum_{l=1}^{L} I_l \right) \tag{3.53}$$

$$P^q(I_q) = \sum_L P_{c_q}(L) \int \left\{ \mathrm{d}P_q(I_l) \right\}_L \delta\left(I_q - \sum_{l=1}^{L} I_l \right) \tag{3.54}$$

$$P^r(I_r) = \sum_L P_{c_r}(L) \int \left\{ \mathrm{d}P_r(I_l) \right\}_L \delta\left(I_r - \sum_{l=1}^{L} I_l \right) \tag{3.55}$$

This concludes the theoretical analysis of our model. In the next sections we consider two cases, defined by properties of the links in the system. We consider cases of **infinite** and of **finite** link capacity.

3.4 Case 1: Infinite link capacity (IC model)

There are physical constraints in real systems. For example the amount of electricity that is managed at one node is restricted by specifications of devices at the substation, or current that flows through a link is restricted by physical properties of wires that link consists of. However, for model that we study here we assume no restrictions on currents

in links at all. This assumption considerably simplifies calculation and it is much easier to handle numerically. We refer to this model as **Infinite Capacity** model (IC).

The absence of any restrictions on the links leads to a particularly convenient form of the link weight interactions, namely, harmonic couplings. The systems with harmonic interactions have been extensively studied and allow exact solutions in many cases. For instance, for systems with harmonic couplings which describe amorphous materials like gels [72] the exact solution can be obtained, due to existence of unique ground states in such systems.

In [72] the case of harmonic couplings has been studied, and for the single-replica potentials an orthogonal function representation has been used. The complete set of Hermite polynomials provides a suitable set of basis functions. The expansion of single-replica potentials is then obtained. Such representation is preferred if one can avoid full functional representation [2].

In the case of harmonic couplings it turns out that the full set of basis functions is not needed. In fact, the space of finite dimensionality defined on the first three basis functions is sufficient to solve saddle point equations. The population dynamics is then reduced to set of simple algebraic updates.

In our model we chose to use quadratic polynomials with real quadratic term and imaginary linear term to represent single-replica functions. The form of such representation is basically dictated by the terms in saddle point equations (3.47). The terms associated with the dissipation are real, while the terms associated with the currents are strictly imaginary.

[2] We will show examples of both approaches. Here we consider particular second order representation of single-replica functions. The anharmonic case considered later in this chapter requires a full functional approach.

3.4.1 Calculation and population dynamics

In case of unrestricted link capacity we can perform the trace over currents I to calculate link weights (3.17)-(3.19). The I turns out to be[3]

$$I_{ij} = \frac{\mathrm{i}\,(x_i - x_j)}{2R_{ij}}, \tag{3.56}$$

and by performing Gaussian integration we obtain

$$U^{qp}(x) = -\beta\frac{x_q^2}{4R_{qp}}, \tag{3.57}$$

$$U^{qr}(x_q, x_r) = -\beta\frac{(x_q - x_r)^2}{4R_{qr}}, \tag{3.58}$$

$$U^{qs}(x_q, x_s) = -\beta\frac{(x_q - x_s)^2}{4R_{qs}} \tag{3.59}$$

Note, that the numerator in (3.56) has the form of a difference of potentials $\Delta V = V_i - V_j = \mathrm{i}(x_i - x_j)$. At the same time the link weights have the form of the scaled dissipation of energy $U_{ij} \simeq I_{ij}^2 R_{ij}$.

Now , to solve our saddle point equations, we assume the following form for ψ and $\hat{\psi}$ functions

$$\psi(x) = Ax^2 + \mathrm{i}Bx \qquad \hat{\psi}(x) = \hat{A}x^2 + \mathrm{i}\hat{B}x, \tag{3.60}$$

where all coefficients are real numbers. This form of functions is dictated by link and single-site weights (quadratic real part and linear imaginary part). We can proceed with the population dynamics algorithm, but instead of pointwise calculation of functions in (3.44)-(3.47), we perform Gaussian integration. Now, our update equations reduce to algebraic updates of coefficients

- Updates of $\hat{A}^r$'s and $\hat{B}^r$'s

$$\hat{A}^r = A^q t, \qquad \hat{B}^r = B^q t, \quad \text{where} \quad t = \frac{1}{1 + 4R_{qr}A^q}. \tag{3.61}$$

[3] Can be done by saddle point method for example.

- Updates of $\hat{A}^q$'s and $\hat{B}^q$'s

$$\hat{A}^q = 0, \qquad \hat{B}^q = \frac{1}{4R_{qp}}, \qquad \text{or}$$
$$\hat{A}^q = A^q t, \qquad \hat{B}^q = B^q t, \quad \text{where} \quad t = \frac{1}{1+4R_{qs}A^q} \quad \text{or}$$
$$\hat{A}^q = A^r t, \qquad \hat{B}^q = B^r t, \quad \text{where} \quad t = \frac{1}{1+4R_{qr}A^r}.$$

- Updates of A^r's and B^r's

$$A^r = \sum_{l=1}^{L} \hat{A}_l^r, \qquad B^r = \sum_{l=1}^{L} \hat{B}_l^r + I_r \quad \text{where} \quad L \quad \text{is drawn from} \quad P_{c_r}(L).$$

- Updates of A^q's and B^q's

$$A^q = \sum_{l=1}^{L} \hat{A}_l^q, \qquad B^q = \sum_{l=1}^{L} \hat{B}_l^q \quad \text{where} \quad L \quad \text{is drawn from} \quad P_{c_q}(L).$$

Only quadratic and linear terms are important in our calculation. The meaning of the quadratic term is quite simple, it is reflects the dissipation in the links. As one would expect the dissipation to be non-negative the A's and $\hat{A}$'s coefficients are initialised as non-negative. The linear coefficients are uniformly sampled from the range $[-1, 1]$. By initialising all A coefficients with non negative values we ensure that updates are numerically stable.

The solutions of (3.16) are meant to be found in the low temperature limit ($\beta \to \infty$). However, in the IC model, the special form of couplings turns out to lead to the correct solution at any temperature. The equation (3.16) can be solved at any temperature, so, for simplicity, we take $\beta = 1$.

3.4.2 Results.

We solve saddle point equations (3.44)-(3.45) at finite temperature for various models of connectivities and distributions of the parameters R_{ij} and I_r using a population dynamics algorithm, the size of populations is 100000. Once the stable distributions of the complex

single-replica functions $\pi[\psi]$ and $\hat{\pi}[\hat{\psi}]$ have been obtained, we calculated relevant physical quantities: the distribution of individual currents (I_{qp}, I_{qs}, I_{qr}) and distribution of the node loads (I_p, I_q, I_r). For the (IC) model we discuss results in terms of these distributions and their statistical characteristics like mean and standard deviation.

Given, that the original network is divided into three subnetworks each of them are defined independently, we analyse the distributions of the currents and loads for each subnetwork. The effects of the connectivity and disorder in this set up can be localised and magnified by tuning corresponding model parameters.

All distributions of currents obtained in the experiments have been calculated in equilibrium. To test if we have reached the equilibrium state we check overall balance.

Furthermore, the calculation results in distributions of optimal currents. For instance, the distribution of currents in the producer network has been found to be determined on $\mathbb{R}^+$, i. e. all the currents from the producer to the distributor nodes are non-negative. This is what one would expect: the extra currents would cause extra dissipation of the energy.

The distribution of currents in the distribution subnetwork is centred at 0, meaning that the distribution part of system takes in exactly as much as it gives out. Hence the zero mean of this distribution.

An increase in the levels of consumption results in an increase of both the mean and standard deviation of the distribution of produced currents as well as an increase of the standard deviation of the distribution of distributed currents (see figure 3.3). Moreover, the growth of mean and standard deviation is linear, as could be expected from the Gaussian form of the distribution of distributed currents and the linearity of the redistribution law at the nodes.

Increasing the number of links at producer nodes results in narrower distributions of produced and distributed currents. A similar effect is observed when the average connectivity in distributor networks is increased (see figures (3.3),(3.9) and (3.12)). In all cases higher connectivity increases the number of possible ways to distribute currents, making it more homogeneous, i.e. current values are less spread out.

In the case when line resistances are different the following trends are observed. In the system where the spread of resistance values is wider, the spread of the currents is

wider as well (see figures (3.14) and (3.17)). As our objective is to minimise dissipation the lines with low resistances might be preferred over the rest. Such lines may carry high currents, resulting in a wider distributions of currents. We have sampled resistance values from uniform distribution. In both cases a wider distribution of link resistances created higher deviations of distributions of produced and distributed currents.

The same trend, but more pronounced, was observed for a random levels of demand. The higher spread resulted in a wider distributions of currents in all subnetworks. Also, in this case we do not observe characteristic peaks in distributions of distribution currents. The peaks at the $(\pm I_r, \pm 2I_r, \pm 3I_r, \ldots)$ correspond to the situations where the distribution network has only one link which connects to the rest of distribution network and the rest of the links attached to the node are producer/receiver links. The same effect was observed in producer networks. Peaks are more pronounced in cases when the average connectivity of the receiver network is 1 (see figures (3.11) and (3.14)).

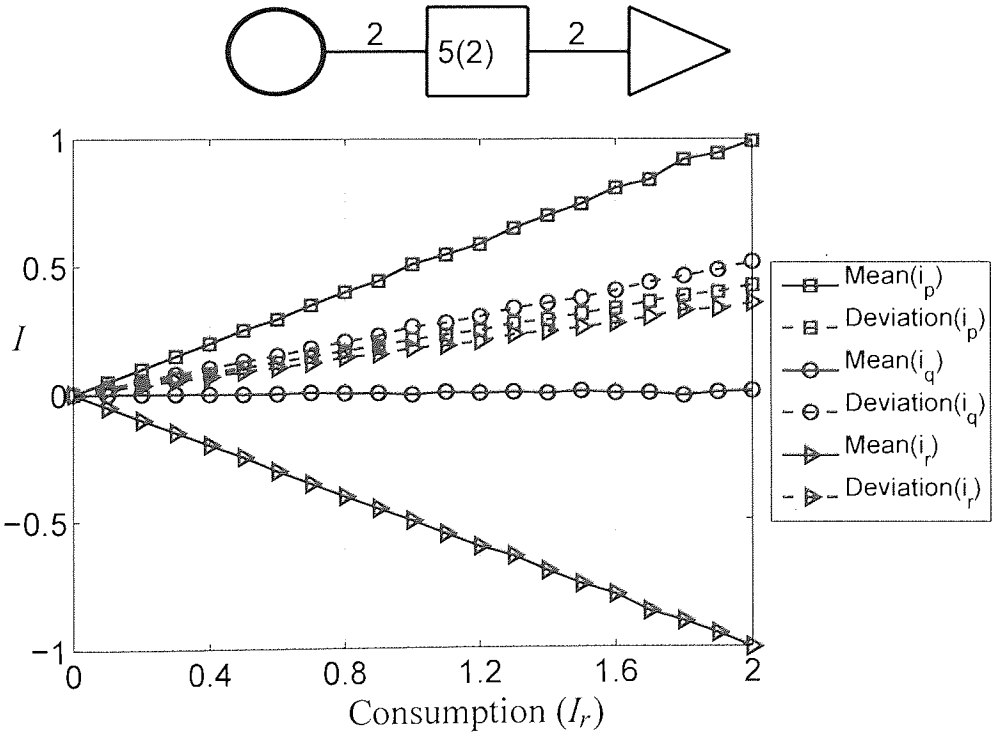

Figure 3.3: Distributions of individual currents obtained via population dynamics, case $c_p = 2$, $c_q = 5(2)$, $c_r = 2$, $R = 1.0$. Each producer has exactly 2 links, average connectivity in distributors network is 5 and lowest connectivity is 2, each receiver has exactly 2 links. Size of the population is 10000. We do 100 equilibrating sweeps and 100 measuring sweeps. Both the means and the standard deviations of distributions of currents exhibit linear dependence on consumption level.

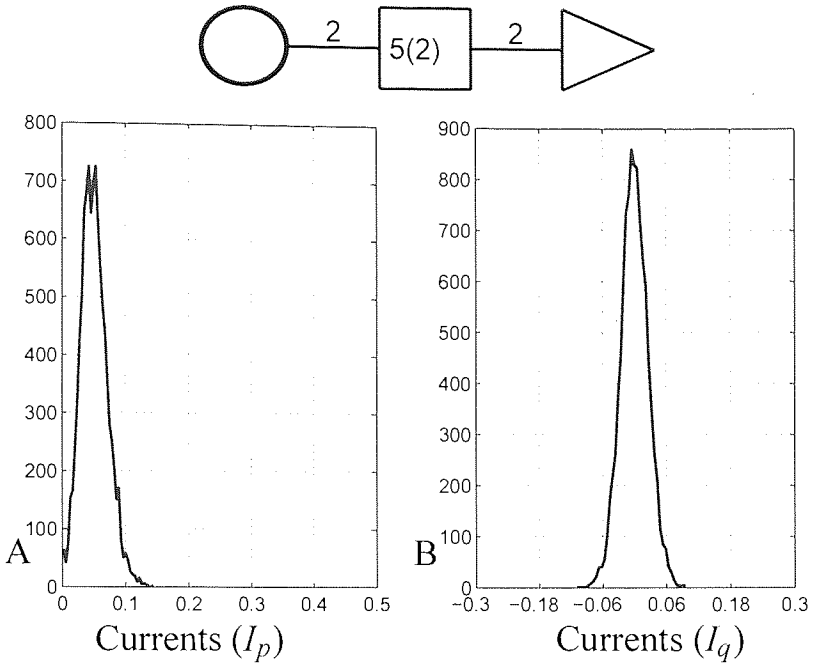

Figure 3.4: Histograms of distributions of individual currents obtained via population dynamics. Consumption $I_r = 0.1$, case $c_p = 2$, $c_q = 5(2)$, $c_r = 2$, $R = 1$. Each producer has exactly 2 links, average connectivity in distributors network is 5 and lowest connectivity is 2, each receiver has exactly 2 links. A: Distribution of currents in the producer-distributor network. B: Distribution of currents in the distribution network.

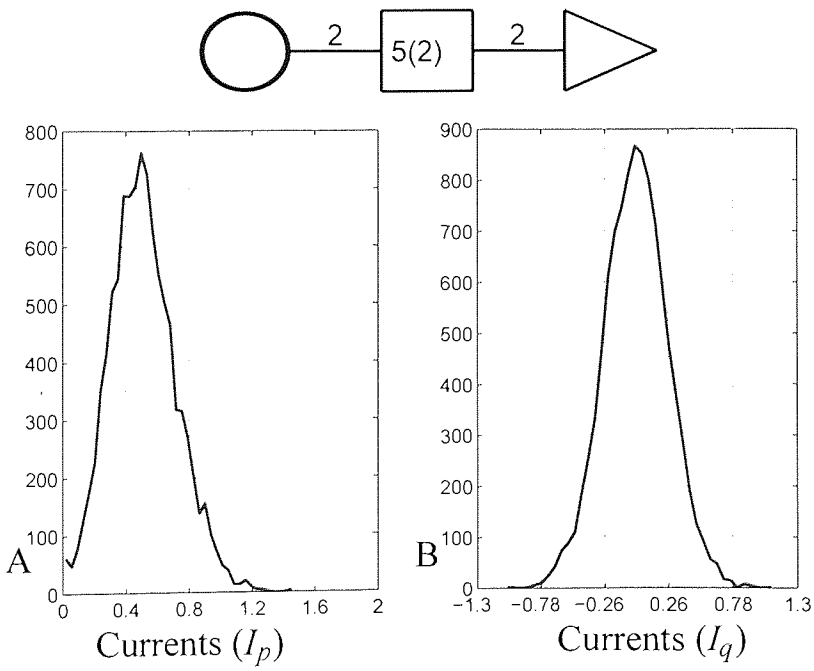

Figure 3.5: Histograms of distributions of individual currents obtained via population dynamics. Consumption $I_r = 1.0$, case $c_p = 2$, $c_q = 5(2)$, $c_r = 2$, $R = 1$. Each producer has exactly 2 links, average connectivity in distributors network is 5 and lowest connectivity is 2, each receiver has exactly 2 links. A: Distribution of currents in the producer-distributor network. B: Distribution of currents in the distribution network.

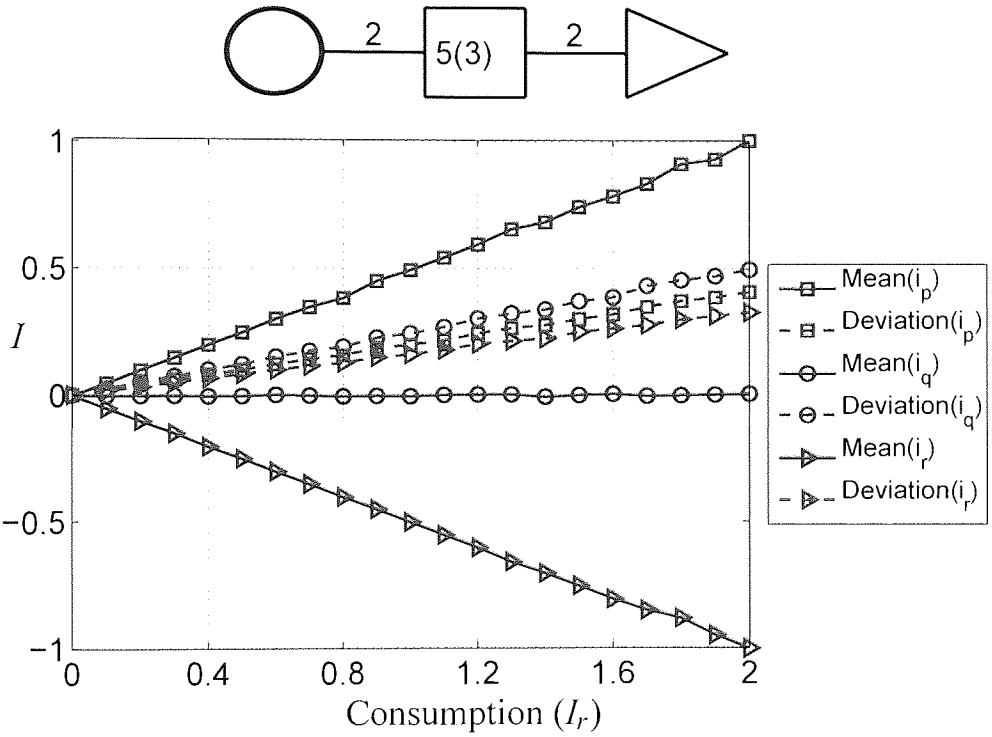

Figure 3.6: Distributions of individual currents obtained via population dynamics, case $c_p = 2, c_q = 5(3), c_r = 2, R = 1$. Each producer has exactly 2 links, average connectivity in distributors network is 5 and lowest connectivity is 3. Size of the population is 10000. We do 100 equilibrating sweeps and 100 measuring sweeps. Both the means and the standard deviations of distributions of currents exhibit linear dependence on consumption level.

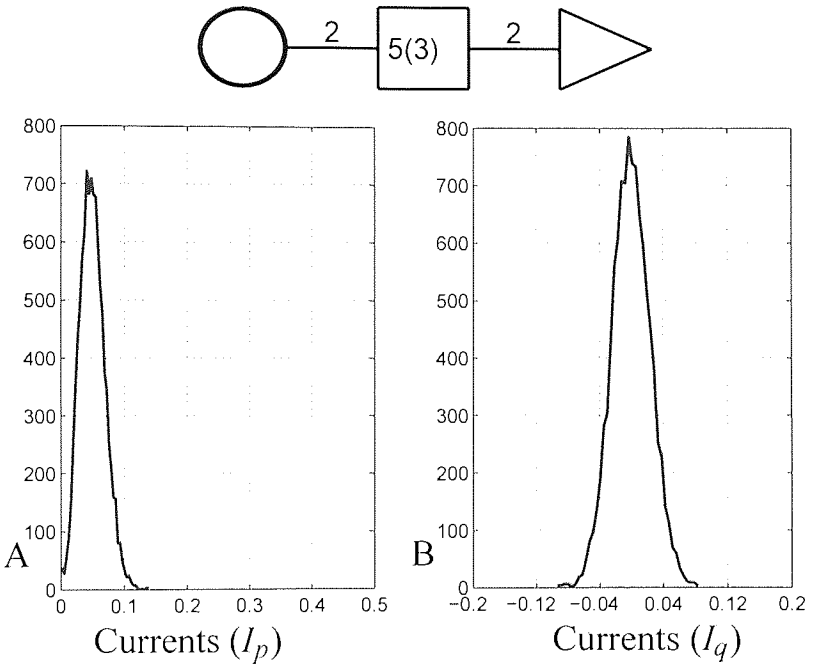

Figure 3.7: Histograms of distributions of individual currents obtained via population dynamics. Consumption $\underline{I_r = 0.1}$, case $c_p = 2, c_q = 5(3), c_r = 2, R = 1$. Each producer has exactly 2 links, average connectivity in distributors network is 5 and lowest connectivity is 3, each receiver has exactly 2 links. A: Distribution of currents in the producer-distributor network. B: Distribution of currents in the distribution network. Solid vertical lines depict mean of distributions while shaded areas highlight a range of 2 units of standard deviation wide.

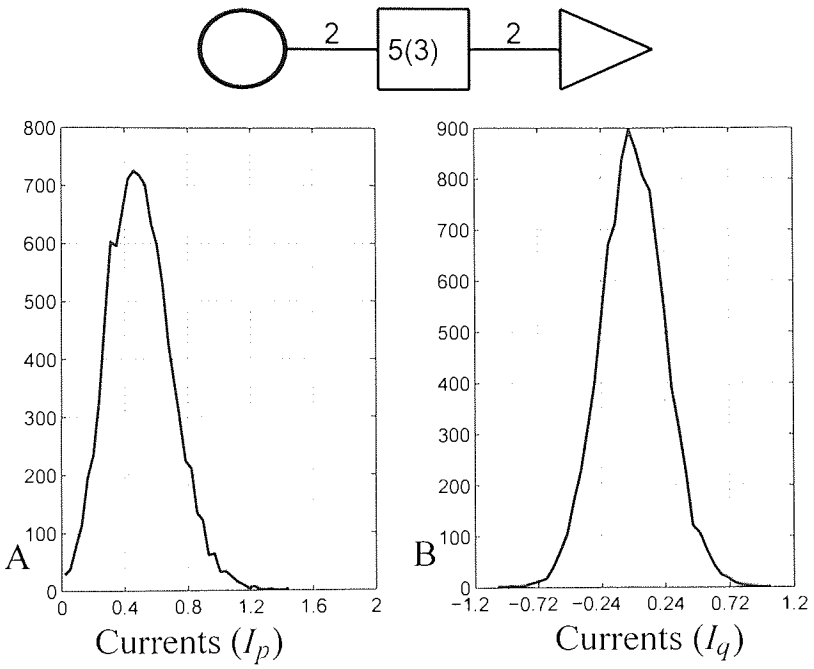

Figure 3.8: Histograms of distributions of individual currents obtained via population dynamics. Consumption $I_r = 1.0$, case $c_p = 2$, $c_q = 5(2)$, $c_r = 2$, $R = 1$. Each producer has exactly 2 links, average connectivity in distributors network is 5 and lowest connectivity is 3, each receiver has exactly 2 links. A: Distribution of currents in the producer-distributor network. B: Distribution of currents in the distribution network. Solid vertical lines depict mean of distributions while shaded areas highlight a range of 2 units of standard deviation wide.

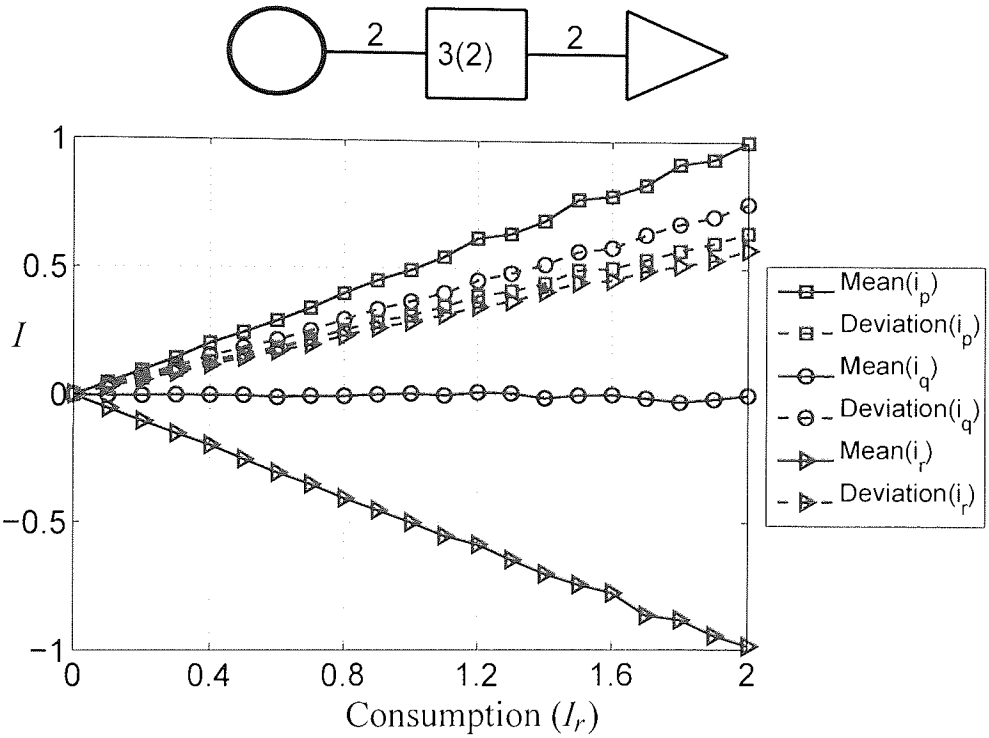

Figure 3.9: Distributions of individual currents obtained via population dynamics, case $c_p = 2$, $c_q = 3(2)$, $c_r = 2$, $R = 1$. Each producer has exactly 2 links, average connectivity in distributors network is 3 and lowest connectivity is 2, each receiver has exactly 2 links. Size of the population is 10000. We do 100 equilibrating sweeps and 100 measuring sweeps. Both the means and the standard deviations of distributions of currents exhibit linear dependence on consumption level.

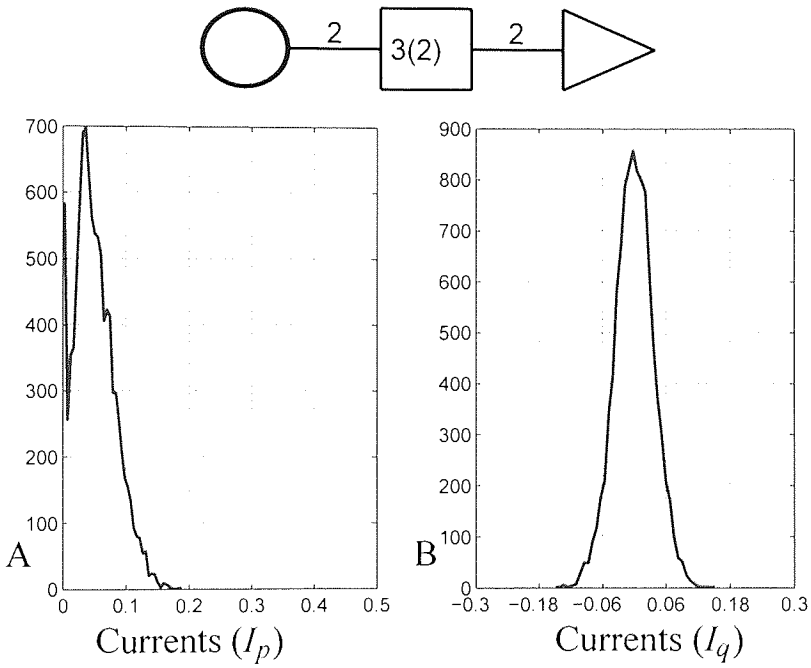

Figure 3.10: Histograms of distributions of individual currents obtained via population dynamics. Consumption $I_r = 0.1$, case $c_p = 2$, $c_q = 3(2)$, $c_r = 2$, $R = 1$. Each producer has exactly 2 links, average connectivity in distributors network is 3 and lowest connectivity is 2, each receiver has exactly 2 links. A: Distribution of currents in the producer-distributor network. B: Distribution of currents in the distribution network. Solid vertical lines depict mean of distributions while shaded areas highlight a range of 2 units of standard deviation wide.

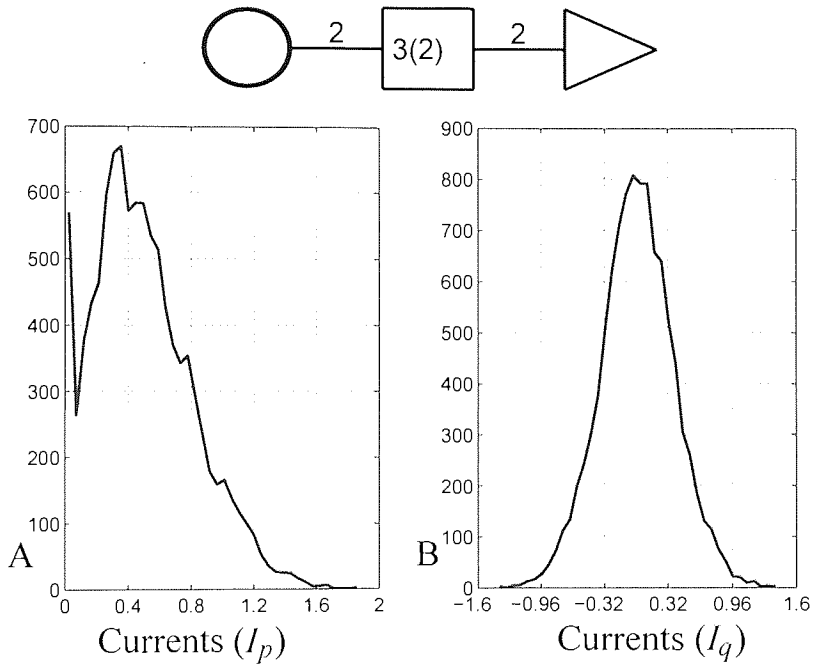

Figure 3.11: Histograms of distributions of individual currents obtained via population dynamics. Consumption $I_r = 1.0$, case $c_p = 2$, $c_q = 3(2)$, $c_r = 2$, $R = 1$. Each producer has exactly 2 links, average connectivity in distributors network is 3 and lowest connectivity is 2, each receiver has exactly 2 links. A: Distribution of currents in the producer-distributor network. B: Distribution of currents in the distribution network. Solid vertical lines depict mean of distributions while shaded areas highlight a range of 2 units of standard deviation wide.

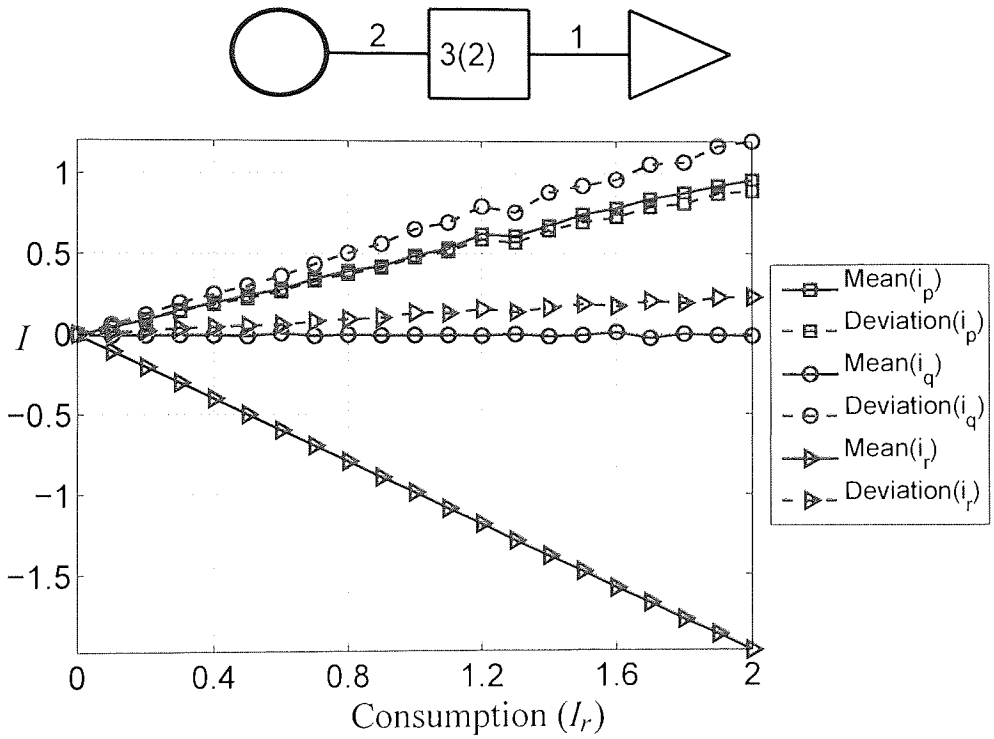

Figure 3.12: Distributions of individual currents obtained via population dynamics, case $c_p = 2$, $c_q = 3(2)$, $c_r = 2$, $R = 1$. Each producer has exactly 2 links, average connectivity in distributors network is 3 and lowest connectivity is 2, each receiver has exactly 1 link. Size of the population is 10000. We do 100 equilibrating sweeps and 100 measuring sweeps. Both the means and the standard deviations of distributions of currents exhibit linear dependence on consumption level.

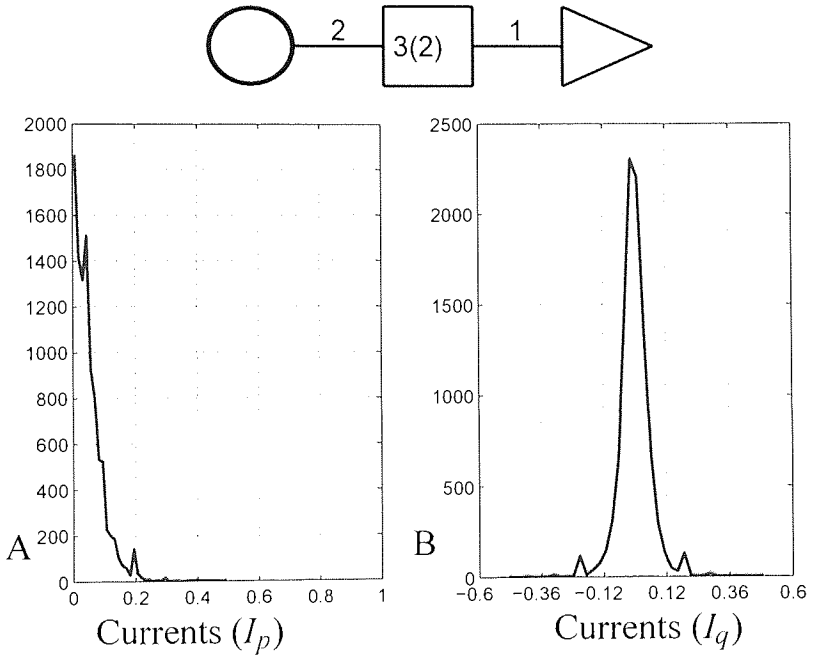

Figure 3.13: Histograms of distributions of individual currents obtained via population dynamics. Consumption $I_r = 0.1$, case $c_p = 2$, $c_q = 3(2)$, $c_r = 1$, $R = 1$. Each producer has exactly 2 links, average connectivity in distributors network is 3 and lowest connectivity is 2, each receiver has exactly 1 link. A: Distribution of currents in the producer-distributor network. B: Distribution of currents in the distribution network. Solid vertical lines depict mean of distributions while shaded areas highlight a range of 2 units of standard deviation wide.

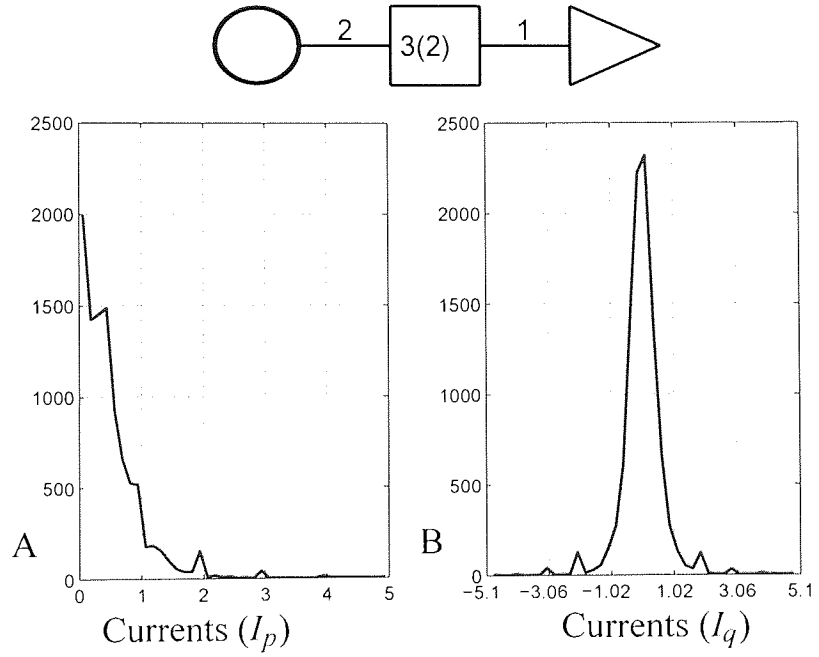

Figure 3.14: Histograms of distributions of individual currents obtained via population dynamics. Consumption $I_r = 1.0$, case $c_p = 2$, $c_q = 3(2)$, $c_r = 1$, $R = 1$. Each producer has exactly 2 links, average connectivity in distributors network is 3 and lowest connectivity is 2, each receiver has exactly 1 link. A: Distribution of currents in the producer-distributor network. B: Distribution of currents in the distribution network. Solid vertical lines depict mean of distributions while shaded areas highlight a range of 2 units of standard deviation wide.

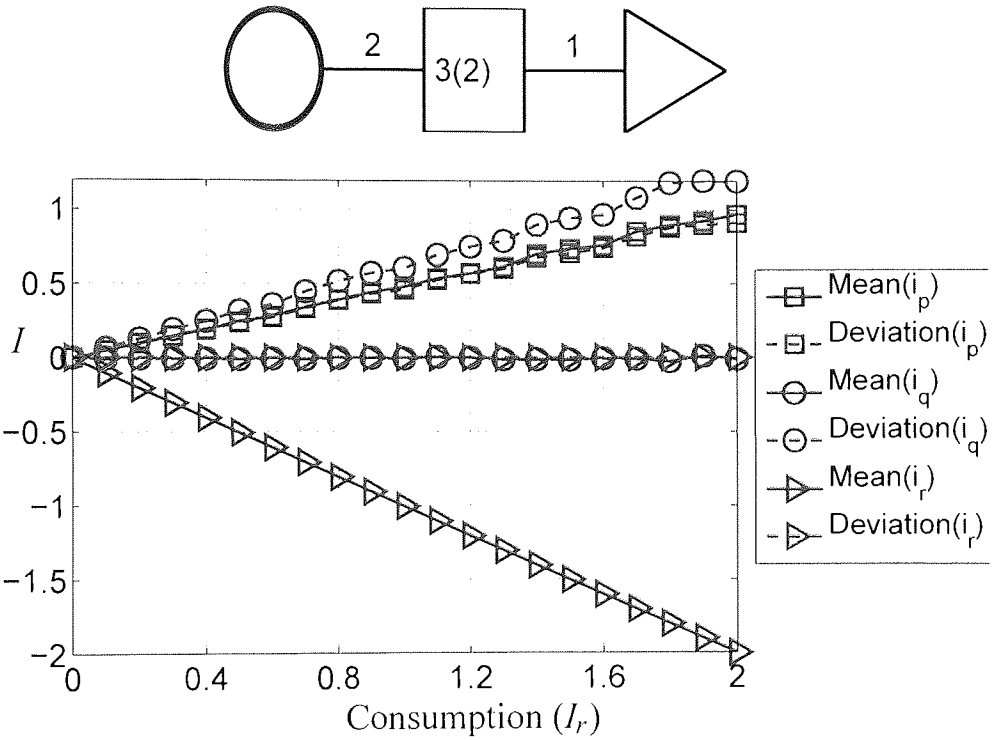

Figure 3.15: Distributions of individual currents obtained via population dynamics, case $c_p = 2$, $c_q = 3(2)$, $c_r = 1$, $R \in (0.5 : 1.5)$. Each producer has exactly 2 links, average connectivity in distributors network is 3 and lowest connectivity is 2, each receiver has exactly 1 link. Size of the population is 10000. We do 100 equilibrating sweeps and 100 measuring sweeps. Both the means and the standard deviations of distributions of currents exhibit linear dependence on consumption level.

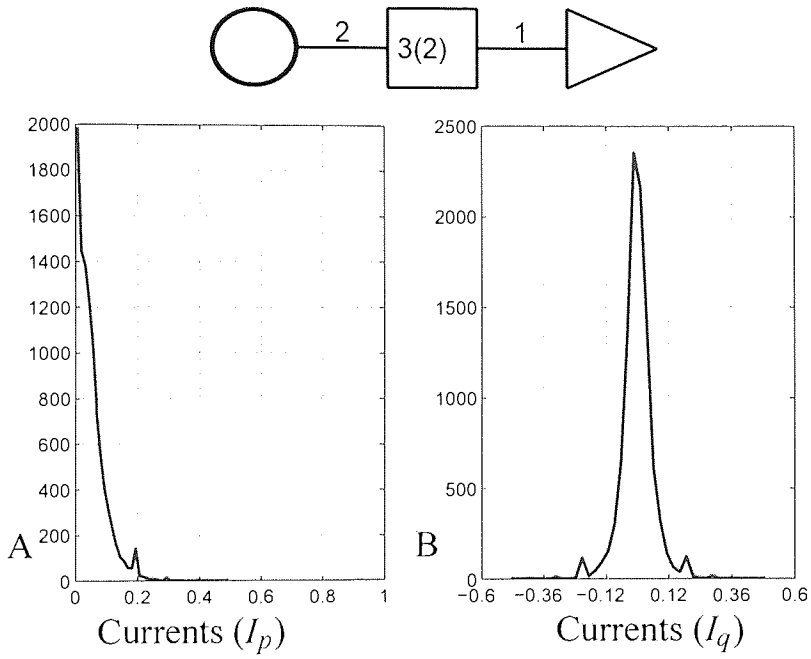

Figure 3.16: Histograms of distributions of individual currents obtained via population dynamics. Consumption $I_r = 0.1$, case $c_p = 2$, $c_q = 3(2)$, $c_r = 1$, $R \in (0.5 : 1.5)$. Each producer has exactly 2 links, average connectivity in distributors network is 3 and lowest connectivity is 2, each receiver has exactly 1 link. A: Distribution of currents in the producer-distributor network. B: Distribution of currents in the distribution network. Solid vertical lines depict mean of distributions while shaded areas highlight a range of 2 units of standard deviation wide.

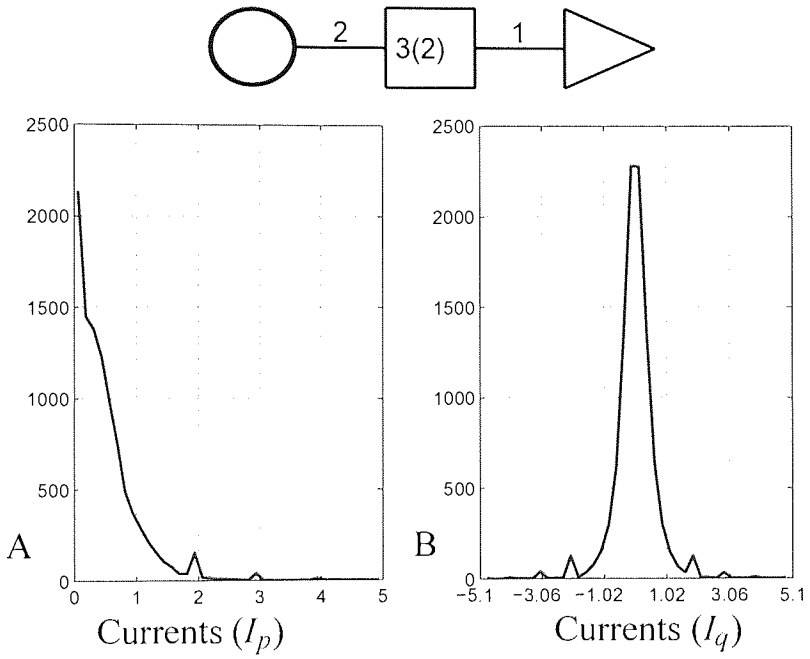

Figure 3.17: Histograms of distributions of individual currents obtained via population dynamics. Consumption $I_r = 1.0$, case $c_p = 2$, $c_q = 3(2)$, $c_r = 1$, $R \in (0.5 : 1.5)$. Each producer has exactly 2 links, average connectivity in distributors network is 3 and lowest connectivity is 2, each receiver has exactly 1 link. A: Distribution of currents in the producer-distributor network. B: Distribution of currents in the distribution network. Solid vertical lines depict mean of distributions while shaded areas highlight a range of 2 units of standard deviation wide.

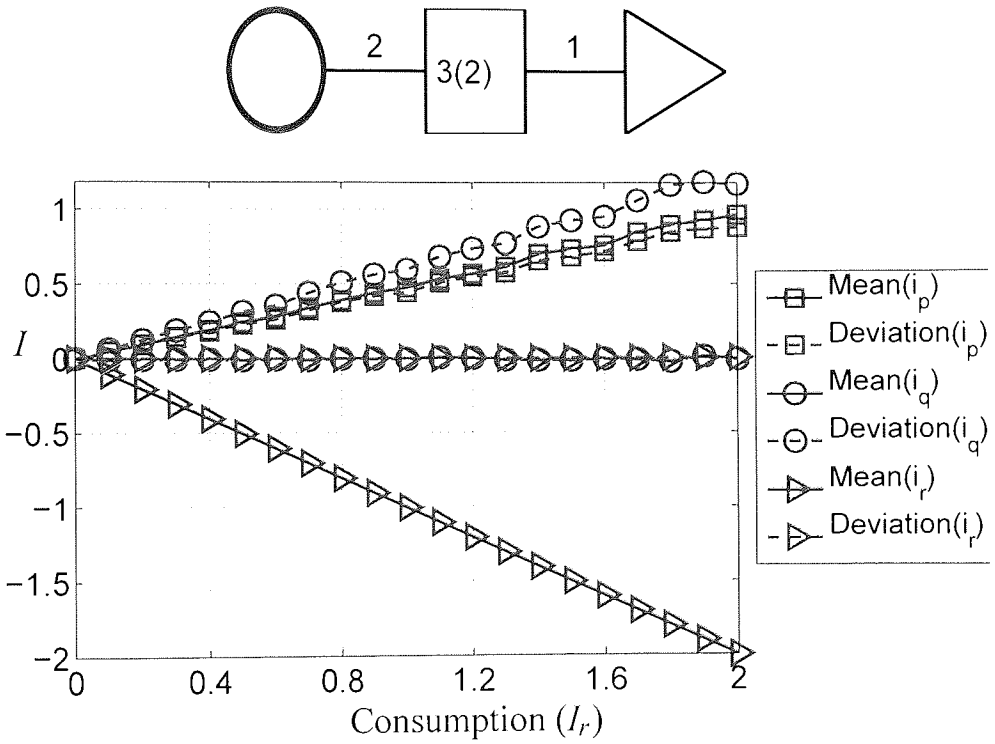

Figure 3.18: Distributions of individual currents obtained via population dynamics, case $c_p = 2$, $c_q = 3(2)$, $c_r = 1$, consumption $I_r \in \left[I \pm \frac{1}{2}I\right]$. Each producer has exactly 2 links, average connectivity in distributors network is 3 and lowest connectivity is 2, each receiver has exactly 1 link. Size of the population is 10000. We do 100 equilibrating sweeps and 100 measuring sweeps. Both the means and the standard deviations of distributions of currents exhibit linear dependence on consumption level.

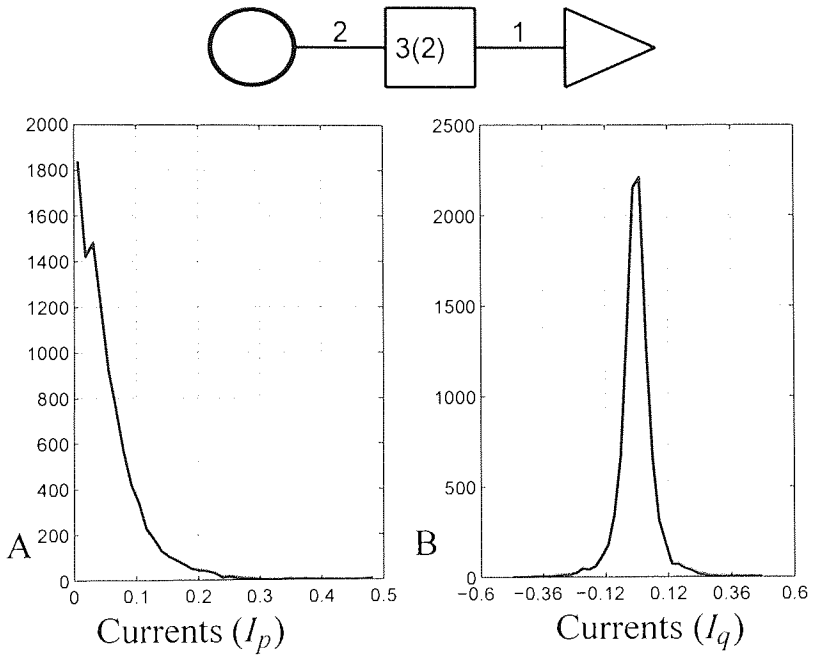

Figure 3.19: Histograms of distributions of individual currents obtained via population dynamics. Consumption $I_r = 0.1$, case $c_p = 2$, $c_q = 3(2)$, $c_r = 1$, $R = 1$, $I_r \in (0.05 : 0.15)$. Each producer has exactly 2 links, average connectivity in distributors network is 3 and lowest connectivity is 2, each receiver has exactly 1 link. A: Distribution of currents in the producer-distributor network. B: Distribution of currents in the distribution network. Solid vertical lines depict mean of distributions while shaded areas highlight a range of 2 units of standard deviation wide.

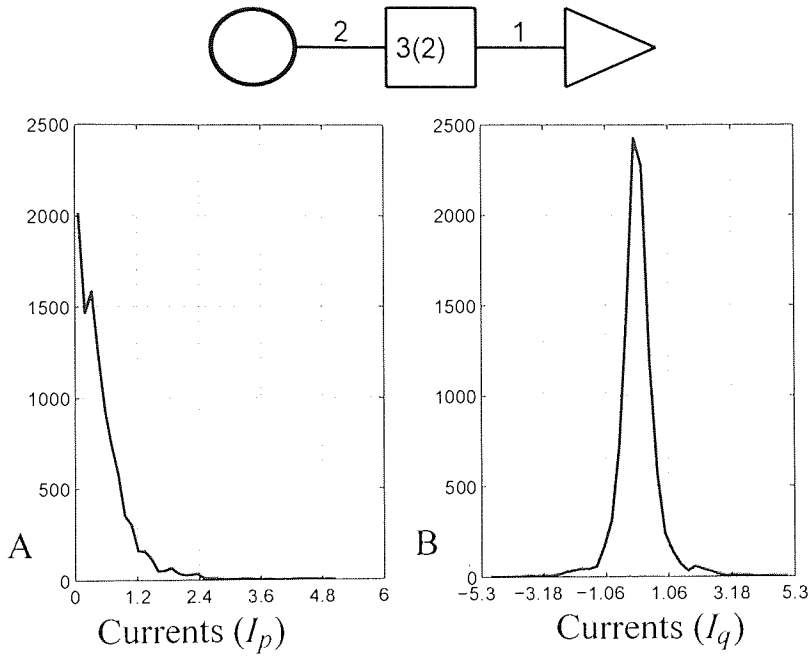

Figure 3.20: Histograms of distributions of individual currents obtained via population dynamics. Consumption $I_r = 1.0$, case $c_p = 2, c_q = 3(2), c_r = 1, R = 1, I_r \in (0.5 : 1.5)$. Each producer has exactly 2 links, average connectivity in distributors network is 3 and lowest connectivity is 2, each receiver has exactly 1 link. A: Distribution of currents in the producer-distributor network. B: Distribution of currents in the distribution network. Solid vertical lines depict mean of distributions while shaded areas highlight a range of 2 units of standard deviation wide.

We also calculate the distributions of loads per node in each subnetwork (see figures (3.21)-(3.22)). Load per node is the amount of net current each node handles. The **load per node** could be applied if one wants to concentrate on the node-associated properties of the network, i.e. monitor critical load. These distributions have similar properties to the distributions of currents.

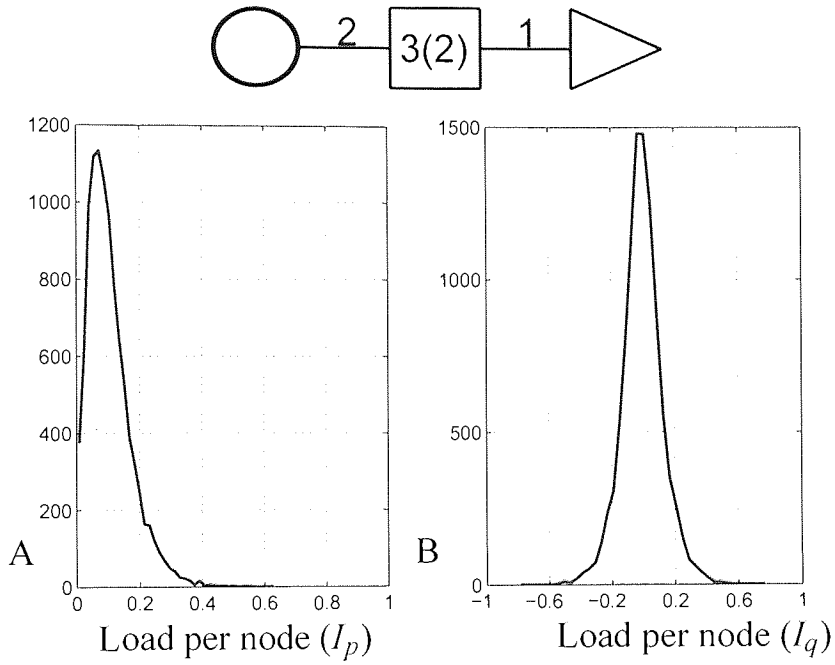

Figure 3.21: Histograms of load per node obtained via population dynamics. Consumption $I_r = 0.1$, case $c_p = 2$, $c_q = 3(2)$, $c_r = 2$, $R = 1$, $I_r \in (0.05 : 0.15)$. Each producer has exactly 2 links, average connectivity in distributors network is 3 and lowest connectivity is 2, each receiver has exactly 1 link. A: Distribution of loads per producer node. B: Distribution of loads per distribution node (This load does not include currents from producers or to receivers).

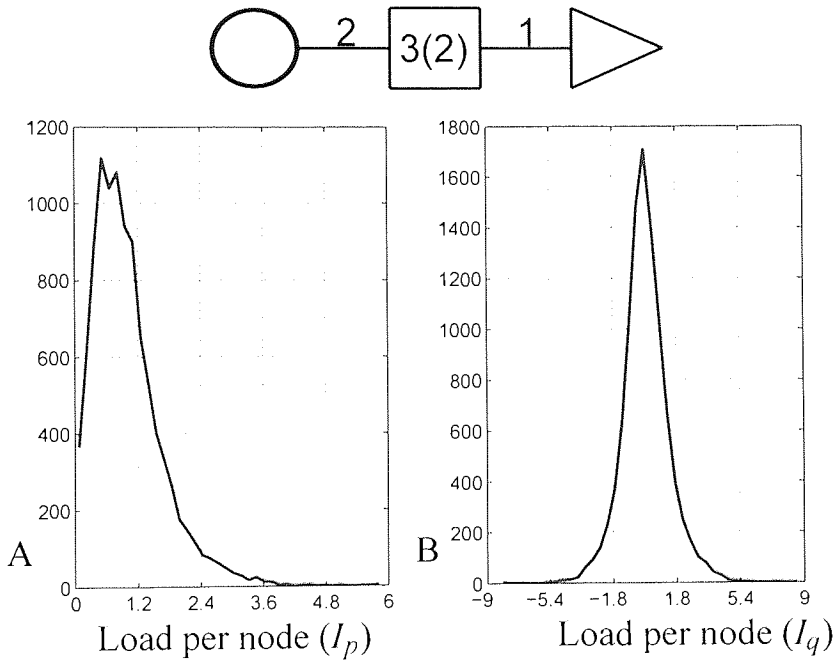

Figure 3.22: Histograms of loads per node obtained via population dynamics. Consumption $I_r = 1.0$, case $c_p = 2$, $c_q = 3(2)$, $c_r = 2$, $R = 1$, $I_r \in (0.5 : 1.5)$. Each producer has exactly 2 links, average connectivity in distributors network is 3 and lowest connectivity is 2, each receiver has exactly 1 link. A: Distribution of loads per producer node. B: Distribution of loads per distribution node (This load does not include currents from producers or to receivers).

3.4.3 Discussion and Conclusions

We have investigated the properties of the DC-like distribution networks without any constraints on link capacity (IC model). The structure of the whole network is assumed to be separable into three functionally distinctive subnetworks. The core is a distribution subnetwork that connects producers and receivers in the system. We analysed different connectivity models for the distribution subnetwork with different combinations of connectivities to producers and receivers. To analyse such systems using equilibrium statistical mechanics, we use the replica method for finitely connected random graphs.

The global properties of interest are distributions of currents in each subnetwork and the distribution of the node loads. We analyse these distributions and dependencies on the system macroparameters. The key macroparameters are connectivities of subnetworks, distribution of link resistances and distribution of levels of demand.

The key observable properties show a linear dependence on the level of demand. As there is no constraints on the link capacity, the currents are able to adapt according to a global minimal dissipation requirement. We monitor the mean and standard deviation of each subnetwork's flow. The increase in the level of demand results in a wider distributions of currents in all subnetworks.

The structural characteristics are also in line with the general observations of distribution systems. We show examples of the beneficial role of redundancy. The increase of average connectivity in any of the subnetworks results in narrower current distributions, not only for this subnetwork, but also narrows the current distributions in other subnetworks.

For each subnetwork, the mean of the distribution of currents in the network is found to exhibit linear dependency on the subnetworks connectivity. However, the standard deviation shows non-trivial dependence on the connectivities and distributions of resistances and levels of demand. We observe qualitatively similar trends for the distributions of node loads in each subnetwork.

Employing an IC model allows us to find optimal distributions of currents in the network. While the absence of any restriction on the capacity of individual elements is not

realistic, yet the analysis of real networks may be achieved. Thus we can assess the spread of currents in the network, and monitor occurrences of currents that exceed some threshold (the threshold represents capacity of the links for example). Such an examination could be beneficial from the design point of view. Both individual characteristics of network elements and network structure may need adjustments for the required flow of currents in the system, or for the existing networks, safe levels of distribution may be obtained.

Finally, if load criticality is the main interest, one may chose to concentrate on the load per node distributions.

3.5 Case 2: Finite link capacity (FC model)

In this section we will consider modification of the (IC) model with a limit on the capacity of links. The maximum capacity is defined in terms of the maximum current that can be passed through the link. We refer to this model as the **Finite Capacity** model (FC).

Unlike the case of harmonic interactions the full functional approach must be applied to find a solution of equations (3.44)-(3.47).

With added local capacity constraint, the problem becomes an optimisation problem. It can be clearly seen that the system becomes spin glass like, in the sense that it shows frustration. Indeed, while in the harmonic case the local distribution constraints could be easily satisfied, the ground state energy corresponds to the minimum of dissipation in the system. However, with introduced limits on the link's capacity the global requirement of minimum dissipation of energy and the local distribution constraints are in direct conflict. At some stage (at some level of demand that passed from producers to receivers) it is likely that current distribution at nodes can not satisfy both requirements simultaneously. The global constraint which tries to split currents might be prevented from doing so by capacity constraint. Similarly, locally optimal flow might not be optimal for the whole system.

In spin glasses and systems that can be viewed as spin glasses frustration prevents finding true minima. As in the SK model one can observe either the spin glass phase or the

true ferromagnetic phase. In the SK model the current phase depends on the temperature and disorder and frustration in the system. While the ferromagnetic phase is characterised by a single ground state, the spin glass phase is usually associated with a large number of metastable states.

A qualitatively similar situation is found in hard optimisation problems. The large number of parameters and constraints in these problems can be thought of as disorder and frustration, and makes finding the true ground state a difficult task.

The practical approach usually followed in problems like TSP and satisfiability problems is to start with some initial configuration, and make small moves by flipping a single spin and see if it results in a better configuration [39, 62]. The better configuration is determined by some global cost function. The problem in this approach is the large number of local minima. Small moves prevent the system from overcoming barriers of locally confined minima. In the spin glasses the difficulty is mainly in the low temperature region, as the number of metastable states increases when the system gets frozen. However, for many optimisation problems the variations of the algorithm described before find near-optimal solutions. The typical procedure is to decrease the temperature slowly, in order to allow the system to settle. The ground state is then hopefully found at zero temperature. For the optimisation problem this would correspond to the true minima of cost function.

For the present model one might also consider an approach used in the harmonic case. The single-replica function might be represented as an expansion over a complete set of basis function. The saddle point equations are then transformed to a set of equations for the coefficients of the expansions. An approximation is achieved by truncating the function basis to a suitable size. Applied to glassy systems at finite temperature this procedure should lead to a sufficient description of the order parameters. However, one must make sure that the set of basis functions is well adapted to the problem studied [72]. Given that such truncated representation is coupled with the RS assumption, the quality of the solution must be checked carefully.

Therefore, we decided to adopt a full functional approach. Some care should be taken with the initialisation of single-replica functions. The form of these functions is naturally expected to be similar to the form used in the harmonic case. Initially we assume a

quadratic form, the final form is determined by population dynamics.

As in the case of the IC model we obtain distributions of currents in each subnetwork. To the existing statistical measures of these distributions we add another one - the **fraction of critical currents** f_{max} in the network. By monitoring $(f^p_{max}, f^q_{max}, f^r_{max})$ we are able to analyse development of critical currents in the system. By monitoring the mean and standard deviation of distributions we can compare the IC and FC models.

3.5.1 Calculation of integrals and population dynamics

The following calculations rely on obtaining value of integral in the large limit β through the constrained optimisation procedure. This procedure follows the same ideas as the saddle point method. We calculate the integral of an exponentially growing (decreasing) function that has unique global maximum (minimum). The value of the integral is estimated from the contribution at the optimal point (optimal single-replica functions), as the contribution of the single-replica functions that are far away from optimal point decays exponentially.

In (3.44) and (3.45) we perform an update of the conjugate single-replica functions. The trace over currents in the link weights and following updates as prescribed by (3.44) and (3.45) are accomplished in the following steps. Firstly, we calculate the most inner integral, by Gaussian integration for example. The capacity restriction is introduced through the integration limits. We assume the unit capacity of every link.

$$e^{-\beta f(x_i,x_j)} = \int_{-1}^{1} \mathrm{d}I_{ij} e^{-\beta(R_{ij}I_{ij}^2 + \mathbf{i}(x_i - x_j)I_{ij})}. \tag{3.62}$$

In (3.62) we use the fact that the difference $\mathbf{i}(x_i - x_j)$ is the voltage drop between two nodes. Therefore, the finite link capacity requirement $I \in [-1, 1]$ implies the following constraint:

$$|x_i - x_j| \leq 2R_{ij}. \tag{3.63}$$

$$e^{-\beta\hat{\psi}(x_j)} = \int_{x_j-2R_{ij}}^{x_j+2R_{ij}} \mathrm{d}x_i e^{-\beta\psi(x_i)-\beta f(x_i,x_j)}. \tag{3.64}$$

(3.64) is solved by maximisation of exponents inside integral. The optimal point (x_i^*) of the integral is found for each point x_j. The correct solution is obtained inside the interval $[-2R_{ij}, 2R_{ij}]$ or on the boundaries, as the (3.63) is KKT (Karush-Kuhn-Tucker) condition for this problem. Note that the limits of integration are dependent on the current point. Updates (3.64) are performed pointwise. The repetition of this procedure for each point x_j yields single update of single-replica function $\hat{\psi}(x)$.

Population dynamics updates (3.46)-(3.47) are also performed pointwise

$$\psi(x_i) = \sum_{l=1}^{L} \hat{\psi}_l(x_i), \quad \text{for distributors,} \tag{3.65}$$

$$\psi(x_i) = \sum_{l=1}^{L} \hat{\psi}_l(x_i) + V(x_i), \quad \text{for receivers.} \tag{3.66}$$

Due to pointwise updates of functions in population dynamics, the accuracy of the algorithm depends on the density and range of the grid, as well as population size in population dynamics. In order to improve speed in the (3.64) the quadratic interpolation has been used to find the critical point.

3.5.2 Calculation of observables

Calculation of the currents is done along the lines described in (3.62) and (3.64) . With added capacity restrictions the expression for $Z_2[\psi_i, \psi_j, U^{ij}]$ becomes

$$Z_2[\psi_i, \psi_j, U^{ij}] = \int_{-\infty}^{\infty} \mathrm{d}x_j \int_{x_j-2R}^{x_j+2R} \mathrm{d}x_i e^{-\beta(\psi_i(x_i)+\psi_j(x_j)} \int_{-1}^{1} \mathrm{d}I_{ij} e^{-\beta(R_{ij}I_{ij}^2+i(x_i-x_j)I_{ij})} \tag{3.67}$$

Here we perform integration twice over x_j and x_i. The value of Z_2 is calculated at the optimal point (x_i^*, x_j^*).To obtain distributions of currents we follow (3.50)-(3.55).

In simulations two outer integrals are calculated via the minimisation procedure on the grid. The size of the grid and the stepsize have been chosen in a way to yield a good

accuracy and speed.

3.5.3 Results

We solve saddle point equations (3.44)-(3.45) at zero temperature for various models of connectivities and distributions of the parameters R_{ij} and I_r using a population dynamics algorithm. The sise of populations in population dynamics is 1000 (single-replica functions). Once the stable distributions of the π's and $\hat{\pi}$'s have been obtained, we calculated relevant physical quantities: the distribution of currents (I_{qp}, I_{qs}, I_{qr}) and distribution of the node loads (I_p, I_q, I_r). In the figures, currents in the producer network are non-negative, in the distribution network are both positive and negative and in the receiver network are mainly non-positive[4].

We discuss results in terms of phase digrams in the space (c_p, c_r, c_q, I_r). We find that presentation of two dimensional diagrams in the plane (c_p, I_r) is sufficient for the qualitative analysis.

Results of the experiments with the following configurations of network parameters are presented

- $c_p = 1$, $c_q = 3(2)$, $c_r = 1$, see figures (3.28) and (3.29).
- $c_p = 1$, $c_q = 3(2)$, $c_r = 2$, see figures (3.30) and (3.31).
- $c_p = 2$, $c_q = 3(2)$, $c_r = 1$, see figures (3.32) and (3.33).
- $c_p = 2$, $c_q = 3(2)$, $c_r = 2$, see figures (3.25), (3.26), (3.27), (3.34) and (3.35).
- $c_q = 3(2)$, $c_r = 1$, see figure (3.36).
- $c_q = 3(2)$, $c_r = 2$, see figure (3.37).
- $c_q = 5(2)$, $c_r = 2$, see figure (3.38).
- $c_q = 5(3)$, $c_r = 2$, see figure (3.39).
- $c_q = 3(2)$, $c_r = 3$, see figure (3.40).

[4] In some cases both positive and negative currents are shown to be present in the receiver network, but this is due to round-off error as well as short equilibrating runs. We discuss this issue later in this section.

We obtain phase diagrams for any subnetwork, by monitoring the fraction of extreme currents in subnetworks. For relatively low levels of consumption we do not observe maximal currents, while for relatively high levels we detect a large number of maximal currents (see figures (3.25)- (3.27)). Therefore, we identify the point when the level of consumption triggers first maximal currents (see figures (3.28), (3.30), (3.32) and (3.34)).

In the phase diagram we plot a line - the critical level of consumption for each configuration of network parameters. The presence of maximal currents signals that some parts of the network reached their capacities, effectively indicating onset of the critical state. Further increase in levels of consumption just increases the strain on the network (see figures (3.36), (3.37), (3.38), (3.39) and (3.40)).

To produce a phase diagram for the whole network, we combine phase diagrams for each subnetwork. The region that lies below all lines is an operational region (O), while the rest may be classified as a critical region (C).

In some cases the subclassification of critical phase is possible. Indeed the boundary between the operational and critical states might be constructed from two lines that depict phase boundaries in subnetworks. In these cases we divide the critical region in two subcritical regions. Depending on which subnetwork develops extreme currents first we identify **P-critical, D-critical** and **R-critical** regions.

In cases where more than one critical region was found we can determine a point where phase boundaries of the corresponding subnetworks cross. This point indicates that both subnetworks develop extreme currents at the same level of consumption. Moving in either way from this point makes one of the subnetworks develop maximal currents before the others.

We have never found more than two different critical regions. Typically, for the unit link capacity in all subnetworks, we found P-critical and R-critical phases. By choosing different capacities in each subnetwork we can obtain all combinations of subdivision of critical phase.

We also monitor the mean and standard deviation of current distributions (see figures (3.29), (3.31), (3.33) and (3.35)). We observe in the operational phase (O) both statistical measures grow linearly with an increase of the level of consumption. In fact, we achieve

agreement with the corresponding measures in the IC model.

Going into the critical phase we observe nonlinear changes in both the mean and standard deviations of distributions of currents. In the critical phase the redistribution constraints are not observed as well, which indicates that replica symmetry does not hold in this region. Here, we can draw an analogy with spin glasses. Namely, the solution of the SK model does not yield physical properties of a material in the spin glass phase, while the solutions in magnetic phases is physical.

For the analysis of network stability against overloading, the classification in terms of operational (O) and critical (C) phases seems to be sufficient. The solutions that corresponds to the operational state satisfies all constraints, while the boundary between phases indicates the onset of instability.

As in the IC model we observe a beneficial role of redundancy. An increase of connectivity in any of subnetworks results in narrower distributions of currents in all subnetworks. Correspondingly, a wider spread of resistances or levels of consumption results in wider distributions of currents.

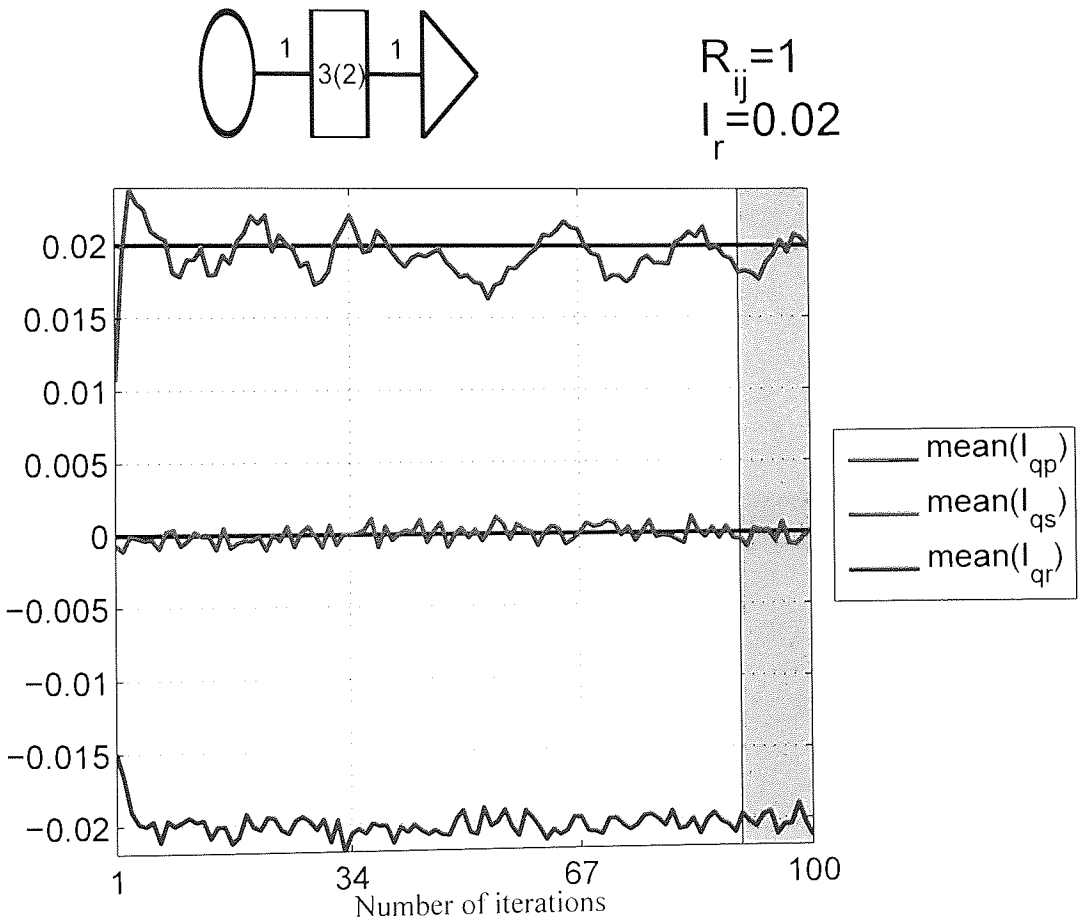

Figure 3.23: Population dynamics updates for three distributions of currents in the network. Average currents. The case $c_p = 1$, $c_q = 3(2)$, $c_r = 1$ and the level of demand is $I_r = 0.02$. Algorithm exhibits good convergence. The measurements are taken in the shaded area only.

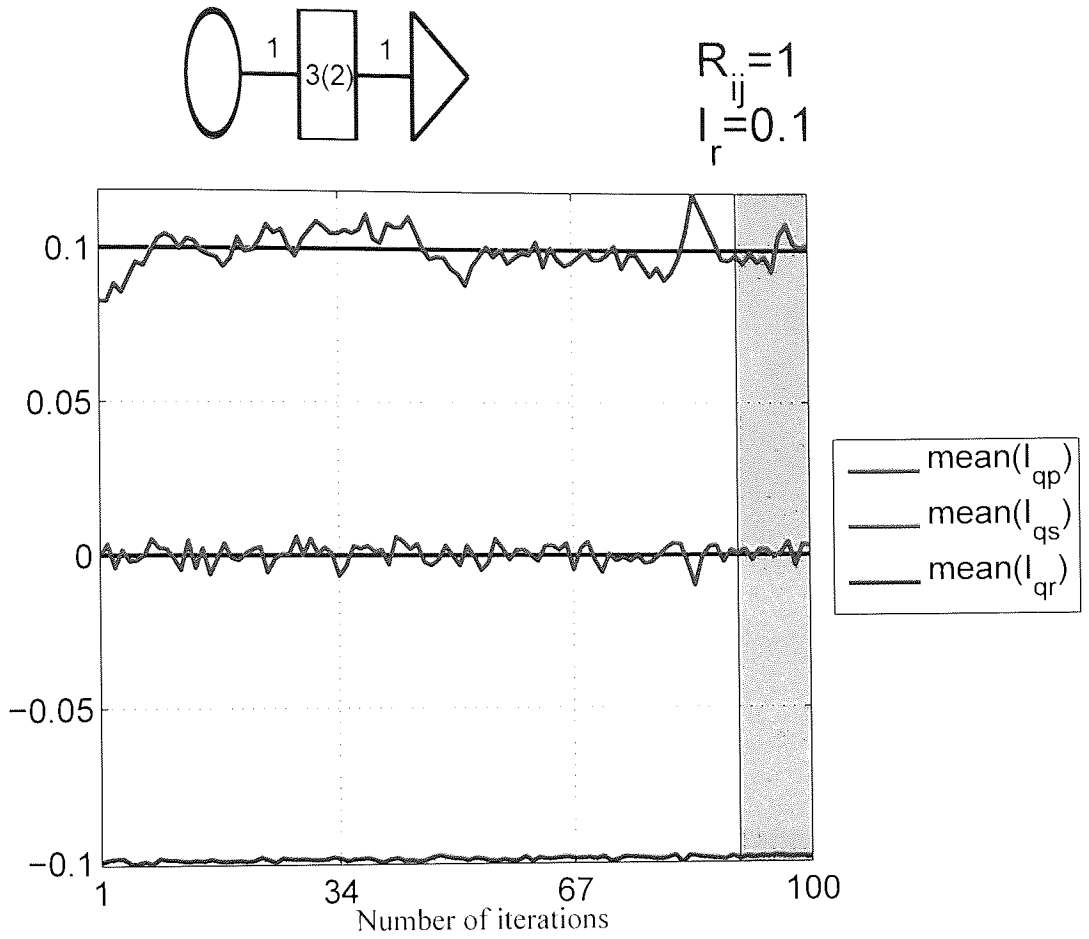

Figure 3.24: Population dynamics updates for three distributions of currents in the network. Average currents. The case $c_p = 1$, $c_q = 3(2)$, $c_r = 1$ and the level of demand is $I_r = 0.1$. Algorithm exhibits good convergence. The measurements are taken in the shaded area only.

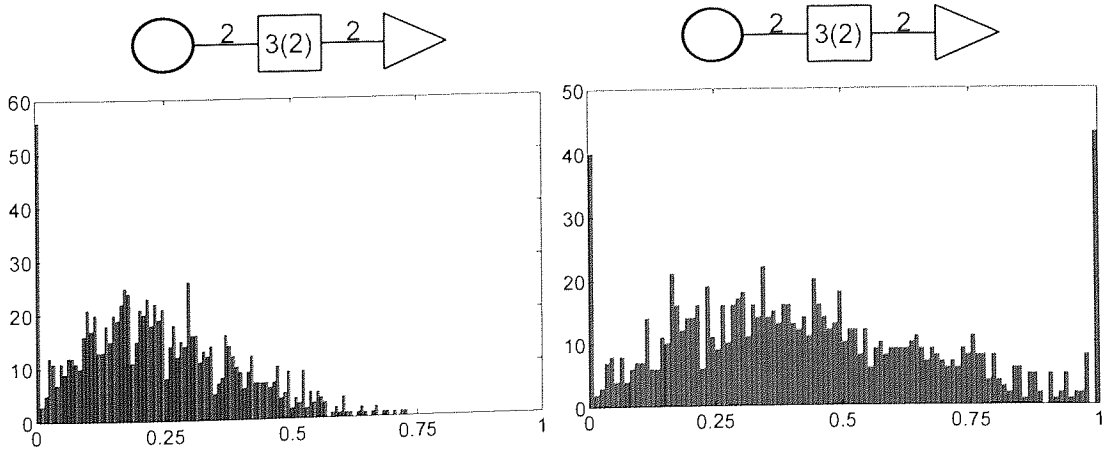

Figure 3.25: Distribution of currents in producer network. The case $c_p = 2$, $c_q = 3$, $c_r = 2$ and the level of demand is 0.5 and 0.9 respectively .

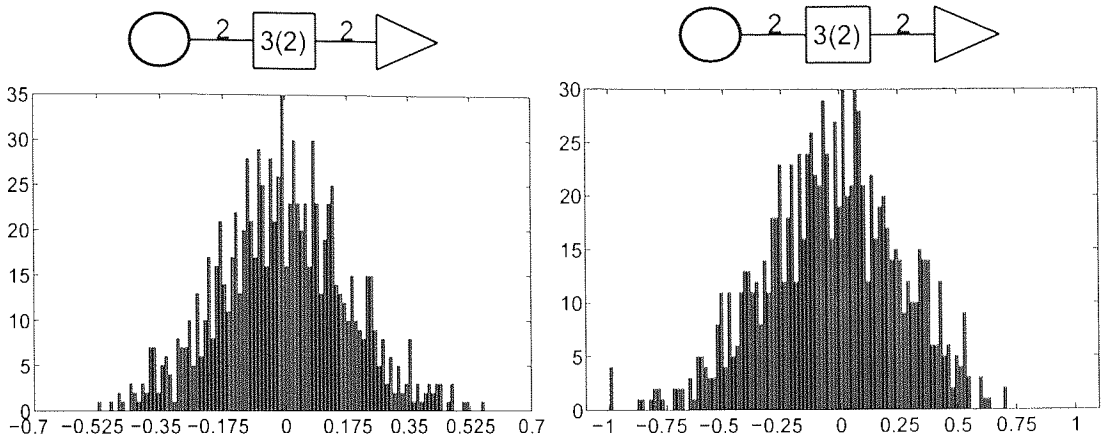

Figure 3.26: Distribution of currents in distribution network. The case $c_p = 2$, $c_q = 3$, $c_r = 2$ and the level of demand is 0.5 and 0.9 respectively .

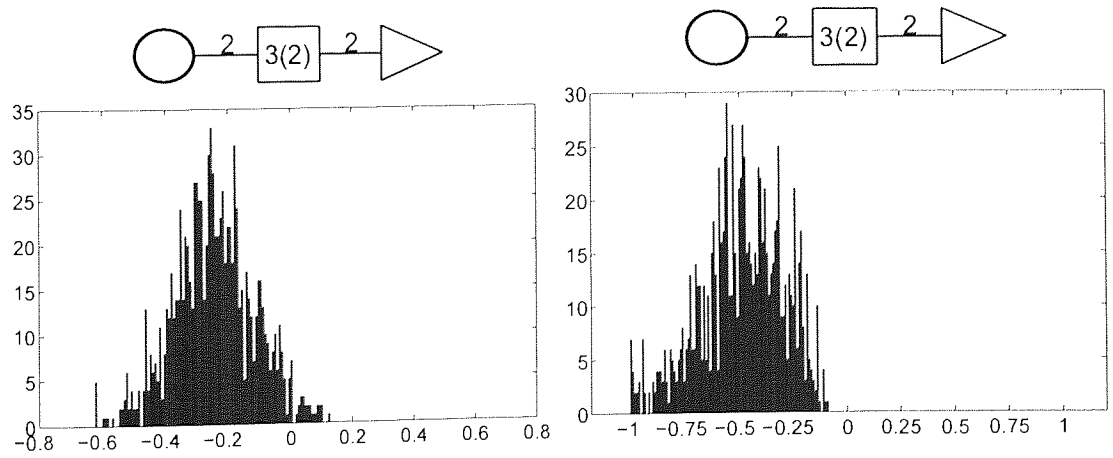

Figure 3.27: Distribution of currents in receiver network. The case $c_p = 2$, $c_q = 3$, $c_r = 2$ and the level of demand is 0.5 and 0.9 respectively .

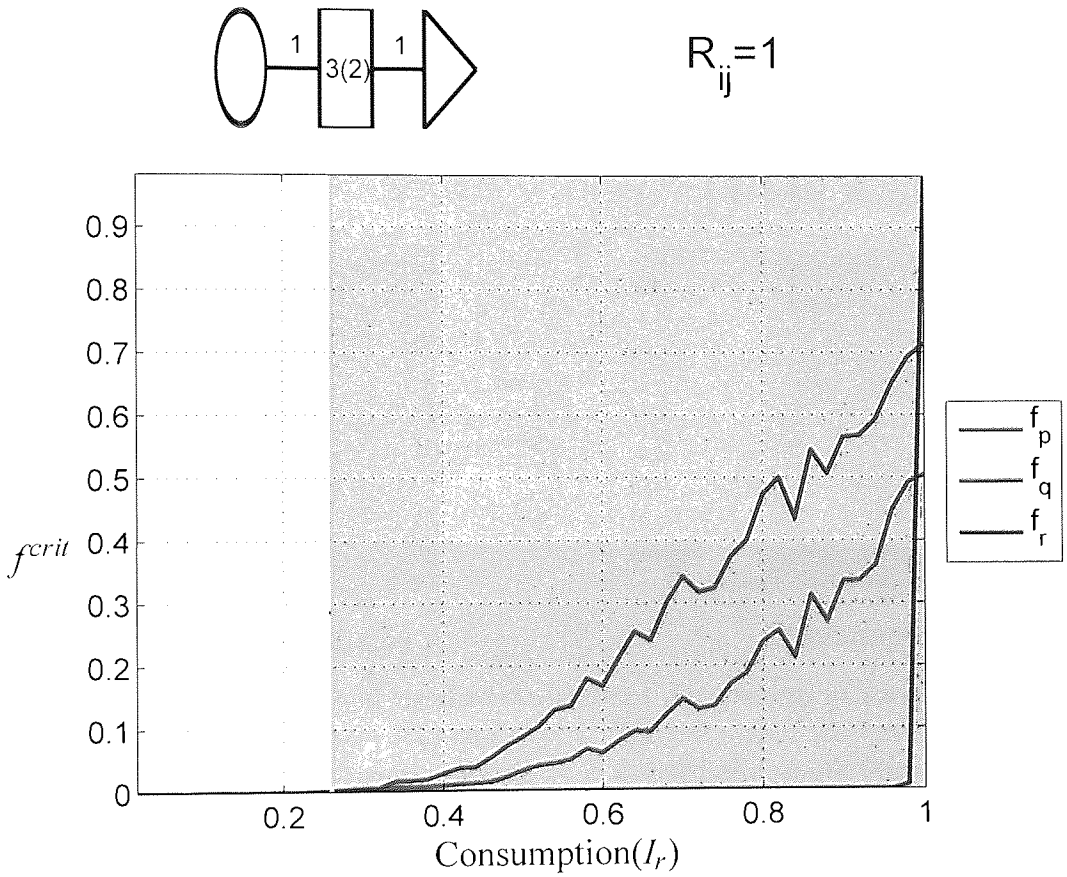

Figure 3.28: Fraction of critical currents (f^{crit}) vs. demand level (I_r) for each subnetwork, with $c_p = 1$, $c_q = 3(2)$ and $c_r = 1$. Fraction of critical currents in producer network (f_p), in distributor network (f_q) and in receiver network (f_r). By monitoring fraction of critical currents we calculate critical level of demand ($I_r^*$the vertical yellow line). Below the critical level of demand we do not find any critical currents in the network, above the critical level of demand (shaded area) we observe occurrence of critical currents. Consequently we classify two intervals of levels of demand (I_r) as operational and critical (below shaded area).

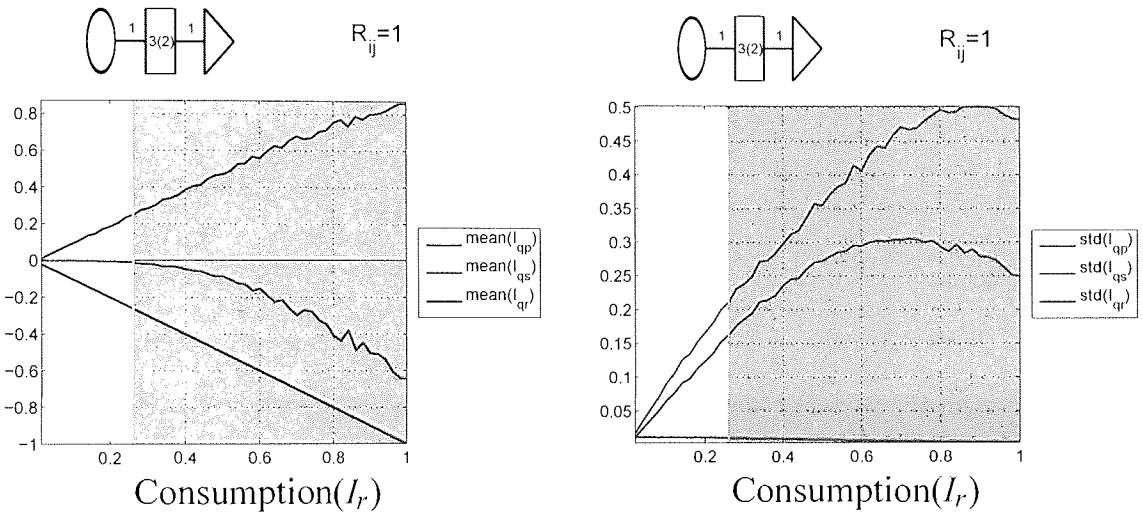

Figure 3.29: The mean and standard deviation of distributions of currents of each subnetwork, with $c_p = 1$, $c_q = 3(2)$ and $c_r = 1$. The left plane: the mean of distributions of currents in producer network (mean(I_{qp}), in distributor network (mean(I_{qs})) and in receiver network (mean(I_{qr})) . The right plane: the standard deviation of distributions of currents in producer network (std(I_{qp}), in distributor network (std(I_{qs})) and in receiver network (std(I_{qr})). The border between operational and critical phases is determined by first occurrences of critical currents in the network. Both statistics exhibit linear dependence on level of demand (I_r) in the operational phase. In the critical phase both statistics are nonlinear on level of demand (I_r). The negative average of currents in receiver network is due to current's definition.

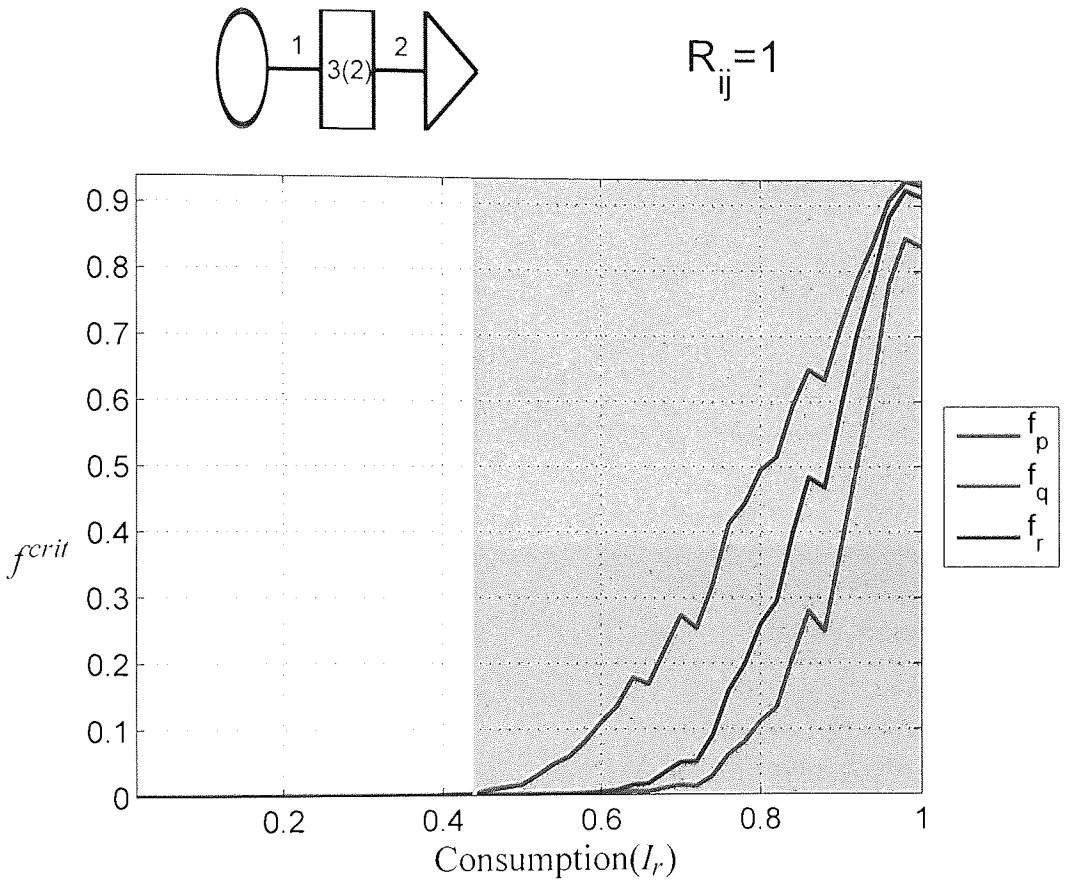

Figure 3.30: Fraction of critical currents (f^{crit}) vs. demand level (I_r) for each subnetwork, with $c_p = 1$, $c_q = 3$ and $c_r = 2$. Fraction of critical currents in producer network (f_p), in distributor network (f_q) and in receiver network (f_r). By monitoring fraction of critical currents we calculate critical level of demand ($I_r^*$the vertical yellow line). Below the critical level of demand we do not find any critical currents in the network, above the critical level of demand (shaded area) we observe occurrence of critical currents. Compared to 3.28 critical level of demand is higher due to the increase of the connectivity in the receiver network.

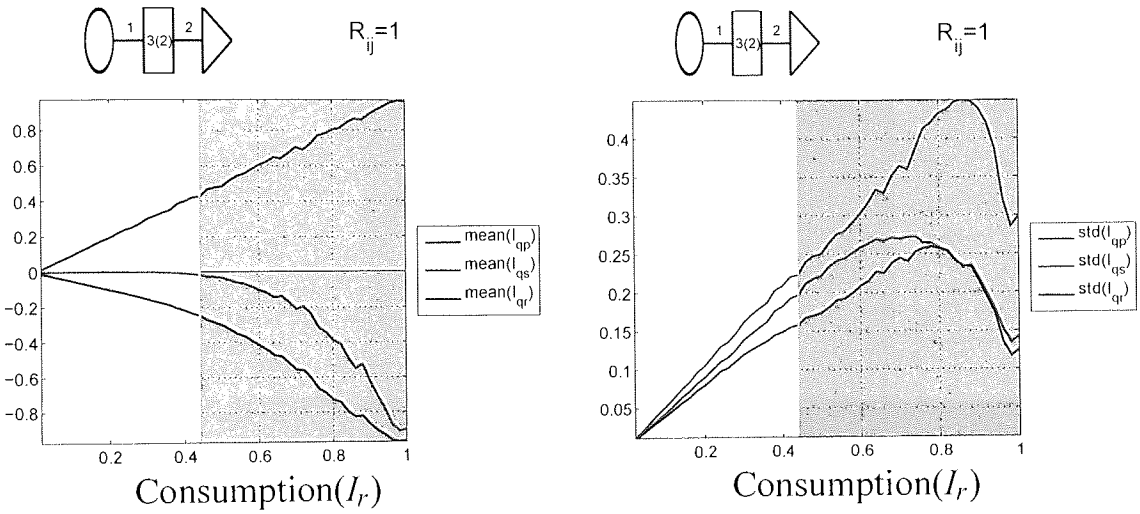

Figure 3.31: The mean and standard deviation of distributions of currents of each sub-network, with $c_p = 1$, $c_q = 3(2)$ and $c_r = 2$. The left plane: the mean of distributions of currents in producer network (mean(I_{qp}), in distributor network (mean(I_{qs})) and in receiver network (mean(I_{qr})) . The right plane: the standard deviation of distributions of currents in producer network (std(I_{qp}), in distributor network (std(I_{qs})) and in receiver network (std(I_{qr})). The border between operational and critical phases is determined by first occurrences of critical currents in the network. Both statistics exhibit linear dependence on level of demand (I_r) in the operational phase. In the critical phase both statistics are nonlinear on level of demand (I_r). The negative average of currents in receiver network is due to current's definition.

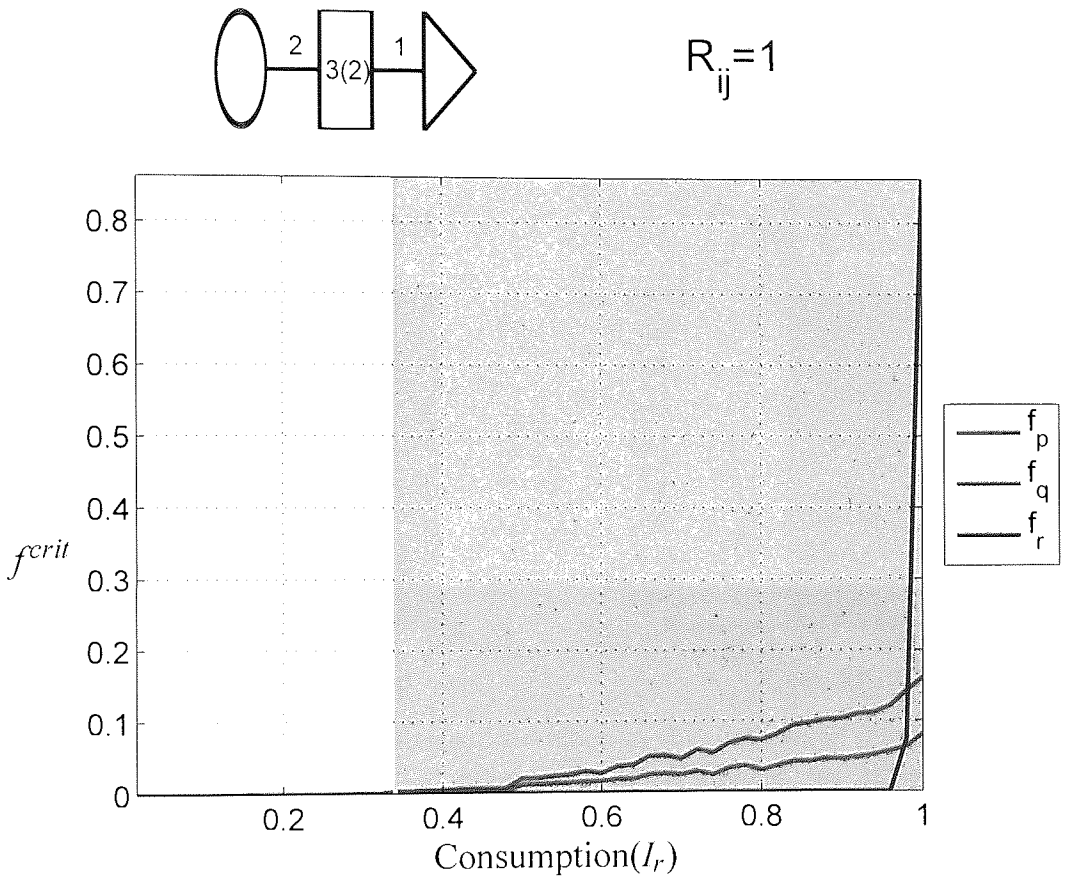

Figure 3.32: Fraction of critical currents (f^{crit}) vs. demand level (I_r) for each subnetwork, with $c_p = 2$, $c_q = 3$ and $c_r = 1$. Fraction of critical currents in producer network (f_p), in distributor network (f_q) and in receiver network (f_r). By monitoring fraction of critical currents we calculate critical level of demand ($I_r^*$the vertical yellow line). Below the critical level of demand we do not find any critical currents in the network, above the critical level of demand (shaded area) we observe occurrence of critical currents. Compared to 3.28 critical level of demand is higher due to the increase in the connectivity in the distributor network. Compared to 3.30 critical level of demand is lower. This means that the increase of connectivity in the distributor network is less beneficial than the increase of connectivity in the receiver network.

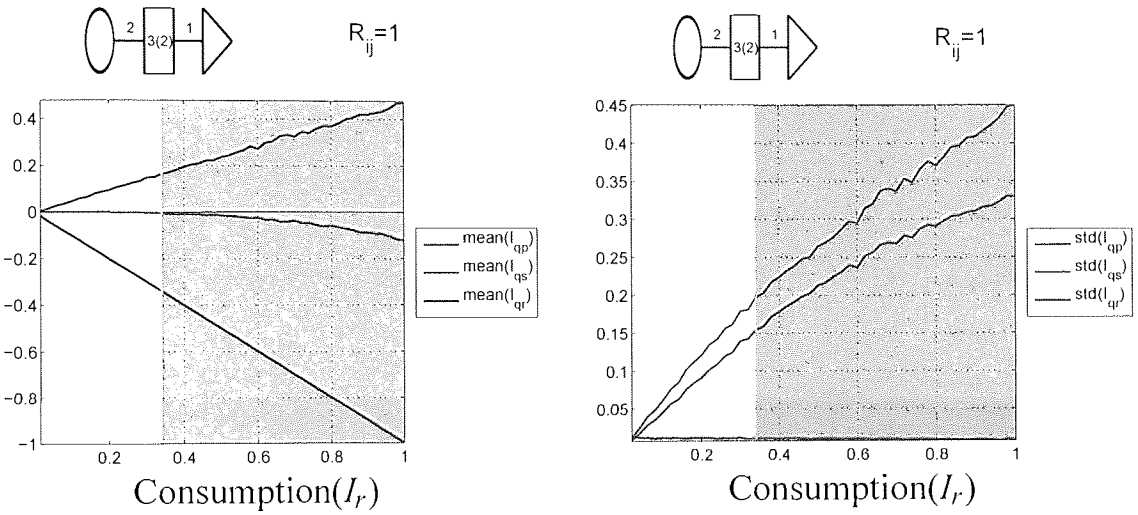

Figure 3.33: The mean and standard deviation of distributions of currents of each sub-network, with $c_p = 2$, $c_q = 3(2)$ and $c_r = 1$. The left plane: the mean of distributions of currents in producer network (mean(I_{qp}), in distributor network (mean(I_{qs})) and in receiver network (mean(I_{qr})) . The right plane: the standard deviation of distributions of currents in producer network (std(I_{qp}), in distributor network (std(I_{qs})) and in receiver network (std(I_{qr})). The border between operational and critical phases is determined by first occurrences of critical currents in the network. Both statistics exhibit linear dependence on level of demand (I_r) in the operational phase. In the critical phase both statistics are nonlinear on level of demand (I_r). The negative average of currents in receiver network is due to current's definition.

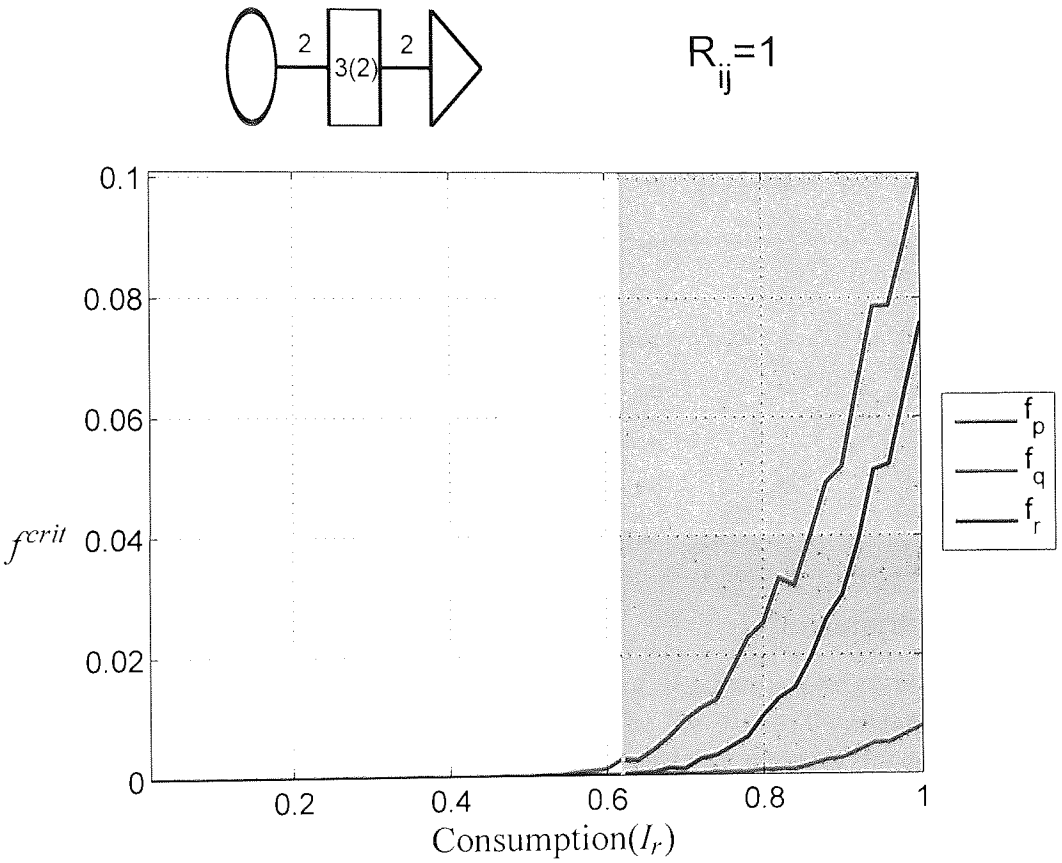

Figure 3.34: Fraction of critical currents (f^{crit}) vs. demand level (I_r) for each subnetwork, with $c_p = 2$, $c_q = 3(2)$ and $c_r = 2$. Fraction of critical currents in producer network (f_p), in distributor network (f_q) and in receiver network (f_r). By monitoring fraction of critical currents we calculate critical level of demand ($I_r^*$the vertical yellow line). Below the critical level of demand we do not find any critical currents in the network, above the critical level of demand (shaded area) we observe occurrence of critical currents. Compared to 3.28 critical level of demand is higher due the increase of the connectivity in the distributor and receiver networks.

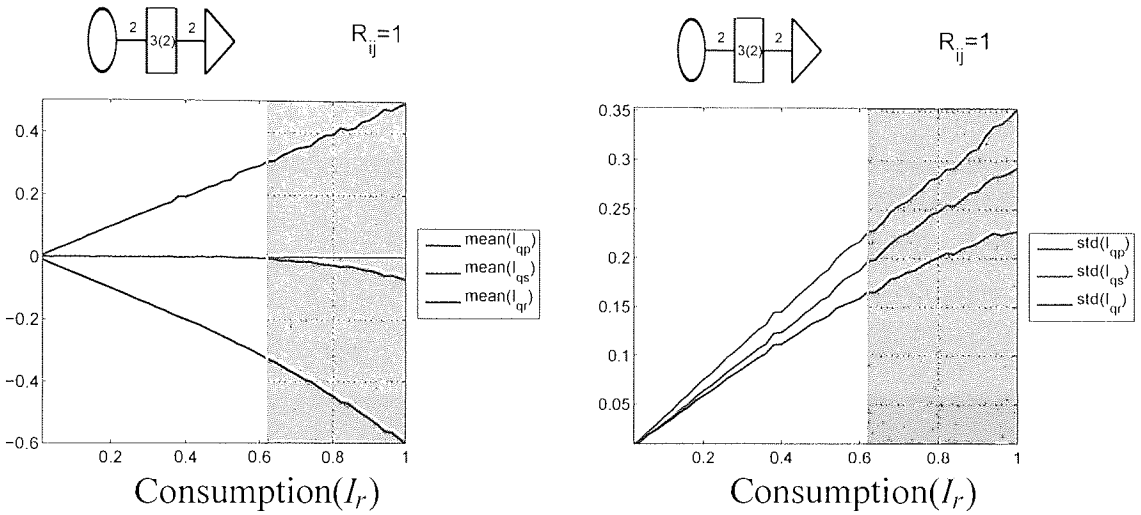

Figure 3.35: The mean and standard deviation of distributions of currents of each sub-network, with $c_p = 2$, $c_q = 3(2)$ and $c_r = 2$. The left plane: the mean of distributions of currents in producer network (mean(I_{qp}), in distributor network (mean(I_{qs})) and in receiver network (mean(I_{qr})) . The right plane: the standard deviation of distributions of currents in producer network (std(I_{qp}), in distributor network (std(I_{qs})) and in receiver network (std(I_{qr})). The border between operational and critical phases is determined by first occurrences of critical currents in the network. Both statistics exhibit linear dependence on level of demand (I_r) in the operational phase. In the critical phase both statistics are nonlinear on level of demand (I_r). The negative average of currents in receiver network is due to current's definition.

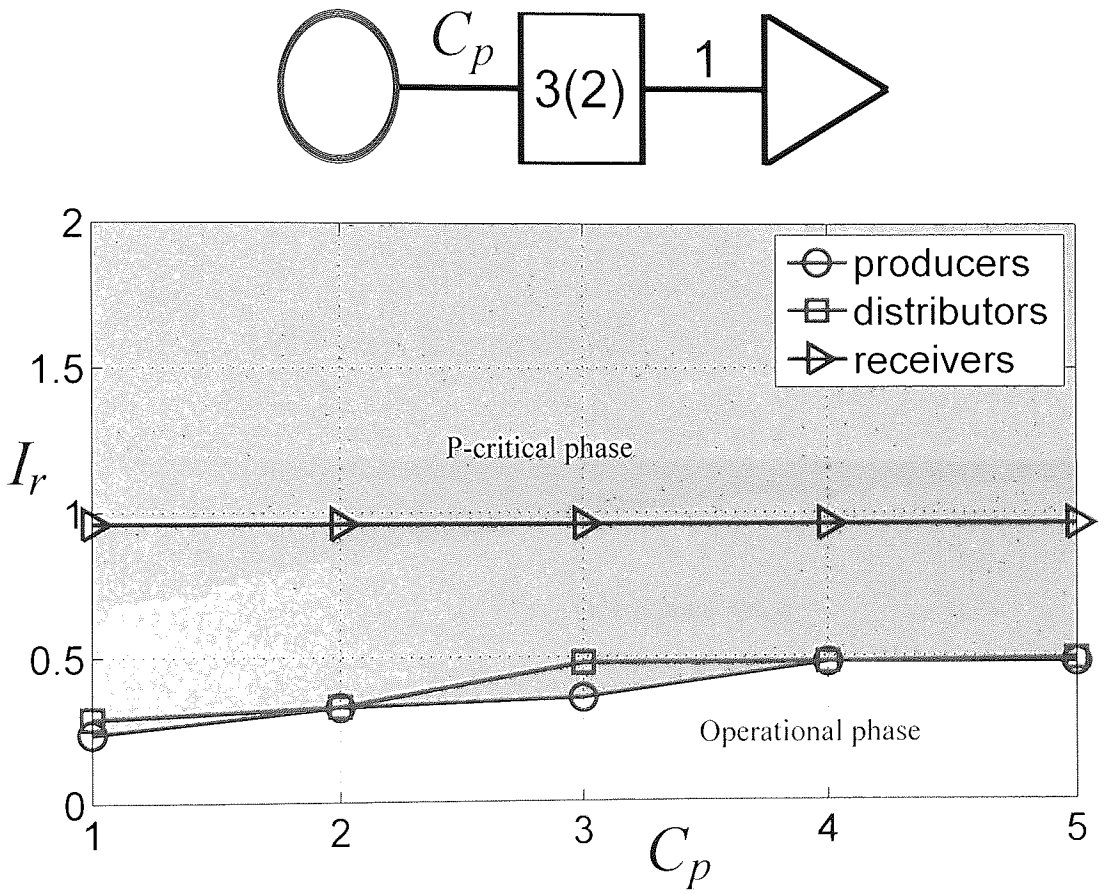

Figure 3.36: Phase diagram with $c_q = 3(2)$, $c_r = 1$, $R = 1$. Lines depict onset of the critical phase for each subnetwork. The lowest line indicates transition between operational and critical phases (shaded area). Only P-critical phase found.

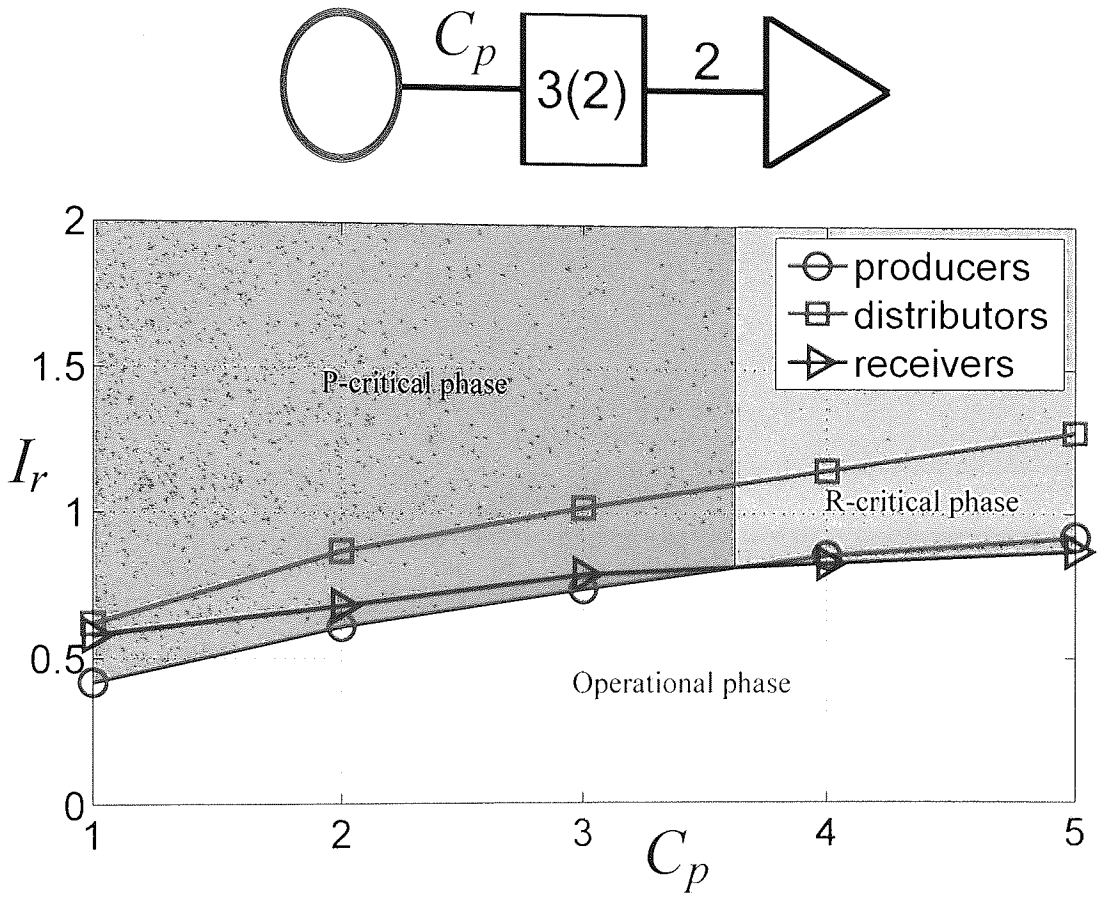

Figure 3.37: Phase diagram with $c_q = 3(2)$, $c_r = 2$, $R = 1$. Lines depict onset of the critical phase for each subnetwork. Compared to 3.36 we see that the P-critical and the R-critical phases have been found. For $C_p < 3.6$ the increase in consumption triggers overload in the producer network, while for $C_p \geq 3.6$ the increase in consumption causes overload in the receiver network. Also, compared to 3.36 we observe higher threshold for consumption that triggers overload in the system due to increased connectivity in the receiver subnetwork.

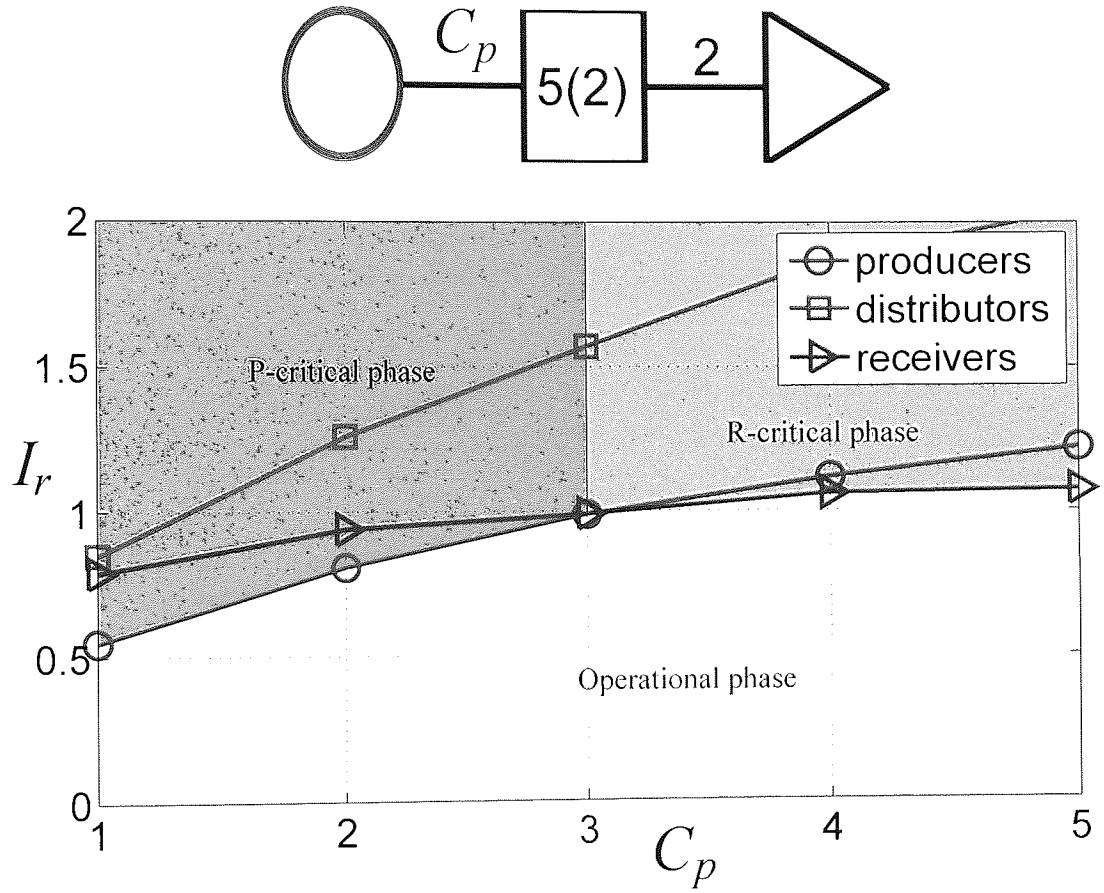

Figure 3.38: Phase diagram with $c_q = 5(2)$, $c_r = 2$, $R = 1$. Lines depict onset of the critical phase for each subnetwork. We see that the P-critical and the R-critical phases have been found. For $C_p < 3$ the increase in consumption triggers overload in the producer network, while for $C_p \geq 3$ the increase in consumption causes overload in the receiver network. Also, compared to 3.37 we observe higher threshold for consumption that triggers overload in the system due to increased connectivity in the distributor network. Moreover, the border between critical phases has been shifted. This reduces P-critical region and increases R-critical region.

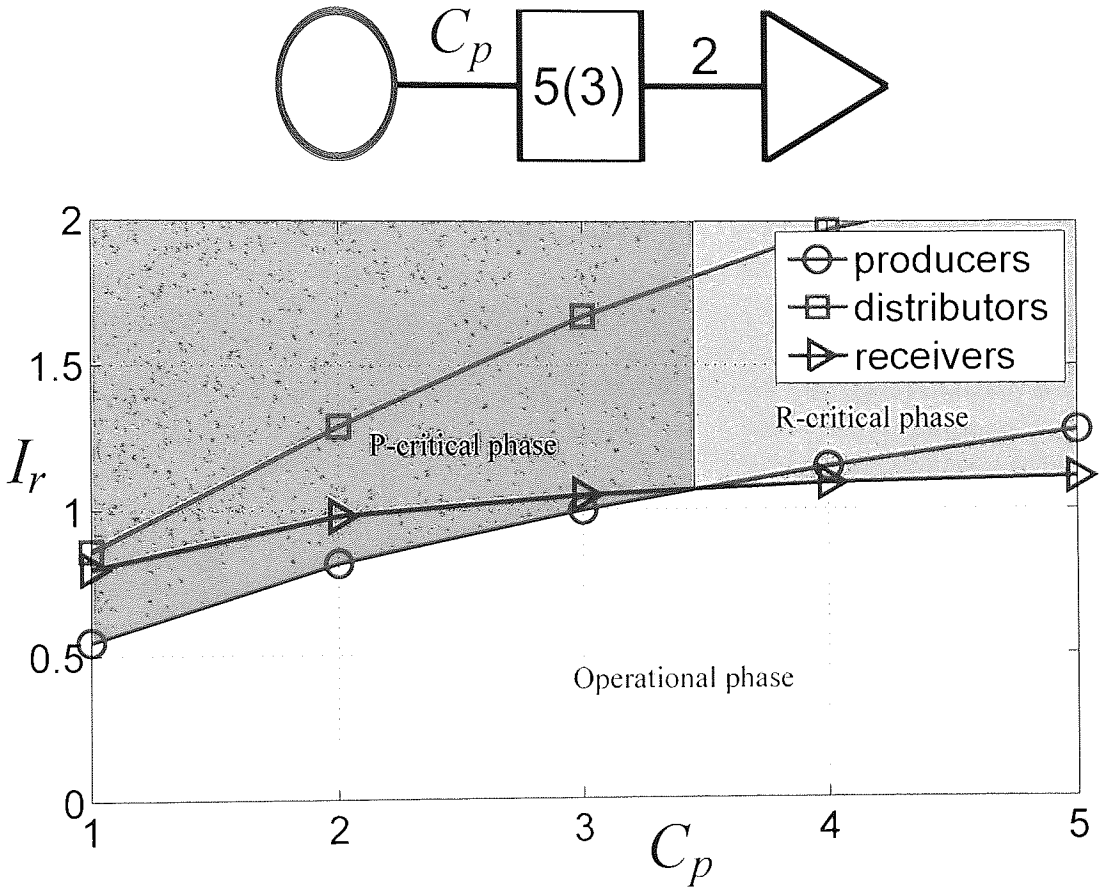

Figure 3.39: Phase diagram with $c_q = 5(3)$, $c_r = 2$, $R = 1$. Lines depict onset of the critical phase for each subnetwork. We see that the P-critical and the R-critical phases have been found. For $C_p < 3.4$ the increase in consumption triggers overload in the producer network, while for $C_p \geq 3.4$ the increase in consumption causes overload in the receiver network. Also, compared to 3.38 we observe slightly higher threshold for consumption that triggers overload in the system due to increased regularity in the distributor network. Moreover, the border between critical phases has been shifted. This reduces R-critical region and increases P-critical region.

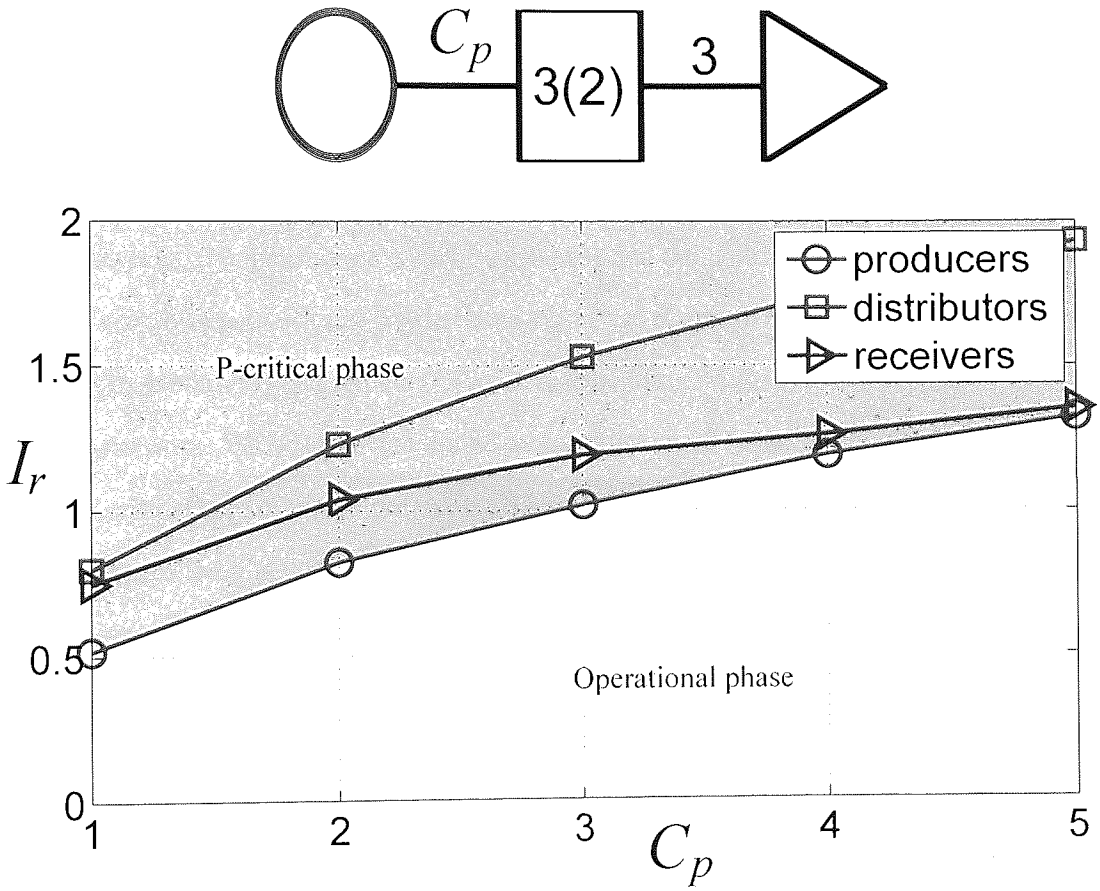

Figure 3.40: Phase diagram with $c_q = 3(2)$, $c_r = 3$, $R = 1$. Lines depict onset of the critical phase for each subnetwork. As in 3.36 we found only P-critical phase. Compared to 3.37 we observe the only critical phase, for the current range of c_p values due to increased connectivity in the receiver network.

3.5.4 Discussion and Conclusions

The FC model is an extension of the IC model described in the current section earlier. The novelty comes from the introduction of the link capacity, i. e. the maximum current that can go through the link. Such a restriction acts at the local level of individual links and adds complexity in finding the balance between global minimal dissipation requirement and local distribution constraints. In order to find an optimal flow of currents in the system the low temperature region is considered.

The global properties of interest are the distributions of currents in each subnetwork and the distributions of the node loads. We analyse these distributions and dependencies on the system macroparameters. The key macroparameters are the connectivities of subnetworks, the distribution of link resistances and the distribution of levels of demand.

We analyse network stability in terms of a phase diagram. We divided parameter space into operational (O) and critical (C) phases, depending on the fraction of critical currents in the network. We observe that the RS assumptions hold in the operational region, while in the critical region we do not expect RS to hold. Indeed, the solution that corresponds to the operational (O) region yields physical properties, while the solution in the critical region is not a true solution, i.e. distributions of currents in the critical region violate local constraints.

Moreover, the critical phase may be subdivided, depending on which subnetwork develops experience overload first. Such a classification allows the detection of the subnetwork that will experience overload first. Also, it is possible to detect a point when two subnetworks develop maximal currents at the same time.

We also assess the influence of redundancy, resistance and levels of demand. We confirm the beneficial role of redundancy. Higher connectivity of any subnetwork results in narrower distributions of currents in all subnetworks. Similarly, narrower distributions of resistances and levels of consumption lead to the narrower distributions of currents in all subnetworks.

In the presented phase diagrams we observe only P-critical and R-critical phases. The absence of a D-critical phase can be understood from the organisation of the network.

The distribution nodes can be connected to both producers and receivers. Consequently, even in case of a highly connected producer and receiver nodes and small connectivity in the distribution subnetwork we observe first extreme currents in either of the side subnetworks, but never in the distribution network. The D-criticality may be observed by either changing the structure of the network (adding an additional layer of distributors for example) or by modification of link resistances (relatively small resistances in distribution network should be sufficient).

3.6 Comparison and Conclusions

In this chapter we analysed the stability of distribution networks with respect to the link overload. We introduced a physical model of the direct current distribution network. We nominated specialised producers, distributors and receivers; and described the system in terms of flow of the currents in such networks. To isolate some effects of connectivity we imposed constraints about interlinks between functionally different nodes, it resulted in the separation of the initial network into three independent (in terms of connectivity) subnetworks.

We have analysed two models of distribution networks. Firstly, we proposed the **infinite capacity (IC)** model of distribution networks. Here we assume that the capacity of all links is unlimited. Secondly, we studied a model with limited capacity. We refer to this model as the **finite capacity (FC)** model.

In order to estimate the system's properties we use distributions of current and of load per node. We rely on monitoring the mean and standard deviation of distributions, but higher order moments may be generated if needed. In addition, in the case of the FC model we check the fraction of critical currents in the network for each subnetwork.

Both IC and FC models were analysed using equilibrium statistical mechanics methods and techniques. The spirit of the methods in both cases is exactly the same, but some subtle changes had to be made in the FC model due to additional constraints. However, despite many similarities the qualitative differences are significant.

3.6.1 IC Model

A description of the system without limits on the link capacity turns out to result in harmonic interactions between connected nodes. The models of this type are known to have certain properties, i.e. we found that the calculation of single-replica functions can be performed at finite temperature. As we apply the replica method we expect the RS approximation to be exact. From the numerical point of view, this form of interaction is advantageous and allows a compact representation of single-replica functions which leads to rapid performance of the population dynamics updates.

In this case we actually managed to obtain observable properties of the system at finite temperature. The optimal current flow exhibited a linear dependence on the level of demand. We also observed a positive influence of redundancy and uniform spread of resources on global properties of the system.

In the IC model we do not have any restrictions on link capacities. Consequently we obtain a solution for the , arguably unrealistic, network set up. However, the solutions, in terms of the distributions of currents in the network, turns out to be a good indicator of the onset of the critical phase in the system, when it is compared to the FC model. By predicting critical currents we can estimate the properties of the network, both of the individual elements and of connectedness in the network, that need to be adjusted.

3.6.2 FC Model

The FC model incorporates an additional restriction - finite link capacity. Inclusion of this constraint introduces significant changes. Indeed the harmonic form of interactions in this case is broken, so to obtain a solution the full functional approach is adopted in population dynamics updates. Moreover, the optimal flow is dependent on the temperature in this case. This is an important feature of this case, as now the optimal flow needs to be computed in the low temperature region.

We managed to classify operational and critical regions of the parameter space, presented in phase diagrams. Existence of two phases in FC model indicates qualitative difference from the IC model, IC model has only operational phase. However, the op-

erational phase is found to qualitatively correspond to the space of solutions of the IC model, e.g. the results of both models match exactly. The critical phase and the boundary between (O) and (C) phases is unique feature of this model.

The qualitative difference between two phases is also marked by the following consideration. The RS assumption holds in the operational region (correct solution), while it is not expected to hold in the critical region (incorrect solution). However, for the stability analysis of networks, it is sufficient to obtain the operational region and the boundary between two phases. The boundary between operational and critical regions yields good predictions of the onset of instability in the system.

Also, the FC model produces subdivision of critical phase that may be insightful. Different types of critical phases indicate subnetworks that develop critical currents before other subnetworks. Such knowledge may be very useful in understanding strong and weak parts of the network, and is desirable for analysis of existing networks, or in design of new complex networks.

Furthermore, the indication of the "weakest link" may be used for tracking overloading failures at the subnetwork level. Note we can not study the spread of individual failures, but we can identify the spread between subnetworks. This could also be used in analysis of the networks , and influence design decisions in modernisation and construction of the networks.

4 Conclusions and Outlook

CONTENTS

In this Thesis we have presented a stability analysis of complex distribution networks. We considered two main types of failures in the networks. The first type of failure is random failure, associated with the reliability of network components [50, 24, 22]. The second type is of overloading failures. Such failures occur due to finite capacity of network elements [70, 25, 28].

In both cases we are interested in the implications of occurrences of failures for the whole network, as well as in investigating the conditions for the occurrences of failures in the first place. In doing so, we managed to express network stability in simple observable physical properties, connected to a comparatively low number of descriptive macroparameters. In both cases we adopted a statistical mechanics approach that enabled to take into account both macro- and microscopic descriptions of the system[32, 58].

In each case we managed to obtain the physical properties that quantify the stability of the system. We are also able to gain a qualitative understanding in the development of a large spread of failures in complex distribution networks. In the case of random failures we observed a phase transition between operational and non-operational phases, as well as a metastable region where system states coexist. This has big implications for the stability of the system, as in this region the working system might experience a sudden collapse of large parts of the network without any prior indications.

In case of failures induced by extreme loads we also observed different phases of the system. For the stability analysis we were only interested in the operational phase and the boundary between operational and critical phases. Moreover, we analysed the robustness of the subnetworks against overloading failures by producing a subclassification of the critical region. This could be very important in understanding the development and propagation of the failures through the system.

4.1 Stability analysis against random failures

In Chapter 2 we addressed stability issues of distribution networks [51]. The main aim of this work was to understand the functioning of the distribution network under random failures. Also we were interested in the spread of failures through the network that could

lead to major blackouts.

We proposed a model that combines a graphical view of the system with quantitative characteristics of network components. Indeed, the model is based on the graphical model of the network with associated variables that represent the state of a given object. The model is based on an existing model of operational research that describes interactions in economic sectors [60]. The feature of that model is the dynamical nature of variables associated with the model entities. The introduction of dynamical variables yields non-trivial system behaviour.

In addition to the dynamical variables associated with nodes in the graph we introduced dynamical links. We considered binary dynamical variables that represents on/off states. Finally, we introduced additional dynamics in the form of a support between network elements.

The method which we use to study this model is inspired by the physics of amorphous materials, namely, spin-glasses. The theoretical analysis which is based on the concepts of statistical mechanics, with the replica method playing a major role. The replica treatment of the system relates a microscopic description with global properties [31, 44, 64].

The model exhibits rich behaviour; we produced phase diagrams that demonstrated a first order phase transition between operational and non-operational phases. Moreover, the intermediate regions has been identified - a coexistence region - which is characterised by coexistence of both operational and non-operational phases. The region is bounded by two dynamical transitions. The lines that represent the boundaries of the coexistence region are spinodals, and they meet at the critical point.

From the stability analysis perspective, the coexistence region is of primary interest. The spinodal lines indicate dynamical transitions from a stable state (the only solution) to a metastable state (two solutions). Once in the metastable region, the transition from one phase to another can not really be noticed, i.e. say initially the operational network moves towards a coexistence region. Once it crosses the spinodal line the state of the system is unstable. Even without moving towards the lower end of the coexistence region the stability of the current state might be affected by random disturbances in the network.

The phase transition in the model points towards a cascading failures phenomenon.

The existence of a phase transition and its characteristics provide a qualitative and quantitative description of the cascading failures propagation.

From the topological prospective we analysed three models of random graphs: exponential random graphs, regular random graphs and scale-free graphs [42, 12]. We reported a qualitative differences between homogeneous structures like the first two and heterogeneous scale-free networks. The first two type of graphs exhibit critical behaviour for systems with average connectivity above the percolation threshold. In contrast, we found that only some of the scale-free structures produced similar behaviour, while others do not exhibit a phase transition at all. For all types of networks we observe a beneficial role of higher connectivities and homogeneous interactions.

4.2 Stability analysis against overload

In Chapter 3 of the thesis we analysed the stability of networks against overload. We aimed to understand what effect the physical limitations of network elements have on local and global properties of the network. We investigated conditions that trigger overloading failures, detectability of critical network load and spreading of load induced failures. The critical load of the network in this context may be referred to as network **capacity**.

Firstly we introduced a model of direct current in the distribution network. The flow is managed at the nodes by distribution rules, e.g. Kirchhoff's law. We order the nodes into three classes : producers, distributors and receivers. We also specified particular requirements on the inter-class interactions. Only distributor nodes are able to connect to any nodes. The flow in the network is driven by consumption demand at the receiver nodes, and propagated over the network through the above mentioned distribution constraints. The optimality of the flow is ensured by a global optimisation requirement of minimal dissipation of the energy. In our model we have chosen to take a quadratic form of the cost function, i.e. a contribution proportional to the resistance of a link and to the square of current that goes through the link.

The microscopic description of the system was formulated via the usual methods of statistical mechanics. The global characteristics are distributions of currents in the net-

work and distributions of node loads. In our analysis we considered two principal cases of networks: those with infinite link capacity (IC) and those with finite link capacity (FC).

The introduction of finite capacity proved to be a critical difference between models. In the IC case our analysis showed the only phase of the system to be an operational one. This operational phase was identified, and its key characteristics (average currents, standard deviation) exhibit linear dependence on the consumption levels.

In contrast, the FC model exhibited non-trivial behaviour. We observed two phases of the system state: operational and critical. This classification is based on the measurable properties of distributions of currents. We monitored a fraction of critical currents in the network, and on that basis classified our system's phases. The operational state corresponded to the lowest level of consumption and is characterised by the absence of critical currents. The standard deviation of the distributions of currents depended linearly on the demand. Both the IC and the FC models can described an operational phase. The critical phase was characterised by presence of critical currents.

For the stability analysis against load induced failures we were interested only in the operational phase and its boundary with the critical phase. As we noticed both the IC and the FC models can exhibit an operational phase. However, due to the harmonicity of the couplings in the former model, and consequently, its much better computational performance, one may prefer to use the IC model. Even without complete knowledge of operational and critical phases the IC model produced a fairly good prediction of the boundary between two phases.

Another important feature of the FC model is its ability to indicate which of the sub-networks represented the "weakest link". Knowledge of not only the criticality of currents in the network, but also of criticality in particular parts of network could be useful for the analysis of existing and expanding networks, as well as at the earliest planning stages of new networks.

Finally, the FC model enabled us the monitoring of the spread of the overloading failures in the network at the level of the distributions of currents. The overload failures developed in one part of the system, spread through the network, triggering overloads in the rest of the system. The mechanism of such failure spreading is understood to be

connected to the capacity of network elements. Strained parts of the network shed the load and trigger overload in the adjacent parts, and so on. The observables we calculated do not allow for a tracking of individual currents, however at the level of subnetworks we can observe such a spread and we can quantify robustness of the network against overload failures.

We should also note that the distribution of currents could be substituted for distribution of loads. Then we may analyse overload failures associated with nodes. Alternatively both of these characteristics could be monitored to identify node and link overload failures.

Also, in the presented work we focused on one specific organisation of network namely, that there is one group of producers, one of distributors, one of receivers and certain constraints on internetwork connections. Such an organisation may not be sufficient in the analysis of complex networks[1]. However, our model can easily be adapted to analyse a network of arbitrary complexity.

[1] The lack of D-critical phases in phase diagrams is a consequence of this particular organisation.

Bibliography

[1] R. Solomonoff and A. Rapoport, "Connectivity of random nets," *Bulletin of Mathematical Biology*, vol. 13, pp. 107–117, 1951.

[2] I. de Sola Pool and M. Kochen, "Contacts and influence," *Social Networks*, vol. 1, pp. 1–48, 1978.

[3] S. Milgram, "The small world problem," *Psychology Today*, vol. 2, pp. 60–67, 1967.

[4] M. Newman, "Scientific collaboration networks. ii. Shortest paths, weighted networks, and centrality," *Phys. Rev. E*, vol. 64, p. 016132, 2001.

[5] M. Newman, "Who is the best connected scientist? A study of scientific coauthorship networks.," *Complex Networks (Lecture Notes in Phys.)*, vol. 650, pp. 337–70, 2004.

[6] F. Ball, D. Mollison, and G. Scala-Tomba, "Epidemics with two levels of mixing," *Ann. Appl. Probab.*, vol. 7, pp. 46–89, 1997.

[7] M. Boguná and R. Pastor-Satorras, "Epidemic spreading in correlated complex networks," *Phys. Rev. E*, vol. 66, p. 047104, 2002.

[8] L. Buzna, K. Peters, and D. Helbing, "Modelling the dynamics of disaster spreading in networks," *Physica A*, vol. 363, pp. 132–140, 2006.

[9] H. Jeong, B. Tombor, R. Albert, Z. Oltvai, and A.-L. Barabasi, "The large-scale organization of metabolic networks," *Nature*, vol. 407, pp. 651–654, 2000.

[10] D. A. Fell and A. Wagner, "The small world of metabolism," *Nat. Biotechnol.*, vol. 18, pp. 1121–1122, 2000.

[11] J. Banavar, A. Maritan, and A. Rinaldo, "Size and form in efficient transportation networks.," *Nature*, vol. 399, pp. 130–132, 1999.

[12] L. A. N. Amaral, A. Scala, M. Barthélémy, and H. E. Stanley, "Classes of small-world networks," *Proc. Natl. Acad. Sci. USA*, vol. 97, p. 11149, 2000.

[13] J. Watts, *Six degrees: the science of a connected age*. W.W. Norton & Company New York London, 2003.

[14] M. Faloutsos, P. Faloutsos, and C. Faloutsos, "On power-law relationships of the internet topology," *Comp. Comm. Rev.*, vol. 29, pp. 251–262, 1999.

[15] R. Albert, H. Jeong, and A.-L. Barabási, "Diameter off the world-wide web," *Nature*, vol. 401, pp. 130–131, 1999.

[16] R. Pastor-Satorras, A. Vázquez, and A. Vespignani, "Dynamical and correlation properties of the internet," *Phys. Rev. Lett.*, vol. 87, p. 258701, 2001.

[17] J. Kleinberg., "Navigation in a small world.," *Nature*, vol. 407, pp. 651–654, 2000.

[18] J. Kleinberg., "Small-world phenomena and the dynamics of information.," *Advances in Neural Information Processing Systems (NIPS)*, vol. 14, pp. 1–14, 2001.

[19] L. A. Adamic, R. M. Lukose, A. R. Puniyani, and B. A. Huberman, "Search in power-law networks," *Phys. Rev.*, vol. 64, p. 046135(8), 2001.

[20] R. Albert, H. Jeong, and A.-L. Barabási, "Error and attack tolerance of complex networks," *Nature*, vol. 406, pp. 378–382, 2000.

[21] D. Callaway, M. Newman, S. Strogatz, and D. Watts, "Network robustness and fragility: percolation on random graphs," *Phys. Rev. Lett.*, vol. 85, pp. 5468–5471, 2000.

[22] R. Cohen, K. Erez, D. ben Avraham, and S. Havlin, "Resilience of the internet to random breakdowns," *Phys. Rev. Lett.*, vol. 85, pp. 4626–4628, 2000.

[23] R. Cohen, K. Erez, D. ben Avraham, and S. Havlin, "Breakdown of the internet under intentional attack," *Phys. Rev. Lett.*, vol. 86, pp. 3682–3685, 2001.

[24] P. Crucitti, V. Latora, M. Marchiori, and A. Rapisarda, "Efficiency of scale-free networks: error and attack tolerance," *Physica A*, vol. 320, pp. 622–642, 2003.

[25] P. Crucitti, V. Latora, and M. Marchiori, "Model for cascading failures in complex networks," *Phys. Rev. E*, vol. 69, p. 45104, 2004.

[26] R. Albert, I. Albert, and G. L. Nakarado, "Structural vulnerability of the North American power grid," *Phys. Rev. E*, vol. 69, p. 025103, 2004.

[27] V. Jacobson, "Congestion avoidance and control," *ACM Computer Communication Review*, vol. 18(4), pp. 314–329, 1988.

[28] R. Kinney, P. Crucitti, R. Albert, and V. Latora, "Modeling cascading failures in the North American power grid," *Eur. Phys. J. B*, vol. 46, pp. 101–107, 2005.

[29] B. A. Carreras, V. E. Lynch, I. Dobson, and D. Newman, "Critical points and transistions in an electric power transmission model for cascading failure blackouts.," *Chaos*, vol. 14, pp. 986–994, 2002.

[30] M. Anghel, K. Werley, and A. Motter, "Stochastic model for power grid dynamics," *Hawaii International Conference on System Sciences*, pp. 113–122, 2007.

[31] D. Sherrington and S. Kirkpatrick, "Solvable model of a spin-glass," *Phys.Rev. Lett.*, vol. 35, pp. 1792–1796, 1975.

[32] D. Sherrington and S. Kirkpatrick, "Infinite-ranged models of spin-glasses," *Phys. Rev. B*, vol. 17(11), pp. 4384–4403, 1978.

[33] G. Parisi, "The order parameter for spin glasses: a function on the interval 0-1," *J. Phys. A: Math. Gen.*, vol. 13, pp. 1101–1112, 1980.

[34] D. J. Amit, H. Gutfreund, and H. Sompolinsky, "Spin-glass models of neural networks.," *Phys. Rev. A*, vol. 32(2), pp. 1007–1018, 1985.

[35] N. Parga and M. A. Virasoro, "The ultrametric organization of memories in a neural network," *J. Physique*, vol. 47, pp. 1857–1864, 1986.

[36] M. Mezard, J. Nadal, and G. Toulouse, "Solvable models of working memories.," *J. Physique*, vol. 47, pp. 1457–1462, 1986.

[37] S. Kirkpatrick, C. Gelatt, and M. Vecchi, "Optimization by simulated annealing," *Science*, vol. 220(4598), pp. 671–680, 1983.

[38] M. Mezard and G. Parisi, "A replica analysis of the travelling salesman problem.," *J. Physique.*, vol. 47, pp. 1285–1296, 1986.

[39] M. Mezard and G. Parisi, "Replicas and optimization," *J. Physique Lett.*, vol. 46, pp. 771–778, 1985.

[40] Y. Fu and P. Anderson, "Application of statistical mechanics to NP-complete problems in combinatorial optimisation.," *J. Phys. A: Math. Gen.*, vol. 19, pp. 1605–1620, 1986.

[41] D. Watts, *Small worlds: the dynamics of networks between order and randomness.* Princeton University Press, 1999.

[42] P. Erdős and A. Rényi, "On the evolution of random graphs," *Publ. Math. Inst. Hung. Acad. Sci*, vol. 5, pp. 17–61, 1960.

[43] M. Newman, S. Strogatz, and D. Watts, "Random graphs with arbitrary degree distributions and their applications," *Phys. Rev. E*, vol. 64, p. 026118, 2001.

[44] L. Viana and A. J. Bray, "Phase diagrams for dilute spin glasses ," *J.Phys. C*, vol. 18, p. 3037, 1985.

[45] J. P. L. Hatchett, B. Wemmenhove, I. Perez Castillo, T. Nikoletopoulos, N. S. Skantzos, and A. C. C. Coolen, "Parallel dynamics of disordered Ising spin systems on finitely connected random graphs," *J. Phys. A*, vol. 37, pp. 6201–6220, 2004.

[46] A. Broder, R. Kumar, F. Maghoul, P. Raghavan, S. Rajagopalan, R. Stat, A. Tomkins, and J. Wiener, "Graph structure in the web," *Comput. Networks*, vol. 33, pp. 309–320, 2000.

[47] A.-L. Barabási and R. Albert, "Emergence of scaling in random networks," *Science*, vol. 286, pp. 509–512, 1999.

[48] S. Strogatz, "Exploring complex networks," *Nature*, vol. 410, pp. 268–276, 2001.

[49] P. Holme and B. Kim, "Growing scale-free networks with tunable clustering," *Phys. Rev. E*, vol. 65, p. 026107, 2002.

[50] P. Holme, B. Kim, C. Yoon, and S. Han, "Attack vulnerability of complex networks," *Phys. Rev. E*, vol. 65, p. 56109, 2002.

[51] D. Nasiev, J. van Mourik, and R. Kühn, "Solvable model for distribution networks on random graphs.," *Phys. Rev. E*, vol. 76, p. 041120, 2007.

[52] R. May, "Will a large complex system be stable?," *Nature*, vol. 238, pp. 413–414, 1972.

[53] A. Perelson and G. Weisbuch, "Immunology for physicists," *Rev. Mod. Phys.*, vol. 69, pp. 1219–1268, 1997.

[54] R. V. Sole and J. M. Montoya, "Complexity and fragility in ecological networks," *Proc. R. Soc. London B*, vol. 268, pp. 2039–2045, 2001.

[55] C. Gadgil, C. H. Lee, and H. Othmer, "Stochastic analysis of first-order reaction networks," *Bull. Math. Biol.*, vol. 67, pp. 901–946, 2005.

[56] A. Aleksiejuk and J. Holyst, "A simple model of bank bankruptcies," *Physica A*, vol. 299, pp. 198–204, 2001.

[57] J. Hatchett and R. Kühn, "Effects of economic interactions on credit risk," *J.Phys. A*, vol. 39, pp. 2231–2251, 2006.

[58] R. Albert and A.-L. Barabási, "Statistical mechanics of complex networks," *Rev. Mod. Phys.*, vol. 74, pp. 47–97, 2002.

[59] S. Dorogovtsev and J. Mendes, *Evolution of Networks: from Biological Networks to the Internet and WWW*. Oxford: Oxford University Press, 2003.

[60] R. Kühn and P. Neu, "Functional correlation approach to operational risk in banking organizations," *Physica A*, vol. 322, pp. 650–666, 2003.

[61] K. Anand and R. Kühn, "Phase transitions and operational risk," *Phys. Rev. E*, vol. 75, p. 016111, 2007.

[62] K. Y. M. Wong and D. Sherrington, "Graph bipartitioning and spin glasses on a random network of fixed finite valence," *J.Phys. A*, vol. 20, pp. L793–L799, 1987.

[63] M. Leone, A. Vázquez, A. Vespignani, and R. Zecchina, "Ferromagnetic ordering in graphs with arbitrary degree distribution," *Eur. Phys. J. B*, vol. 28, pp. 191–197, 2002.

[64] B. Wemmenhove and A. C. C. Coolen, "Finite connectivity attractor neural networks," *J.Phys. A*, vol. 36, pp. 9617–9633, 2003.

[65] I. Syozi, "Transformation of Ising models," in *Phase Transitions and Critical Phenomena* (C. Domb and M. S. Green, eds.), vol. 1, p. 269, London, New York, San Francisco: Academic Press, 1972.

[66] M. Mézard and G. Parisi, "The Bethe lattice spin glass revisited," *Eur. Phys. J. B*, vol. B 20, pp. 217–233, 2001.

[67] D. Kempe, J. Kleinberg, and E. Tardos., "Maximizing the spread of influence through a social network," in *Proc. 9th ACM SIGKDD Intl. Conf. on Knowledge Discovery and Data Mining*, pp. 137–146, ACM New York, NY, USA, 2003.

[68] Y. Moreno, J. Gomez, and A. Pacheco, "Instability of scale-free networks under node-breaking avalanches," *Europhys. Lett.*, vol. 58, pp. 630–636, 2002.

[69] Y. Moreno, R. Pastor-Satorras, A. Vázquez, and A. Vespignani, "Critical load and congestion instabilities in scale-free networks," *Europhys. Lett.*, vol. 62, pp. 292–298, 2003.

[70] P. Holme, "Edge overload breakdown in evolving networks," *Phys. Rev. E*, vol. 66, p. 036119, 2002.

[71] H. Hassenmuller, "Tomorrow's power grids getting smarter and safer," *Pictures of the future, Siemens*, vol. 1, pp. 50–52, 2008.

[72] R. Kühn, J. van Mourik, M. Weigt, and A. Zippelius, "Finitely coordinated models for low-temperature phases of amorphous systems," *J. Phys. A*, vol. 40, p. 9227, 2007.

A Mathematical tools

A number of transformations are required in replica calculations. Many of these transformations allow analytic continuations of discrete quantities, which is essential to the replica method. We provide a brief overview of transformations we used in our calculations.

A.1 Delta function

We extensively use the Dirac and Kronecker delta functions to enforce constraints in the problems. We often used integral representations of both functions. The Fourier transform of the Dirac delta function is

$$\delta(x-y) = \frac{1}{2\pi}\int_{-\infty}^{\infty} \exp\left[-is(x-y)\right] \mathrm{d}s. \tag{A.1}$$

Constraints on discrete variables can be enforced by the Kronecker delta function. In

the replica method we use constraints on integer quantities and use the Cauchy integral formula

$$\delta_{K,L} = \oint_C \frac{\mathrm{d}z}{2\pi \mathrm{i} z} z^{(K-L)}, \tag{A.2}$$

where K, L are integer numbers and the path C is an arbitrary contour in the complex plane about the point 0. We also use the property

$$\oint_C \frac{\mathrm{d}z}{2\pi \mathrm{i} z} z^{-L} f(z) = \frac{1}{L!} \frac{\partial^L f(z)}{\partial z^L}\bigg|_{z=0}. \tag{A.3}$$

B Stability of distribution networks against random failures

In the Chapter 2 we considered a spin model on graphs with finite connectivity. Here, we present details of steps taken to perform connectivity averages, details of replica method and the replica symmetry ansatz.

B.1 Detailed balance

Here, we show that under the conditions stated in equations (2.24)-(2.26), the dynamics (2.18)-(2.18) satisfies detailed balance with respect to the Gibbs-Boltzmann distribution with Hamiltonian (2.27). We first consider a transition $\{v,l\} \rightarrow \{v,l\}'$ with $v_i = 0$, $v_i' = 1$ and $v_j = v_j', l_j = l_j' \quad \forall \quad j(\neq k)$, for which

$$Prob(\{v,l\}') = W(\{v,l\}'|\{v,l\}) = \phi_\beta(h_i), \tag{B.1}$$

where $W(\{\nu,l\}'|\{\nu,l\})$ is the transition probability and $h_i = h(\{\nu,l\})$ is the node support (2.11) for node i in the state $\{\nu,l\}$.

For the reverse transition $\{\nu,l\}' \to \{\nu,l\}$ we have that $W(\{\nu,l\}|\{\nu,l\}') = \phi_\beta(-h_i)$, with the node support h_i unchanged, as it is independent of ν_i. Hence,

$$\frac{W(\{\nu,l\}'|\{\nu,l\})}{W(\{\nu,l\}|\{\nu,l\}')} = \frac{\phi_\beta(h_i)}{\phi_\beta(-h_i)} = e^{\beta h_i} = e^{-\beta(H(\{\nu,l\}')-H(\{\nu,l\}))}, \tag{B.2}$$

i.e. the ratio of the equilibrium distributions of the states $\{\nu,l\}$ and $\{\nu,l\}'$. This establishes detailed balance for all transitions involving node variables.

Next, we consider transition $\{\nu,l\} \to \{\nu,l\}'$ with $l_{ij} = 0$, l'_{ij} and $\nu_i = \nu'_i \quad \forall \quad il_{kl} = l'_{kl} \quad (kl) \neq (ij)$. Using the symmetry conditions (2.24)-(2.26), we obtain the corresponding ratio of transition probabilities.

$$\frac{W(\{\nu,l\}'|\{\nu,l\})}{W(\{\nu,l\}|\{\nu,l\}')} = \frac{\phi_\beta(h_{ij})}{\phi_\beta(-h_{ij})} = e^{\beta h_i} = e^{-\beta(H(\{\nu,l\}')-H(\{\nu,l\}))}, \tag{B.3}$$

where h_{ij} is the link support (2.12) which is independent of l_{ij}. This establishes detailed balance for all transitions involving link variables.

B.2 Averaging the replicated partition function

The underlying network is fully described by the connectivity matrix $\mathbf{c} = \{c_{ij}\}$. We consider ensemble of graphs which have degree distribution $P_C(L)$, where C is the average connectivity and L is a node coordination number.

The degree distribution is

$$P_C(L) = \frac{1}{N}\sum_i \delta_{L,L_i}, \tag{B.4}$$

and the compatibility with the average connectivity is ensured by

$$p_C(c_{ij}) = \left(1 - \frac{C}{N}\right)\delta_{c_{ij},0} + \frac{C}{N}\delta_{c_{ij},1}. \tag{B.5}$$

Now, given the distribution of connectivity matrices, the average (2.28) of the repli-

cated partition function has the following structure

$$\langle Z^n \rangle = \frac{\mathbb{T}}{\mathbb{N}}$$

where

$$\mathbb{T} = \operatorname*{Tr}_{\{c_{ij}\}} \operatorname*{Tr}_{\{\nu_i^\alpha\}} \operatorname*{Tr}_{\{l_{ij}^\alpha\}} \left(e^{\beta \sum_{(ij)} c_{ij} \sum_\alpha l_{ij}^\alpha \left(a_{ij} \nu_i^\alpha \nu_j^\alpha + b_{ij} \left(\nu_i^\alpha + \nu_j^\alpha \right) + d_{ij} \right) + \beta \sum_i \sum_\alpha \mu_i \nu_i^\alpha} \right) \times \tag{B.6}$$

$$\times \prod_L \delta_{P_c(L)} \prod_k \delta \left(\sum_{j(\neq k)} c_{kj} - L_k \right)$$

$$\mathbb{N} = \operatorname*{Tr}_{\{c_{ij}\}} \prod_L \delta_{P_c(L)} \prod_k \delta \left(\sum_{j(\neq k)} c_{kj} - L_k \right) \tag{B.7}$$

$$\delta_{P_c(L)} = \delta \left(P_c(L) - \frac{1}{N} \sum_i \delta_{L,L_i} \right) \tag{B.8}$$

We start with the calculations of all possible configurations ($\mathbb{N}$):

$$\begin{aligned}
\mathbb{N} &= \operatorname*{Tr}_{\{c_{ij}\}} \prod_L \delta_{P_c(L)} \prod_k \delta \left(\sum_{j(\neq k)} c_{kj} - L_k \right) \\
&= \operatorname*{Tr}_{\{c_{ij}\}} \prod_L \delta_{P_c(L)} \oint \left(\prod_k \frac{\mathrm{d}\hat{L}_k}{2\pi \mathrm{i}} \right) \left(e^{\mathrm{i} \sum_{j(\neq k)} (\hat{L}_k + \hat{L}_j) c_{ij}} \right) \left(e^{-\mathrm{i} \sum_i \hat{L}_k L_k} \right) \\
&= \prod_L \delta_{P_c(L)} \oint \left(\prod_k \frac{\mathrm{d}\hat{L}_k}{2\pi \mathrm{i}} e^{-\mathrm{i} \sum_k \hat{L}_k L_k} \right) \operatorname*{Tr}_{\{c_{ij}\}} \prod_{(ij)} \left(e^{\mathrm{i} \sum_{j(\neq k)} (\hat{L}_k + \hat{L}_j) c_{kj}} \right) \\
&= \prod_L \delta_{P_c(L)} \oint \left(\prod_k \frac{\mathrm{d}\hat{L}_k}{2\pi \mathrm{i}} e^{-\mathrm{i} \sum_k \hat{L}_k L_k} \right) \prod_{(ij)} \left(\left(1 - \frac{c}{N} \right) + \frac{c}{N} e^{\mathrm{i} \sum_{j(\neq k)} (\hat{L}_k + \hat{L}_j)} \right) \\
&= \prod_L \delta_{P_c(L)} \oint \left(\prod_k \frac{\mathrm{d}\hat{L}_k}{2\pi \mathrm{i}} e^{-\mathrm{i} \sum_k \hat{L}_k L_k} \right) \prod_{(ij)} \left(\frac{c}{N} \left(e^{\mathrm{i} \sum_{j(\neq k)} (\hat{L}_k + \hat{L}_j)} - 1 \right) + 1 \right)
\end{aligned}$$

substitution

$$\chi_{kj} = e^{\mathrm{i} \sum_{j(\neq k)} (\hat{L}_k + \hat{L}_j)} - 1$$

$$\prod_{(kj)}\left(1+\frac{c}{N}\chi_{kj}\right)=e^{\ln\prod_{(kj)}\left(1+\frac{c}{N}\chi_{kj}\right)}=e^{\sum_{(kj)}\ln\left(1+\frac{c}{N}\chi_{kj}\right)}\approx e^{\sum_{(kj)}\frac{c}{N}\chi_{kj}}$$

$$\begin{aligned}
\mathbb{N} &= \prod_L \delta_{P_c(L)} \oint \left(\prod_k \frac{d\hat{L}_k}{2\pi i} e^{-i\sum_k \hat{L}_k L_k}\right) e^{\frac{c}{N}\sum_{(kj)}\left(e^{i(\hat{L}_k+\hat{L}_j)}-1\right)} \\
&= \prod_L \delta_{P_c(L)} \oint \left(\prod_k \frac{d\hat{L}_k}{2\pi i} e^{-i\sum_k \hat{L}_k L_k}\right) e^{\frac{c}{2N}\sum_k\sum_j\left(e^{i(\hat{L}_k+\hat{L}_j)}-1\right)} \\
&= \prod_L \delta_{P_c(L)} \oint \left(\prod_k \frac{d\hat{L}_k}{2\pi i} e^{-i\sum_k \hat{L}_k L_k}\right) e^{\frac{c}{2N}\sum_k\sum_j e^{i\hat{L}_k}e^{i\hat{L}_j}-\frac{cN}{2}} \\
&= |z=e^{i\hat{L}_k}, dz=ie^{i\hat{L}_k}d\hat{L}_k| = \\
&= \prod_L \delta_{P_c(L)} \oint \left(\prod_k \frac{dz}{z} z^{-L_k}\right) e^{\frac{c}{2N}\sum_k\sum_j e^{i\hat{L}_k}e^{i\hat{L}_j}-\frac{cN}{2}} \delta\left(\rho_0-\frac{1}{N}\sum_k e^{i\hat{L}_k}\right) \\
&= \prod_L \delta_{P_c(L)} \oint \left(\prod_k \frac{dz}{z} z^{-L_k}\right) \frac{1}{(2\pi)^N}\int D(\rho,\hat{\rho}_0) e^{\frac{cN}{2}\left(\rho_0^2-1\right)} e^{N\hat{\rho}_0\rho_0} e^{-\sum_k \hat{\rho}_0 e^{i\hat{L}_k}} \\
&= \frac{1}{(2\pi)^N}\prod_L \delta_{P_c(L)} \int D(\rho,\hat{\rho}_0) \oint \left(\prod_k \frac{dz}{z} z^{-L_k} e^{-\hat{\rho}_0 z}\right) e^{\frac{cN}{2}\left(\rho_0^2-1\right)+N\hat{\rho}_0\rho_0} \\
&= \frac{1}{(2\pi)^N}\prod_L \delta_{P_c(L)} \int D(\rho,\hat{\rho}_0) \oint \left(\prod_k \left(\frac{\hat{\rho}_0^{L_k}}{L_k!}\right)\right) \left(e^{\frac{cN}{2}\left(\rho_0^2-1\right)+N\hat{\rho}_0\rho_0}\right) \\
&= \frac{1}{(2\pi)^N}\int D(\rho,\hat{\rho}_0) \left(\prod_L \delta_{P_c(L)} e^{\sum_k \delta_{L,L_k}\sum_L \ln\left(\frac{\hat{\rho}_0^{L_k}}{L_k!}\right)} \left(e^{\frac{cN}{2}\left(\rho_0^2-1\right)+N\hat{\rho}_0\rho_0}\right)\right) \\
&= \frac{1}{(2\pi)^N}\int D(\rho,\hat{\rho}_0) \left(e^{N\sum_L P_c(L)\delta_{L,L_k}\ln\left(\frac{\hat{\rho}_0^{L_k}}{L_k!}\right)} \left(e^{\frac{cN}{2}\left(\rho_0^2-1\right)+N\hat{\rho}_0\rho_0}\right)\right) \\
\mathbb{N} &= \frac{1}{(2\pi)^N}\int D(\rho,\hat{\rho}_0) \left(e^{N\left(\frac{c}{2}\left(\rho_0^2-1\right)-\hat{\rho}_0\rho_0+\sum_L P_c(L)\ln\left(\frac{\hat{\rho}_0^L}{L!}\right)\right)}\right)
\end{aligned}$$

to find ρ_0 and $\hat{\rho}_0$, we use saddle point method. This involves taking the derivatives with respect to ρ and $\hat{\rho}_0$:

$$\begin{aligned} \frac{d\mathbb{N}}{d\rho_0} = 0 \quad &\Rightarrow \quad c\rho_0 = \hat{\rho}_0, \\ \frac{d\mathbb{N}}{d\hat{\rho}_0} = 0 \quad &\Rightarrow \quad \rho_0\hat{\rho}_0 = c, \end{aligned} \tag{B.9}$$

and we obtain a solution

$$\begin{aligned} \rho_0 &= 1 \\ \hat{\rho}_0 &= c \end{aligned}$$

and

$$\mathbb{N} \sim e^{N\left(\sum_L P_c(L) \ln\left(\frac{c^L}{L!}\right) - c\right)}$$

For the nominator $\mathbb{T}$ we proceed in a similar way:

$$
\begin{aligned}
\mathbb{T} &= \operatorname*{Tr}_{\{c_{ij}\}}\operatorname*{Tr}_{\{v_i^\alpha\}}\operatorname*{Tr}_{\{l_{ij}^\alpha\}}\left(e^{\beta\sum_{(ij)}c_{ij}\sum_\alpha l_{ij}^\alpha\left(a_{ij}v_i^\alpha v_j^\alpha+b_{ij}\left(v_i^\alpha+v_j^\alpha\right)+d_{ij}\right)+\beta\sum_i\sum_\alpha\mu_i v_i^\alpha}\right)\times \\
&\quad\times\prod_L\delta_{P_c(L)}\prod_k\delta\left(\sum_{j(\neq k)}c_{kj}-L_k\right) \\
&= \operatorname*{Tr}_{\{c_{ij}\}}\operatorname*{Tr}_{\{v_i^\alpha\}}\operatorname*{Tr}_{\{l_{ij}^\alpha\}}\left(e^{\beta\sum_{(ij)}c_{ij}\sum_\alpha l_{ij}^\alpha\left(a_{ij}v_i^\alpha v_j^\alpha+b_{ij}\left(v_i^\alpha+v_j^\alpha\right)+d_{ij}\right)+\beta\sum_i\sum_\alpha\mu_i v_i^\alpha}\right)\times \\
&\quad\times\prod_L\delta_{P_c(L)}\oint\left(\prod_k\frac{\mathrm{d}\hat{L}_k}{2\pi\mathrm{i}}\right)e^{-\mathrm{i}\hat{L}_kL_k+\mathrm{i}\hat{L}_k\sum_{j(\neq k)}c_{kj}} \\
&= \prod_L\delta_{P_c(L)}\left(\operatorname*{Tr}_{\{v_k^\alpha\}}\oint\left(\prod_k\frac{\mathrm{d}\hat{L}_k}{2\pi\mathrm{i}}\right)e^{-\mathrm{i}\hat{L}_kL_k}e^{\beta\sum_\alpha\mu_kv_k^\alpha}\right)\times \\
&\quad\times\prod_{(kj)}\left(\operatorname*{Tr}_{\{l_{kj}^\alpha\}}\operatorname*{Tr}_{\{c_{kj}\}}e^{\beta\sum_{(kj)}c_{kj}\sum_\alpha l_{ij}^\alpha\left(a_{kj}v_i^\alpha v_j^\alpha+b_{kj}\left(v_i^\alpha+v_j^\alpha\right)+d_{kj}\right)}e^{\mathrm{i}(\hat{L}_k+\hat{L}_j)c_{kj}}\right) \\
&= \prod_L\delta_{P_c(L)}\left(\operatorname*{Tr}_{\{v_k^\alpha\}}\oint\left(\prod_k\frac{\mathrm{d}\hat{L}_k}{2\pi\mathrm{i}}\right)e^{-\mathrm{i}\hat{L}_kL_k}e^{\beta\sum_\alpha\mu_kv_k^\alpha}\right)\times \\
&\quad\times\prod_{(kj)}\left(\left(1-\frac{c}{N}\right)+\frac{c}{N}\left(\operatorname*{Tr}_{\{l_{kj}^\alpha\}}e^{\beta\sum_\alpha l_{kj}^\alpha\left(a_{kj}v_i^\alpha v_j^\alpha+b_{kj}\left(v_i^\alpha+v_j^\alpha\right)+d_{kj}\right)}e^{\mathrm{i}(\hat{L}_k+\hat{L}_j)}\right)\right) \\
&= \prod_L\delta_{P_c(L)}\left(\operatorname*{Tr}_{\{v_i^\alpha\}}\oint\left(\prod_k\frac{\mathrm{d}\hat{L}_k}{2\pi\mathrm{i}}\right)e^{-\mathrm{i}\hat{L}_kL_k}e^{\beta\sum_\alpha\mu_kv_k^\alpha}\right)\prod_{(kj)}\left(1+\frac{c}{N}\chi_{kj}\right)
\end{aligned}
$$

where

$$
\chi_{kj}=\operatorname*{Tr}_{\{l_{kj}^\alpha\}}e^{\beta\sum_\alpha l_{kj}^\alpha\left(a_{kj}v_i^\alpha v_j^\alpha+b_{kj}\left(v_i^\alpha+v_j^\alpha\right)+d_{kj}\right)}e^{\mathrm{i}(\hat{L}_k+\hat{L}_j)}-1 \tag{B.10}
$$

We can transform $\prod_{(kj)}\left(1+\frac{c}{N}\chi_{kj}\right)$:

$$\prod_{(kj)}\left(1+\frac{c}{N}\chi_{kj}\right)=e^{\ln\prod_{(kj)}\left(1+\frac{c}{N}\chi_{kj}\right)}=e^{\sum_{(kj)}\ln\left(1+\frac{c}{N}\chi_{kj}\right)}\approx e^{\frac{c}{N}\sum_{(kj)}\chi_{kj}}$$

$$=\exp\left(\frac{c}{N}\sum_{(kj)}\left(\operatorname*{Tr}_{\{l_{kj}^{\alpha}\}}e^{\beta\sum_{\alpha}l_{kj}^{\alpha}\left(a_{ij}v_i^{\alpha}v_j^{\alpha}+b_{ij}\left(v_i^{\alpha}+v_j^{\alpha}\right)+d_{ij}\right)}e^{\mathrm{i}(\hat{L}_k+\hat{L}_j)}-1\right)\right)$$

$$=\exp\left(\frac{c}{2N}\sum_{k}\sum_{j}\left(\operatorname*{Tr}_{\{l_{kj}^{\alpha}\}}e^{\beta\sum_{\alpha}l_{kj}^{\alpha}\left(a_{kj}v_i^{\alpha}v_j^{\alpha}+b_{kj}\left(v_i^{\alpha}+v_j^{\alpha}\right)+d_{kj}\right)}e^{\mathrm{i}(\hat{L}_k+\hat{L}_j)}-1\right)\right)$$

$$=\exp\left(\frac{c}{2N}\sum_{k}\sum_{j}\left(e^{\mathrm{i}(\hat{L}_k+\hat{L}_j)}\prod_{\alpha}\left(1+e^{\beta\sum_{\alpha}l_{kj}^{\alpha}\left(a_{kj}v_i^{\alpha}v_j^{\alpha}+b_{kj}\left(v_i^{\alpha}+v_j^{\alpha}\right)+d_{kj}\right)}\right)\right)-\frac{cN}{2}\right).$$

The exponent can be transformed :

$$N^2\sum_{k}\sum_{j}\left(e^{\mathrm{i}(\hat{L}_k+\hat{L}_j)}\prod_{\alpha}\left(1+e^{\beta\left(a_{kj}v_i^{\alpha}v_j^{\alpha}+b_{kj}\left(v_i^{\alpha}+v_j^{\alpha}\right)+d_{kj}\right)}\right)\right)=\left|\rho(\bar{v})\equiv\frac{1}{N}\sum_{k}e^{\mathrm{i}\hat{L}_k}\delta_{\bar{v},\bar{v}_k}\right|$$

$$=\sum_{k}e^{\mathrm{i}\hat{L}_k}\sum_{j}e^{i\hat{L}_j}\operatorname*{Tr}_{v}\delta_{\bar{v},\bar{v}_k}\operatorname*{Tr}_{w}\delta_{\bar{w},\bar{v}_j}\prod_{\alpha}\left(1+e^{\beta\left(a_{kj}\bar{v}\bar{w}+b_{kj}(\bar{v}+\bar{w})+d_{kj}\right)}\right)=\operatorname*{Tr}_{v}\operatorname*{Tr}_{w}f(\bar{v},\bar{w})\rho(\bar{v})\rho(\bar{w})$$

Incorporating transformitions and substituting traces for integrals, we obtain

$$
\begin{aligned}
\mathbb{T} &= \int D(\rho)\prod_L \delta_{P_c(L)}\left(\operatorname*{Tr}_{\{\nu_k^\alpha\}}\oint\left(\prod_k\frac{d\hat{L}_k}{2\pi i}\right)e^{-i\hat{L}_k L_k}e^{\beta\sum_\alpha\mu_k\nu_i^\alpha}\right)\\
&\quad\times e^{\frac{cN}{2}\left(\operatorname{Tr}_{\bar{\nu}}\operatorname{Tr}_{\bar{w}}f(\bar{\nu},\bar{w})\rho(\bar{\nu})\rho(\bar{w})-1\right)}\delta\left(N\rho(\bar{\nu})-\sum_k e^{i\hat{L}_k}\delta_{\bar{\nu},\bar{\nu}_i}\right)\\
&= \frac{1}{(2\pi)^N}\int D(\rho,\hat{\rho})\prod_L\delta_{P_c(L)}\left(\operatorname*{Tr}_{\{\nu_k^\alpha\}}\oint\left(\prod_k\frac{d\hat{L}_k}{2\pi i}\right)e^{-i\hat{L}_k L_k}e^{\beta\sum_\alpha\mu_k\nu_i^\alpha}\right.\\
&\quad\left.\times e^{\frac{cN}{2}G_l(\rho)}e^{-N\operatorname{Tr}_{\bar{\nu}}\rho(\bar{\nu})\hat{\rho}(\bar{\nu})}e^{\operatorname{Tr}_{\bar{\nu}}\hat{\rho}(\bar{\nu})\sum_k e^{i\hat{L}_k}\delta_{\bar{\nu},\bar{\nu}_k}}\right)\\
&= \frac{1}{(2\pi)^N}\int D(\rho,\hat{\rho})e^{N\left(\frac{c}{2}G_l(\rho)-G_m[\rho]\right)}\prod_L\delta_{P_c(L)}\left(\operatorname*{Tr}_{\nu_k}\oint\left(\prod_k\frac{d\hat{L}_k}{2\pi i}\right)e^{-i\hat{L}_k L_k}e^{\beta\sum_\alpha\mu_k\nu_i^\alpha}e^{\hat{\rho}(\bar{\nu}_k)e^{i\hat{L}_k}}\right)\\
&= \frac{1}{(2\pi)^N}\int D(\rho,\hat{\rho})e^{N\left(\frac{c}{2}G_l(\rho)-G_m[\rho]\right)}\prod_L\delta_{P_c(L)}\exp\left(\sum_k\ln\left(\operatorname*{Tr}_{\nu_k}\oint\frac{d\hat{L}_k}{2\pi i}e^{-i\hat{L}_k L_k}e^{\beta\sum_\alpha\mu_k\nu_i^\alpha}e^{\hat{\rho}(\bar{\nu}_k)e^{i\hat{L}_k}}\right)\right)\\
&= \frac{1}{(2\pi)^N}\int D(\rho,\hat{\rho})e^{N\left(\frac{c}{2}G_l(\rho)-G_m[\rho]\right)}\prod_L\delta_{P_c(L)}\exp\left(\sum_k\ln\left(\operatorname*{Tr}_{\nu_k}e^{\beta\sum_\alpha\mu_k\nu_i^\alpha}\frac{\hat{\rho}(\bar{\nu}_k)^{L_k}}{L_k!}\right)\right)\\
&= \frac{1}{(2\pi)^N}\int D(\rho,\hat{\rho})e^{N\left(\frac{c}{2}G_l(\rho)\right)-G_m[\rho]}\exp\left(N\sum_L\delta_{P_c(L)}\ln\left(\operatorname*{Tr}_{\nu_i}e^{\beta\sum_\alpha\mu_k\nu_i^\alpha}\frac{\hat{\rho}(\bar{\nu}_i)^L}{L!}\right)\right)\\
&= \frac{1}{(2\pi)^N}\int D(\rho,\hat{\rho})\exp\left(N\left(\frac{c}{2}G_l(\rho)-G_m[\rho]+\sum_L\delta_{P_c(L)}\ln\left(\operatorname*{Tr}_{\nu_k}e^{\beta\mu_k|\bar{\nu}_k|}\frac{\hat{\rho}(\bar{\nu}_k)^L}{L!}\right)\right)\right).
\end{aligned}
$$

Now, functionals are given as

$$G_l[\rho] = \operatorname*{Tr}_{\tilde{\nu}}\left[\operatorname*{Tr}_{\tilde{w}}[f(\tilde{\nu},\tilde{w})\rho(\tilde{\nu})\rho(\tilde{w})]\right], \tag{B.11}$$

$$G_m[\rho] = -\operatorname*{Tr}_{\tilde{\nu}}[\rho(\tilde{\nu})\hat{\rho}(\tilde{\nu})], \tag{B.12}$$

$$G_s[\hat{\rho}] = \sum_L P_C(L)\ln\operatorname*{Tr}_{\tilde{\nu}}e^{\beta\mu_i|\tilde{\nu}|}\frac{\hat{\rho}(\tilde{\nu})^L}{L!}. \tag{B.13}$$

B.3 Replica symmetry

In our next step we introduce RS ansatz in the form:

$$\rho(\bar{\nu}) = \lambda\int_0^\infty dx\pi(x)\frac{\prod_\alpha x^{\nu_\alpha}}{(1+x)^n}, \tag{B.14}$$

$$\hat{\rho}(\bar{\nu}) = \hat{\lambda}\int_0^\infty dx\hat{\pi}(x)\frac{\prod_\alpha x^{n^\alpha}}{(1+x)^n}, \tag{B.15}$$

where $\pi(x)$ and $\hat{\pi}(x)$ are normalised. We then express functionals (B.12)-(B.13) in terms of $\pi(x)$ and $\hat{\pi}(x)$ to the first order in n using RS ansatz (B.14) and (B.15):

$$\begin{aligned} G_l[\pi] &\backsimeq \lambda^2 + n\int_0^\infty \mathrm{d}\pi(x_1)\mathrm{d}\pi(x_2)\,\langle \ln[C_0 + C_1(x_1+x_2) + C_2 x_1 x_2]\rangle_{a,b,d}\,, \\ G_m[\pi,\hat{\pi}] &\backsimeq \lambda\hat{\lambda} + n\int_0^\infty \mathrm{d}\pi(x)\mathrm{d}\hat{\pi}(\hat{x})\ln[1+x\hat{x}]\,, \\ G_s[\hat{\pi}] &\backsimeq \sum_L P_C(L)\left[\ln\left(\frac{\hat{\lambda}^L}{L!}\right) + n\int_0^\infty \{\mathrm{d}\hat{\pi}(\hat{x}_l)\}_L \ln\left[1+e^{\beta\mu}\{\hat{x}\}_L\right]\right]. \end{aligned} \tag{B.16}$$

Here we used shorthands

$$C_0 = 1 + e^{\beta d_{ij}}, \quad C_1 = 1 + e^{\beta(b_{ij}+d_{ij})}, \quad C_2 = 1 + e^{\beta(a_{ij}+2b_{ij}+d_{ij})}. \tag{B.17}$$

We solve the saddle-point equations to $O(1)$ in n, and we obtain the prefactors $\lambda = 1$ and $\hat{\lambda} = C$. This leads to a cancellation of the $O(n^0)$ contributions to $\mathbb{T}$ with $\mathbb{N}$. Finally, the partition function can be expressed in terms of functionals (2.38).

$$\langle Z^n\rangle_D, \mathbf{c} \sim \int D\pi D\hat{\pi} \exp\left[nN\left\{\frac{C}{2}G_l[\pi] - CG_m[\pi,\hat{\pi}] + \sum_L P_C(L)G_s[\hat{\pi}]\right\}\right]. \tag{B.18}$$

B.4 Calculation of observable properties

From the free energy we can obtain physically relevant quantities.

$$F = -\frac{1}{\beta}\left(\frac{C}{2}G_l[\pi] - CG_m[\pi,\hat{\pi}] + G_s[\hat{\pi}]\right). \tag{B.19}$$

The fraction m_n of working nodes is given

$$m_n = \frac{\partial F}{\partial \mu} = \sum_L P_C(L)\int_0^\infty \{\mathrm{d}\hat{\pi}(\hat{x}_l)\}_L \left\langle \frac{e^{\beta\mu}\{\hat{x}_l\}_L}{1+e^{\beta\mu}\{\hat{x}_l\}_L}\right\rangle_\mu, \tag{B.20}$$

the fraction m_l of working links,

$$m_e = \frac{\partial F}{\partial a} = \int_0^\infty \mathrm{d}\pi(x_1)\mathrm{d}\pi(x_2)\left\langle \frac{M_0 + M_1(x_1+x_2) + M_2 x_1 x_2}{C_0 + C_1(x_1+x_2) + C_2 x_1 x_2}\right\rangle_{a,b,d}, \tag{B.21}$$

in which $M_i = C_i - 1$, C_i are given in (2.34) and (2.35). The internal energy is given

$$U = -\frac{C}{2}\int_0^\infty d\pi(x_1)d\pi(x_2)\left\langle \frac{E_0 + E_1(x_1+x_2) + E_2 x_1 x_2}{C_0 + C_1(x_1+x_2) + C_2 x_1 x_2}\right\rangle_{a,b,d}$$
$$-\sum_L P_C(L)\int_0^\infty \{d\hat{\pi}(\hat{x}_l)\}_L \left\langle \frac{\mu e^{\beta\mu}\{\hat{x}_l\}_L}{1+e^{\beta\mu}\{\hat{x}_l\}_L}\right\rangle_\mu ,$$

with $E_0 = de^{\beta d}$, $E_1 = (b+d)e^{\beta(b+d)}$ and $E_2 = (a+2b+d)e^{\beta(a+2b+d)}$.

C Capacity of Power Grids

In Chapter 3 we worked with the distribution network which has specific constraints on structure. Recall that the structure of the network is specialised, so the distributor nodes can be connected to any type of nodes, while both producers and receivers can not be directly connected either between these two groups or inside each group.

C.1 Averaging the replicated partition function

To work with the replicated partition function on such a structure we write the average over connectivities. This is very similar to the strategy we used for performing averages in Chapter 2 and appendix B. In fact the only major difference is the presence of three subnetworks and consequent factorisation of the partition function.

$$\langle Z^n \rangle = \frac{\mathbb{T}}{\mathbb{N}}, \tag{C.1}$$

where $\mathbb{N}$ is the normalisation constant and given by

$$\begin{aligned}\mathbb{N} &= \prod_{qp} \mathrm{Tr}_{c_{qp}} \left[p_{c_p}(c_{qp}) \delta_{c_{qp},c_{pq}} \prod_p \delta_{L_p,\sum_q c_{qp}} \right] \\ &\times \prod_{(qs)} \mathrm{Tr}_{c_{qs}} \left[p_{c_q}(c_{qs}) \delta_{c_{qs},c_{sq}} \prod_q \delta_{L_q,\sum_{s(\neq q)} c_{qs}} \right] \\ &\times \prod_{qr} \mathrm{Tr}_{c_{qr}} \left[p_{c_r}(c_{qr}) \delta_{c_{qr},c_{rq}} \prod_r \delta_{L_r,\sum_q c_{qr}} \right]\end{aligned}$$

Here we achieved factorisation as three subnetworks are independent. The distributions that ensure compatibility withe given average connectivity are

$$\begin{aligned}p_{C_p}(c_{qp}) &= \left(1 - \frac{c_p}{Nq}\right) \delta_{c_{qp},0} + \frac{c_p}{Nq} \delta_{c_{qp},1}, \\ p_{C_q}(c_{qs}) &= \left(1 - \frac{c_q}{Nq}\right) \delta_{c_{qs},0} + \frac{c_q}{Nq} \delta_{c_{qs},1}, \\ p_{C_r}(c_{qr}) &= \left(1 - \frac{c_r}{Nq}\right) \delta_{c_{qr},0} + \frac{c_r}{Nq} \delta_{c_{qr},1},\end{aligned}$$

and the average connectivities c_p and c_r are defined on the producer and receiver sides respectively. Also the coordination numbers $\{L_p, L_q, L_r\}$ are drawn from the corresponding degree distribution $P_{c_i}(L)$. The general strategy is to express $\mathbb{N}$ in terms of a path integral and use saddle-point method. First, we use the integral representation of the Kronecker delta function (??) expressing constraints on the local coordination numbers L_i.

The $\mathbb{N}$ is then transformed exactly as in (??) and we obtain

$$\begin{aligned}\mathbb{N} &= \int \frac{\mathrm{d}\hat{\rho}_p^0 \mathrm{d}\rho_p^0}{2\pi/N_p} \exp\left[N_p \left\{ c_p(\rho_p^0 \rho_q^0 - 1) - \rho_p^0 \hat{\rho}_p^0 + \sum_L P_{c_p}(L) \ln\left(\frac{\hat{\rho}_p^L}{L!}\right) \right\} \right] \\ &\times \int \frac{\mathrm{d}\hat{\rho}_r^0 \mathrm{d}\rho_r^0}{2\pi/N_r} \exp\left[N_r \left\{ c_r(\rho_r^0 \rho_q^0 - 1) - \rho_r^0 \hat{\rho}_r^0 + \sum_L P_{c_r}(L) \ln\left(\frac{\hat{\rho}_r^L}{L!}\right) \right\} \right] \\ &\times \int \frac{\mathrm{d}\hat{\rho}_q^0 \mathrm{d}\rho_q^0}{2\pi/N_q} \exp\left[N_q \left\{ \frac{c_q}{2}((\rho_q^0)^2 - 1) - \rho_q^0 \hat{\rho}_q^0 + \sum_L P_{c_q} \ln\left(\frac{(\hat{\rho}_q^0)^L}{L!}\right) \right\} \right].\end{aligned} \tag{C.2}$$

In the saddle point we obtain

$$\rho_p^0 = \rho_r^0 = \rho_q^0 = 1, \tag{C.3}$$

$$\hat{\rho}_p^0 = C_p, \hat{\rho}_r^0 = C_r, \hat{\rho}_q^0 = C_q, \tag{C.4}$$

and have

$$\begin{aligned} \mathbb{N} \sim & \left[\exp\left(N\sum_L P_{C_p}(L)\ln\left(\frac{C_p^L}{L!}\right)\right) - C_p\right] \\ \times & \left[\exp\left(N\sum_L P_{C_r}(L)\ln\left(\frac{C_r^L}{L!}\right)\right) - C_r\right] \\ \times & \left[\exp\left(N\sum_L P_{C_q}(L)\ln\left(\frac{C_q^L}{L!}\right)\right) - C_q\right] \end{aligned} \tag{C.5}$$

Before we proceed to the calculation of $\mathbb{T}$ we introduce shorthand notation for a replicated vector $\tilde{x} = (x^1, \ldots, x^n)$. Also, it is useful to introduce replica link weights

$$\begin{aligned} U^{qp}(\tilde{x}_q) &\equiv \operatorname*{Tr}_{\tilde{I}} \exp\left[-\beta\sum_\alpha \left(R_{qp} I_{qp}^{\alpha^2} + i x_q^\alpha I_{qp}^\alpha\right)\right] \\ U^{qr}(\tilde{x}_q, \tilde{x}_r) &\equiv \operatorname*{Tr}_{\tilde{I}} \exp\left[-\beta\sum_\alpha \left(R_{qr} I_{qr}^{\alpha^2} + i\left(x_r^\alpha - x_q^\alpha\right) I_{qr}^\alpha\right)\right] \\ U^{qs}(\tilde{x}_q, \tilde{x}_s) &\equiv \operatorname*{Tr}_{\tilde{I}} \exp\left[-\beta\sum_\alpha \left(R_{qs} I_{qs}^{\alpha^2} + i\left(x_q^\alpha - x_s^\alpha\right) I_{qs}^\alpha\right)\right]. \end{aligned}$$

In our next step we introduce replica density functions

$$\rho^r(\tilde{x}) = \frac{1}{N_r}\sum_r z_r \delta(\tilde{x} - \tilde{x}_r), \quad \rho^q(\tilde{x}) = \frac{1}{N_q}\sum_q z_q \delta(\tilde{x} - \tilde{x}_q) \tag{C.6}$$

and obtain a representation of a replicated partition function in terms of ρ's and $\hat{\rho}$'s.

$$\langle Z^n \rangle_R = \int D\rho D\hat{\rho} \exp\left\{N\left(G_l[\rho] - G_m[\rho, \hat{\rho}] + G_s[\hat{\rho}]\right)\right\} \tag{C.7}$$

where

$$G_l[\rho] = \lambda_q C_p G_l^p[\rho^q] + \lambda_q C_r G_l^r[\rho^q, \rho^r] + \lambda_q \frac{C_q}{2} G_l^q[\rho^q] \quad \text{(C.8)}$$

$$G_m[\rho, \hat{\rho}] = -\lambda_r G_m^r[\rho^r, \hat{\rho}^r] - \lambda_q G_m^q[\rho^q, \hat{\rho}^q], \quad \text{(C.9)}$$

$$G_s[\hat{\rho}] = \sum_L P_{C_r}(L) G_{r,L}[\hat{\rho}^r] + \sum_L P_{C_q}(L) G_{q,L}[\hat{\rho}^q] \quad \text{(C.10)}$$

C.2 Replica symmetry

In the next step , we introduce the RS ansatz in the form

$$\rho^r(\tilde{x}) = \int D\psi \pi^r[\psi] \prod_\alpha \frac{e^{-\beta\psi(x^\alpha)}}{Z[\psi]}, \qquad \hat{\rho}^r(\tilde{x}) = \rho_r^0 \int D\hat{\psi}\hat{\pi}^r[\hat{\psi}] \prod_\alpha \frac{e^{-\beta\hat{\psi}(x^\alpha)}}{Z[\hat{\psi}]} \quad \text{(C.11)}$$

$$\rho^q(\tilde{x}) = \int D\psi \pi^q[\psi] \prod_\alpha \frac{e^{-\beta\psi(x^\alpha)}}{Z[\psi]}, \qquad \hat{\rho}^q(\tilde{x}) = \rho_q^0 \int D\hat{\psi}\hat{\pi}^q[\hat{\psi}] \prod_\alpha \frac{e^{-\beta\hat{\psi}(x^\alpha)}}{Z[\hat{\psi}]} \quad \text{(C.12)}$$

The functionals in RHS in (C.8)-(C.10) can be expressed in terms of functionals π's and $\hat{\pi}$'s.

$$G_l^p[\pi^q] \sim \rho_p^0 \rho_q^0 + n \int D\pi^q[\psi^q] \left\langle \ln\left(\frac{Z_1[\psi^q, U^{qp}]}{Z[\psi^q]}\right)\right\rangle_R, \quad \text{(C.13)}$$

$$G_l^r[\pi^q, \pi^r] \sim \rho_q^0 \rho_r^0 + n \int D\pi^q[\psi^q] D\pi^r[\psi^r] \left\langle \ln\left(\frac{Z_2[\psi^q, \psi^r, U^{qr}]}{Z[\psi^q]Z[\psi^r]}\right)\right\rangle_R, \quad \text{(C.14)}$$

$$G_l^q[\pi^q] \sim (\rho_q^0)^2 + n \int D\pi^q[\psi^q] D\pi^q[\psi^s] \left\langle \ln\left(\frac{Z_2[\psi^q, \psi^s, U^{qs}]}{Z[\psi^q]Z[\psi^s]}\right)\right\rangle_R, \quad \text{(C.15)}$$

$$G_m[\pi^r, \hat{\pi}^r] \sim \rho_r^0 \hat{\rho}_r^0 + n \int D\pi^r[\psi^r] D\hat{\pi}^r \ln\left(\frac{Z[\psi^r + \hat{\psi}^r]}{Z[\psi^r]Z[\hat{\psi}^r]}\right), \quad \text{(C.16)}$$

$$G_m[\pi^q, \hat{\pi}^q] \sim \rho_q^0 \hat{\rho}_q^0 + n \int D\pi^r[\psi^q] D\hat{\pi}^r \ln\left(\frac{Z[\psi^q + \hat{\psi}^q]}{Z[\psi^q]Z[\hat{\psi}^q]}\right), \quad \text{(C.17)}$$

$$G_s[\hat{\pi}^r] \sim \sum_L P_C(L) \left(\ln\left(\frac{(\hat{\rho}_r^0)^L}{L!}\right) + n \int \{D\hat{\pi}\}_L \langle \frac{Z[\sum_l^L \hat{\psi}_l^r + V]}{\{Z[\hat{\psi}_l^r]\}_L} \rangle_V \right) \quad \text{(C.18)}$$

$$G_s[\hat{\pi}^q] \sim \sum_L P_C(L) \left(\ln\left(\frac{(\hat{\rho}_q^0)^L}{L!}\right) + n \int \{D\hat{\pi}\}_L \langle \frac{Z[\sum_l^L \hat{\psi}_l^q + V]}{\{Z[\hat{\psi}_l^q]\}_L} \rangle_V \right) \quad \text{(C.19)}$$

Firstly , we solve the saddle-point equations to $O(1)$ in n. The saddle point is

$$\rho_p^0 = \rho_r^0 = \rho_q^0 = 1, \tag{C.20}$$

$$\hat{\rho}_p^0 = C_p, \quad \hat{\rho}_r^0 = C_r, \quad \hat{\rho}_q^0 = C_q. \tag{C.21}$$

This ensures that $O(n^0)$ contributions to $\mathbb{T}$ cancels with $\mathbb{N}$. Then we obtain

$$\langle Z^n \rangle_{D,\mathbf{c}} \sim \int D\pi D\hat{\pi} \exp\left[nN \left\{ G_l[\pi] - G_m[\pi,\hat{\pi}] + \sum_L P_C(L) G_{s,L}[\hat{\pi}] \right\} \right] \tag{C.22}$$

where functionals over π's and $\hat{\pi}$'s are given in (3.37, 3.38 and 3.39).